

# Nonlinear Analysis of Reinforced Concrete Frames Subjected to Abnormal Loads

by

Ignac Joseph Emil Zajac

A thesis  
presented to the University of Waterloo  
in fulfillment of the  
thesis requirement for the degree of  
Master of Applied Science  
in  
Civil Engineering

Waterloo, Ontario, Canada, 2007

©Ignac Zajac, 2007

## **Author's Declaration**

I hereby declare that I am the sole author of this thesis. This is a true copy of the thesis, including any required final revisions, as accepted by my examiners.

I understand that my thesis may be made electronically available to the public.

Signature

## Abstract

The purpose of this study is to analyze reinforced concrete frames subjected to abnormal loads. Structures are rarely subjected to abnormal loads, however, when they are subjected to them, it can lead to a progressive collapse. The World Trade Centers in New York City and the Alfred P. Murrah building in Oklahoma City are examples of structures being deliberately subjected to abnormal loads. Structures can also experience unintentional abnormal loading. Examples include the Ronan Point apartment building in Canning Town, England and Husky Stadium at the University of Washington. Consequently, many analysis and design standards now explicitly account for abnormal loads and try to mitigate their effects.

This study presents the development of a nonlinear computer analysis program for reinforced concrete frames. The method of analysis involves discretizing a two dimensional reinforced concrete frame into a series of beam-column elements. The element is linear-elastic, however, its end-sections model nonlinear behaviour of a total member by a series of springs. The springs represent the post-elastic stiffness of the end-sections. The post-elastic stiffness of a member-section is obtained from a post-elastic force-deformation response, which is first obtained by performing sectional analysis on a reinforced concrete section using a public domain computer program. The post-elastic force-deformation responses are modeled as either bilinear or trilinear. So-called stiffness degradation factors, which are defined as the ratio of elastic to elastic plus post-elastic deformation of a member-section, are used in modifying the elastic stiffness coefficients in the element stiffness matrix to account for the nonlinear behaviour.

Once a reinforced concrete frame enters the post-elastic range of response the analysis procedure becomes incremental. The stiffness degradation factors are calculated at each load increment and the degree of post-elastic stiffness degradation is progressively tracked throughout the load history. The program also has the capability of performing a progressive collapse analysis whereby debris loads caused by falling members are calculated and applied to the structure.

A series of example problems are presented to demonstrate the computer analysis program. The first analysis example is for a simple portal frame used to illustrate the program outputs. The second analysis example is for a 2 bay-2 storey more redundant frame. The third analysis example is for the same 2 bay-2 storey frame but with some initial damage caused by an abnormal load. This example is used to illustrate the program's capabilities in performing a progressive collapse analysis.

## **Acknowledgements**

I would like to thank my supervisors, Professor Donald E. Grierson and Professor Marianna Polak, for their guidance in the preparation of this thesis. A lot of time was spent discussing concepts and ideas and reviewing my work in general and their help was very much appreciated.

A special thanks goes out to Yuxin Liu for always taking the time to offer an opinion or assistance whenever it was needed.

Finally, I would especially like to thank my parents and family for their love and support throughout my studies. They have always wholeheartedly supported me in all my endeavors and for this I am truly grateful.

## Table of Contents

Author's Declaration .....	ii
Abstract.....	iii
Acknowledgements.....	iv
List of Figures.....	vii
List of Tables .....	xi
Chapter 1 Introduction.....	1
1.1 Scope of Study.....	2
1.2 Assumptions and Idealizations .....	3
Chapter 2 Analysis Concept .....	6
2.1 Beam-Column Model for Analysis.....	6
2.2 Post-Elastic Range of Response .....	7
2.3 Sectional Analysis of Reinforced Concrete Members.....	8
2.3.1 Sectional Analysis in Bending.....	9
2.3.2 Sectional Analysis in Shear .....	10
2.3.3 Sectional Analysis in Compression .....	11
2.4 Approximating Member-End Deformations from Strains.....	12
2.5 Post-Elastic Stiffness and Force-Deformation Response .....	14
2.5.1 General Force-Deformation Response.....	14
2.5.2 Examples of Post-Elastic Force-Deformation Response and Post-Elastic Stiffness .....	17
2.6 Stiffness Degradation Factors.....	20
2.6.1 Bending Stiffness Degradation Factor.....	20
2.6.2 Shear Stiffness Degradation Factor .....	24
2.6.3 Axial Stiffness Degradation Factor.....	25
2.7 Member Stiffness Matrix .....	26
Chapter 3 Analysis Procedure.....	43
3.1 Stage Zero Elastic Analysis .....	43
3.2 Stage One Inelastic Incremental Analysis .....	45
3.3 Stage Two Elastic-Unloading Analysis .....	49
3.4 Stage Three Reloading Inelastic Analysis .....	50
Chapter 4 Example Problems .....	56
4.1 Reinforced Concrete Frame Design.....	56

4.2 Analysis Program Outputs .....	57
4.3 Portal Frame.....	58
4.3.1 Post-Elastic Bending Stiffness Degradation .....	58
4.3.2 Post-Elastic Shear Stiffness Degradation.....	62
4.3.3 Post-Elastic Axial Stiffness Degradation.....	64
4.4 2 Bay - 2 Storey Frame .....	66
4.4.1 Post-Elastic Bending Stiffness Degradation .....	66
4.4.2 Post-Elastic Shear Stiffness Degradation.....	72
4.4.3 Post-Elastic Axial Stiffness Degradation.....	76
4.5 2 Bay-2 Storey Frame with Initial Damage .....	79
Chapter 5 Conclusions .....	119
5.1 Summary .....	119
5.2 Conclusions.....	120
5.3 Future Work.....	121
Appendix A Examples of Calculating $\mu$ .....	122
Appendix B Axial Stiffness Reduction Coefficient.....	126
Appendix C Frame Design .....	129
Appendix D 2 Bay - 2 Storey Frame Members Post-Elastic Force-Deformation Response .....	133

## List of Figures

Figure 1.1: Ronan Point Apartment Building 1968 (© Daily Telegraph, 1968) .....	4
Figure 1.2: Husky Stadium 1987 (© John Stamets, 1987) .....	5
Figure 1.3: Alfred P. Murrah Building, Oklahoma 1995 (Hinman, 1997) .....	5
Figure 2.1: Beam-column analysis model (Xu <i>et al</i> , 2005).....	30
Figure 2.2: Typical moment-rotation response for an under-reinforced concrete section.....	31
Figure 2.3: Typical force-deformation response for axial compression .....	31
Figure 2.4: Summary of a reinforced concrete column section ( <i>Response-2000</i> ) .....	32
Figure 2.5: Sectional analysis in bending - output results ( <i>Response-2000</i> ) .....	32
Figure 2.6: Moment-curvature control plot ( <i>Response-2000</i> ) .....	33
Figure 2.7: Sectional analysis in shear - output results ( <i>Response-2000</i> ).....	33
Figure 2.8: Shear force-shear strain control plot ( <i>Response-2000</i> ) .....	34
Figure 2.9: Sectional analysis in compression - output results ( <i>Response-2000</i> ).....	34
Figure 2.10: Compressive force-axial strain control plot ( <i>Response-2000</i> ) .....	35
Figure 2.11: Curvature along a beam.....	35
Figure 2.12: Shear strain along a beam.....	35
Figure 2.13: General post-elastic force-deformation response .....	36
Figure 2.14: Post-elastic moment-curvature for a 500x350 mm section, 35 MPa, $\rho = 1.31\%$ .....	36
Figure 2.15: General post-elastic force-deformation response .....	37
Figure 2.16: Post-elastic moment-rotation response for an under-reinforced section .....	37
Figure 2.17: Post-elastic moment-rotation response for an over-reinforced section .....	38
Figure 2.18: Post-elastic shear force-shear deformation response for a section with transverse reinforcement.....	38
Figure 2.19: Post-elastic shear force-shear deformation response for a section without transverse reinforcement.....	39
Figure 2.20: Post-elastic axial tension-axial deformation.....	39
Figure 2.21: Post-elastic axial compression-axial deformation .....	40
Figure 2.22: Model for bending stiffness degradation factor (Xu <i>et al</i> , 2005) .....	40
Figure 2.23: Beam cross section.....	41
Figure 2.24: Model for shear stiffness degradation factor (Xu <i>et al</i> , 2005) .....	42
Figure 2.25: Model for axial stiffness degradation factor (Xu <i>et al</i> , 2005) .....	42
Figure 3.1: Four-stage analysis procedure.....	52

Figure 3.2: General trilinear post-elastic force-deformation response .....	52
Figure 3.3: Local instability.....	53
Figure 3.4: Member-end forces at time of disengagement .....	53
Figure 3.5: Elastic-unloading nodal loads .....	53
Figure 3.6: Falling debris load.....	54
Figure 3.7: Analysis procedure.....	55
Figure 4.1: Symbol legend.....	84
Figure 4.2: Portal frame geometry and loading .....	84
Figure 4.3: Portal frame analysis model .....	85
Figure 4.4: Column cross section .....	85
Figure 4.5: Beam cross section .....	85
Figure 4.6: Beam post-elastic moment-rotation graph .....	86
Figure 4.7: Column post-elastic moment-rotation graph.....	87
Figure 4.8: Load factor $\lambda = 0.124$ .....	87
Figure 4.9: Bending moment diagram (kN-m) $\lambda = 0.124$ .....	88
Figure 4.10: Load factor $\lambda = 0.126$ .....	88
Figure 4.11: Bending moment diagram (kN-m) $\lambda = 0.126$ .....	88
Figure 4.12: Load factor $\lambda = 0.128$ .....	89
Figure 4.13: Bending moment diagram (kN-m) $\lambda = 0.128$ .....	89
Figure 4.14: Load factor $\lambda = 0.266$ .....	89
Figure 4.15: Bending moment diagram (kN-m) $\lambda = 0.266$ .....	90
Figure 4.16: Load factor $\lambda = 0.984$ .....	90
Figure 4.17: Bending moment diagram (kN-m) $\lambda = 0.984$ .....	90
Figure 4.18: Bending moment diagram (kN-m) $\lambda = 1.00$ .....	91
Figure 4.19: Load factor $\lambda = 1.12$ .....	91
Figure 4.20: Bending moment diagram (kN-m) $\lambda = 1.12$ .....	91
Figure 4.21: Load factor $\lambda = 1.25$ .....	92
Figure 4.22: Bending moment diagram (kN-m) $\lambda = 1.25$ .....	92
Figure 4.23: Beam post-elastic shear force-shear deformation response.....	93
Figure 4.24: Column post-elastic shear force-shear deformation response.....	94
Figure 4.25: Load factor $\lambda = 0.716$ .....	94



Figure 4.26: Shear diagram $\lambda = 0.716$ .....	95
Figure 4.27: Shear diagram $\lambda = 1.0$ .....	95
Figure 4.28: Load factor $\lambda = 1.10$ .....	95
Figure 4.29: Shear diagram $\lambda = 1.10$ .....	96
Figure 4.30: Load factor $\lambda = 1.25$ .....	96
Figure 4.31: Shear diagram $\lambda = 1.25$ .....	96
Figure 4.32: Column post-elastic compression-axial deformation graph .....	97
Figure 4.33: Load factor $\lambda = 1.0$ .....	97
Figure 4.34: Load factor $\lambda = 12.35$ .....	97
Figure 4.35: Load factor $\lambda = 30.6$ .....	98
Figure 4.36: Frame geometry and loading .....	98
Figure 4.37: Node and member numbering .....	99
Figure 4.38: Beam cross-section .....	99
Figure 4.39: Column cross-section .....	99
Figure 4.40: Load factor $\lambda = 1.0$ .....	100
Figure 4.41: Bending moment diagram (kN-m) $\lambda = 1.0$ .....	100
Figure 4.42: Load factor $\lambda = 1.51$ .....	101
Figure 4.43: Bending moment diagram (kN-m) $\lambda = 1.51$ .....	101
Figure 4.44: First member-end failure $\lambda = 1.51$ .....	102
Figure 4.45: Bending moment diagram from elastic unloading (kN-m) .....	102
Figure 4.46: After elastic unloading .....	103
Figure 4.47: Bending moment diagram from after elastic unloading (kN-m) .....	103
Figure 4.48: Load factor $\lambda = 1.0$ .....	104
Figure 4.49: Shear diagram (kN) $\lambda = 1.0$ .....	104
Figure 4.50: Load factor $\lambda = 1.12$ .....	105
Figure 4.51: Shear diagram (kN) $\lambda = 1.12$ .....	105
Figure 4.52: First member-end failure .....	106
Figure 4.53: Shear diagram from elastic unloading (kN) .....	106
Figure 4.54: After elastic unloading .....	107
Figure 4.55: Shear diagram after elastic unloading (kN) .....	107
Figure 4.56: Load factor $\lambda = 1.0$ (kN) .....	108

Figure 4.57: Load factor $\lambda = 7.92$ (kN) .....	108
Figure 4.58: After first elastic unloading.....	109
Figure 4.59: After second elastic unloading .....	109
Figure 4.60: Geometry and loading with initial damage .....	110
Figure 4.61: Normal and reverse bending post-elastic moment-rotation response.....	111
Figure 4.62: Load factor $\lambda = 0.22$ .....	111
Figure 4.63: Bending moment diagram(kN-m) $\lambda = 0.22$ .....	112
Figure 4.64: First unloading nodal loads .....	112
Figure 4.65: Bending moment diagram from first unloading (kN-m) .....	113
Figure 4.66: After first unloading.....	113
Figure 4.67: Bending moment diagram for after first unloading (kN-m).....	114
Figure 4.68: Reloading loads.....	114
Figure 4.69: Load factor $\lambda = 0.55$ .....	115
Figure 4.70: Bending moment diagram (kN-m) $\lambda = 0.55$ .....	115
Figure 4.71: Second unloading nodal loads.....	116
Figure 4.72: Bending moment diagram for second unloading (kN-m).....	116
Figure 4.73: After second elastic-unloading.....	117
Figure 4.74: Bending moment diagram for after second unloading (kN-m) .....	117
Figure 4.75: Remaining structure .....	118

## List of Tables

Table 2.1: Degradation factors and curvature integration length.....	41
--	----

# Chapter 1

## Introduction

The purpose of this study is to analyze reinforced concrete frames subjected to abnormal loads which can potentially lead to progressive collapse. This is accomplished by developing a nonlinear computer analysis program. The analysis and design for progressive collapse is explicitly accounted for in many standards including Unified Facilities Criteria 4-023-03 "Design of Buildings to Resist Progressive Collapse" (DoD, 2005) and the United States General Services Administration "Progressive Collapse Analysis and Design Guidelines for New Federal Office Buildings and Major Modernization Projects" (GSA, 2003). England was one of the first nations to account for progressive collapse in the design of structures after the Ronan Point apartment building in Canning Town, England suffered a progressive collapse in 1968. A gas explosion blew out two exterior walls of a corner apartment at an upper floor triggering the progressive collapse (Figure 1.1) (CAC, 1995). The building was constructed with precast walls and floors.

The Cement Association of Canada (CAC) defines progressive collapse as when a localized damage or failure of a structural member, which may be initiated by an abnormal loading event, leads to collapse of a disproportionately large part of the structure. The type of abnormal load can range from impact loads, explosions or construction errors during erection of a building. There are many examples of structures that have been subjected to abnormal loads. In 1987 a new grandstand was being erected at Husky Stadium at the University of Washington. A series of guylines temporarily supporting the structure during construction were removed too early resulting in complete collapse of the grandstand (Figure 1.2). Another example of a structure subjected to abnormal load is the Alfred P. Murrah building in Oklahoma City. In 1995 a deliberately set explosion destroyed one third of the building and killed 168 people, of which, 160 were in the building at the time (Figure 1.3). Arguably the most famous incident of a structure being subjected to abnormal load is the World Trade Centers of New York City. In 2001 they were subject to impact loads and extreme fires as a consequence of airplanes being deliberately flown into them.

Similar to the GSA (2003) standard, however, this study uses a threat independent approach whereby the abnormal loading event is not explicitly known or quantified. This is because abnormal loads vary greatly in type and intensity. In the analysis program presented in this study, the intact structures are instead loaded beyond the normal range of applied loads, i.e., when the reinforcement yields, to show that they are subjected to some abnormal loading event. Alternatively, a critical

member of the structure is removed and the modified structure is analyzed by the program. The critical member is assumed to have been damaged by an abnormal loading event.

Progressive collapse is rare because it requires both an abnormal load to create a localized damage and also a structure that lacks sufficient redundancy to resist the progression of damage (DoD, 2005). However, abnormal loads and progressive collapse do exist and thus efforts should be made to minimize their impact on structures. In order to do that, however, a structure's response to an abnormal load must be understood. Such is the focus of this study.

## **1.1 Scope of Study**

This study presents a computer analysis technique for reinforced concrete frames subjected to abnormal loads. The method of analysis involves discretizing a two-dimensional frame into a series of beam-column elements, whose end-sections model the nonlinear behaviour of the element. The degree of post-elastic stiffness degradation is tracked through the use of stiffness degradation factors. The load is incrementally applied to the structure until the full design load is reached, or a failure state occurs before that point.

Chapter 2 presents the analysis concepts and includes:

- The analysis model and member properties used to analyze a reinforced concrete frame.
- The concept of the post-elastic range of response.
- The public domain program used to obtain force-strain and moment-curvature data for any type of reinforced concrete section.
- The method for modifying the public domain program's force-strain and moment-curvature data into the required force-deformation and moment-rotation data.
- The definition of the post-elastic stiffness of a member-section and the force-deformation responses modeled in this study.
- The definition and derivation of the stiffness degradation factors and how they apply to this study.
- The derivation of the element stiffness matrix.

Chapter 3 presents the four stages of the analysis program and includes:

- Stage zero elastic analysis which is performed on the structure up to the point that the structure no longer exhibits linear-elastic behaviour.
- Stage one inelastic incremental analysis where the degree of post-elastic behaviour is tracked.
- Stage two elastic-unloading analysis which is performed only after a member-section exceeds its ultimate load resistance and fails.
- Stage three reloading inelastic analysis which also tracks the degree of post-elastic behaviour of the structure, but also applies amplified debris loads on the structure caused by falling members that have disengaged from the main structure.

Chapter 4 presents a series of example problems used to illustrate the computer analysis program and includes:

- A simple portal frame used to illustrate the features of the analysis procedure and various outputs from the program.
- A 2 bay-2 storey more redundant frame.
- The same 2 bay-2 storey frame, but with some initial damage caused by some abnormal loading event. This example serves to illustrate the program's capability to conduct a progressive collapse analysis.

Chapter 5 presents a summary of the work discussed in this study, some specific conclusions regarding the analysis of reinforced concrete frames and finally, areas of future work.

## **1.2 Assumptions and Idealizations**

The following assumptions and idealizations are made in this study:

- Plane sections remain plane such that the strain distribution across a member-section is linear.
- There are no out-of-plane actions, i.e., the structure is laterally braced.
- A member is in the elastic range when the modulus of elasticity is constant and its force-deformation response is linear.

- Beyond the elastic range, the member is assumed to be fully or partially plastic.
- A member's nonlinear behaviour is modeled by a series of springs and is confined to the end-sections of the member.
- The unloading phenomenon whereby a member-section experiences increasing deformation through decreasing load after the member-section reaches its ultimate load resistance is ignored. This study assumes that once a member-section reaches its ultimate load resistance it has also reached the end of its load history.
- The post-elastic force-deformation or moment-rotation response of a member-section is modeled as either trilinear or bilinear, depending on the case being studied.
- When determining the degree of post-elastic stiffness degradation, only single stress states are looked at, i.e., moment-shear or moment-axial force interaction is ignored.



**Figure 1.1: Ronan Point Apartment Building 1968 (© Daily Telegraph, 1968)**

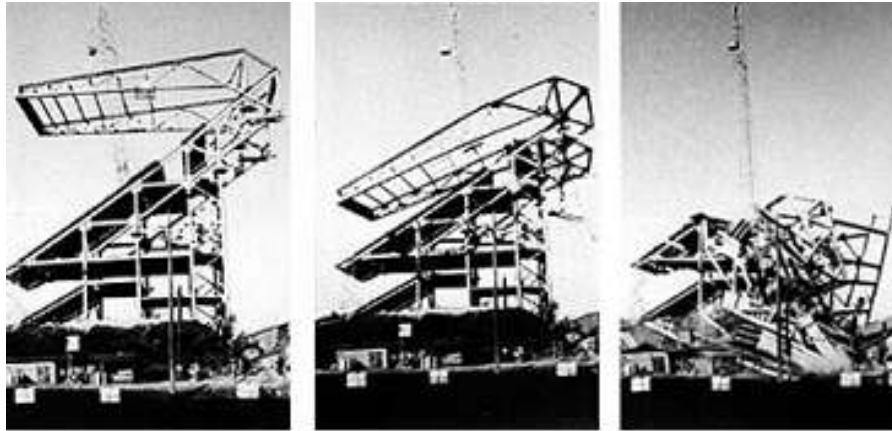


**Figure 1.2: Husky Stadium 1987 (© John Stamets, 1987)**



**Figure 1.3: Alfred P. Murrah Building, Oklahoma 1995 (Hinman, 1997)**



## Chapter 2

### Analysis Concept

The following presents the concepts and theory behind the analysis procedure. Section 2.1 presents the analysis model and member properties used to analyze a reinforced concrete frame. Section 2.2 explains the concept of the post-elastic range of response of a member-section. Section 2.3 explores a public domain program used to obtain information about the sectional behaviour of reinforced concrete considered in this study. It also refers to the theory on which the public domain program is based. Section 2.4 shows how member-section deformations and rotations are approximated from given strains and curvatures. Section 2.5 defines the post-elastic stiffness of a member-end section and presents the force-deformation responses modeled in this study. Section 2.6 derives the stiffness degradation factors and explains their purpose in the analysis and how initial values are selected. Finally, Section 2.7 presents the member stiffness matrix and how it is derived.

#### 2.1 Beam-Column Model for Analysis

The method of analysis in this study involves discretizing a two dimensional reinforced concrete frame into an assemblage of the beam-column elements shown in Figure 2.1 . The element has length  $L$ , modulus of elasticity  $E$ , moment of inertia  $I$ , cross-sectional area  $A$  and shear modulus  $G$ . All properties are constant. In the presented study they are all based on the gross concrete section. The element has six local member-end forces  $f_i$  ( $i = 1$  to  $6$ ) consisting of axial forces, shear forces and bending moments. The element also has six local member-end deformations  $d_i$  ( $i = 1$  to  $6$ ) consisting of axial deformations, shear deformations and rotations. The element without springs is linear-elastic; however, its end-sections model nonlinear behaviour of a total member by a series of springs, which represent the post-elastic stiffness of the end-sections. The springs in the horizontal direction, designated by  $N_i$  ( $i = 1$  to  $2$ ), represent post-elastic axial stiffness; the springs in the vertical direction, designated by  $T_i$  ( $i = 1$  to  $2$ ), represent post-elastic shear stiffness, while the rotational springs, designated by  $R_i$  ( $i = 1$  to  $2$ ), represent post-elastic bending stiffness. Furthermore, the bending, shearing and axial stiffness degradation factors,  $r_i$ ,  $t_i$ ,  $n_i$  ( $i = 1$  to  $2$ ), respectively, are included in the model. They modify the elastic stiffness coefficients of the element stiffness matrix to account for the post-elastic behaviour of the end-sections of the member.

There are three issues then that should be discussed further to fully develop the analysis model: 1) the post-elastic range of response must be defined; 2) the calculation of the post-elastic sectional stiffness, modeled here by the end springs, must be given; 3) the purpose and derivation of the stiffness degradation factors must be illustrated.

## 2.2 Post-Elastic Range of Response

Reinforced concrete members show a strong material nonlinearity when subjected to loads. This is due to the nonlinear response in both tension and compression due to cracking, yielding of reinforcement and nonlinear concrete compressive behaviour. When a member exhibits a tension type of response (through flexure, shear or axial loads) it is assumed that the response is linear until cracking. After that, if the load is increased, the response becomes nonlinear. When a member exhibits a compression type of response, it is assumed that the linear elastic range is up to 40% of the maximum load ( $0.4f_c$  is the limit of elasticity). A reinforced concrete member's nonlinear response to loads, when applied to structural analysis, is one of the problems addressed in this study.

It is assumed that a reinforced concrete member is in the elastic range when the modulus of elasticity is constant and the force-deformation response is linear. Beyond that, the member is assumed to be fully or partially plastic and in the post-elastic range. Figure 2.2 shows a typical moment-rotation response for an under-reinforced concrete section.  $M_{cr}$  represents the moment at which initial flexural cracking in the tension zone of the member occurs.  $M_y$  represents the moment at which the tensile reinforcement begins to yield, while  $M_{ult}$  represents the full moment capacity of the member and the point at which the concrete crushes in the compression zone. The elastic domain of the response is small due to the member's low cracking moment resistance. Up until the point of flexural cracking, denoted by  $M_{cr}$ , the moment-rotation response is elastic. At this point the concrete begins to crack and there is a change in the sectional properties of the member, indicated in the figure by the change in slope of the moment-rotation response at  $M_{cr}$ . Beyond this point and for the remainder of the load history the member section is in the post-elastic range.

For members in compression, it is typically said that linear-elastic behaviour ends and nonlinear behaviour begins when the member is subjected to a compressive stress of approximately  $0.4f_c$  (Pillai, Kirk & Erki, 1999). A constant value of Young's modulus for concrete in compression is obtained by the secant method, whereby a line is drawn through the origin of the stress-strain curve and a point that is 40 percent of the compressive strength. The slope of this line represents the

average value of the modulus throughout the normal range of applied loads (Pillai, Kirk & Erki, 1999). When a member is subjected to loads beyond this range, the effective modulus continuously changes making the response nonlinear. Figure 2.3 shows a typical force-deformation response for a member section subjected to axial compression. The member-section is in the elastic range up until 40% of the ultimate compressive force is reached. Beyond this point nonlinear behaviour begins and for the remainder of the load history the section is said to be in the post-elastic range.

### **2.3 Sectional Analysis of Reinforced Concrete Members**

The post-elastic sectional stiffness of the member-sections is modeled by a series of end springs. The bending, shearing and axial elastic member stiffness is defined as the force required to produce a unit deformation (Timoshenko & Gere, 1972). Elastic axial member stiffness for example, has a value of  $AE/L$ , which is obtained by calculating the slope of the force-deformation response of a member in the elastic range. Similarly, the post-elastic bending, shearing or axial stiffness of a member-section is obtained by calculating the slope of the post-elastic force-deformation response. The post-elastic force-deformation response of a member-section then, is first needed in order to calculate the post-elastic stiffness. In order to obtain the post-elastic force-deformation response of a member-section, the post-elastic force-strain response is first obtained through sectional analysis.

For this study, the sectional behaviour of reinforced concrete members is obtained from a public domain analysis program titled *Response-2000* Version 1.0.5, hereafter referred to as *Response*. *Response* is based on the Modified Compression Field Theory (MCFT). It was created by Evan C. Bentz of the University of Toronto as part of his PhD thesis work (Bentz, 2000), under the supervision of Professor M.P. Collins. The program is available free of charge from the World Wide Web at: <http://www.ecf.utoronto.ca/~bentz/r2k.htm>. The program can be used to determine the sectional force-strain relationship of a variety of reinforced concrete members subjected to moment, shear force, axial force, or a combination thereof. The user may analyze any type of cross section by inputting parameters such as concrete compressive strength, type of reinforcement, type of prestressing steel and section geometry. The user may also select predefined AASHTO, CPCI, PCI or WSDOT standard sections. Pertinent section information is then summarized for the user as shown in Figure 2.4, and includes such data as cross sectional area and moment of inertia.

As mentioned, the program is based on the MCFT to analyze sections subjected to load using average stresses and average strains in the calculations (Collins & Mitchell, 1991). Due to the fact

that average stresses are used, things such as dowel action force, shear stresses on cracks, etc., need not be explicitly calculated, thus simplifying the procedure (Bentz, 2000). The program uses an incremental layered approach whereby the sectional forces are solved for by assuming a global strain state (comprised of the longitudinal strain, the curvature, and the average shear strain) for the cross section (Bentz, 2000). *Response* was tested and compared to a database of 534 beams, to find an average experimental-over-predicted shear strength ratio equal to 1.05 with a coefficient of variation of 12.0% (Bentz, 2000). The reader is referred to Bentz (2000) for more detailed information regarding the theoretical models used in *Response*, the internal workings of the program and the experimental data the program is compared to. What follows now is an example of the sectional force-strain behaviour given by *Response* that is used in this study.

### **2.3.1 Sectional Analysis in Bending**

In order for *Response* to obtain a moment-curvature plot for a reinforced concrete section subjected to bending moment only, the ratio of bending moment to shear force to axial force is set to 1:0:0 in the program. Using the reinforced concrete section in Figure 2.4 as an example, the sectional analysis is run and the results are output as shown in Figure 2.5.

Two control plots are shown along the left-hand side of the figure to aid the user in determining specific information about the cross-section at any particular load level. The moment-curvature plot (bottommost plot on the left-hand side) is of most importance to this study. The moment-curvature plot is used to obtain the moment-rotation plot that is then used to obtain the post-elastic bending stiffness of a member-section at a particular load level (discussed in detail in Section 2.5).

When the user selects a moment level on the control plot, nine additional pieces of information for that cross section at that moment level are shown in the plots on the right. Information such as approximate crack width, longitudinal concrete stress, and longitudinal reinforcement stress are shown. Of particular importance to this study (which will become evident in Section 2.5) is the moment and curvature magnitudes at which flexural cracking initiates in the section, the reinforcement yields, and the section reaches its ultimate capacity.

The moment-curvature control plot produced by *Response* is shown by itself in Figure 2.6, in which the maximum moment and curvature are shown to have values of 231.1 kN-m and 207.3 rad/km, respectively. By moving the cross-hairs along the control plot, one can obtain information about the cross section at the load level indicated, from the nine graphs of Figure 2.5. The moment

and curvature magnitude at which initial flexural cracking occurs in the section is now determined as an example.

For this particular cross section, the concrete tensile strength has a value of 1.87 MPa. If the cross-hairs, starting at the origin, move along the control plot, the longitudinal concrete stress - shown in one of the nine graphs of Figure 2.5- changes for each load level of the control plot. At a moment level of 16 kN-m the longitudinal concrete stress at the bottom fibers of the section has a value of 1.8 MPa, while at a moment level of 20.3 kN-m the longitudinal concrete stress has a value of 1.9 MPa, which exceeds the tensile strength of the concrete. Furthermore, at 16 kN-m the crack diagram shows a completely uncracked section, while at 20.3 kN-m the crack diagram shows that a small flexural crack has developed. From this information, one may infer that at a moment level of 16 kN-m the section is on the verge of cracking. The curvature at the 16 kN-m moment level may then be obtained from the moment-curvature control plot. The point of initial cracking due to shear or axial force is found in a similar way.

### **2.3.2 Sectional Analysis in Shear**

In order for *Response* to obtain a force-strain plot for a reinforced concrete section subjected to shear only, it is first noted that shear cannot exist alone without some degree of bending moment and, as such, the ratio of shear force to bending moment to axial force is set to 1:0.01:0 in the program.

Using the same reinforced concrete section as in Figure 2.4, the analysis is run and the results are output as shown in Figure 2.7. The two control plots at the left hand side are shear force-shear strain (top plot) and shear force-axial strain (bottom plot). The shear force-shear strain plot is of most importance to this study. This plot is used to obtain the post-elastic force-deformation response of the member-section which is then used to obtain the post-elastic shear stiffness of the cross-section at a particular load level (discussed in detail in Section 2.5).

When the user selects a shear level on the control plot, nine additional pieces of information for the cross section at that shear level are shown on the plots to the right. Information such as longitudinal reinforcement stress, transverse strain, and stirrup stress are shown. The magnitude of the shear force and corresponding shear strain at the point of stirrup yielding is required for this study (which will become evident in Section 2.5) and is now presented as an example.

The shear force-shear strain control plot produced by *Response* is shown by itself in Figure 2.8. The maximum shear resistance and shear strain are indicated to have magnitudes of 265.3 kN and

18.0 mm/m, respectively. Again, by moving the cross-hairs along the control plot, one can obtain information about the cross section at any load level from the nine graphs of Figure 2.7. The reinforcement properties for this cross section are consistent with CSA G30.12 steel with a yield strength of 400 MPa. To determine the point at which the reinforcement yields, the cross hairs are moved along the control plot of Figure 2.8 and the values in the nine plots of Figure 2.7 are observed, particularly the stirrup stress level. Once the stirrup stress level reaches 400 MPa the reinforcement has yielded. This is also indicated on the dynamic cross section diagram whereby the stirrups change colour at their middle to indicate that initial yielding is occurring. One may then note the shear force from the control plot as well as the corresponding shear strain. In this case, the shear force and shear strain have magnitudes of 223 kN and 2.13 mm/m, respectively. The point at which the longitudinal reinforcement yields in flexure or due to tensile axial load is found in an analogous way.

### **2.3.3 Sectional Analysis in Compression**

In order for *Response* to obtain a force-strain plot for a reinforced concrete section subjected to compression only, the ratio of axial force to bending moment to shear force is set to -1:0:0 in the program (the negative sign indicates a compressive force). Using the same reinforced concrete cross section as in Figure 2.4, the analysis is run and the results output as shown in Figure 2.9. There is only 1 control plot in this case (albeit repeated) along the left side of the figure which shows compressive force-axial strain data. This data is used to obtain the post-elastic force-deformation response of the member section in order to obtain the post-elastic axial stiffness of the section at some load level. Longitudinal strain, longitudinal reinforcement stress, longitudinal concrete stress, and other data are shown in the nine additional plots to the right, which change depending on the load level selected in the control plot. A final piece of data important in this study is the force and deformation at which the section reaches its ultimate capacity. This is now presented as an example.

The compressive force-axial strain control plot produced by *Response* is shown by itself in Figure 2.10. The maximum compressive force and axial strain are indicated to have values of 5780.3 kN and 10.9 mm/m, respectively. The nine plots in Figure 2.9 show information about the cross section at the load level selected from the control plot. The compressive stress of the concrete is 35 MPa. As the cross hairs move along the control plot and the load level increases, the longitudinal concrete stress also increases. Once it reaches a stress level of 35 MPa, the section has reached its ultimate capacity and fails due to crushing of concrete. Furthermore, the crack diagram changes colour once crushing occurs. The compressive force and corresponding axial strain at the ultimate capacity can be

recorded. In this case they have magnitudes of 5780.3 kN and 1.96 mm/m, respectively. In the case of a section in compression, it is not necessary to check the concrete stress level or the crack diagram to determine the section's ultimate capacity. One can simply record the force and deformation magnitudes at the peak point of the graph shown in the control plot. In the other loading cases however, the ultimate capacity is determined by observing the information presented in the nine plots and comparing those values to the material properties of the section. Figure 2.10 also shows a distinctive unloading, whereby the compressive force decreases with an increase in strain. In this study, the unloading portion of the curve is ignored such that there is no further increase in strain beyond the ultimate compressive load.

## 2.4 Approximating Member-End Deformations from Strains

### Flexure

The output data from *Response* for sectional analysis in bending includes a moment-curvature graph; however, a moment-rotation graph is needed to calculate the post-elastic bending stiffness. The curvature values from *Response* are the maximum curvatures for the end-section of a beam. The curvature, however, changes along the length of a member. Curvature is defined as the change in slope per unit length along the member. Integrating the curvature  $\phi$  over a length  $a$  produces a rotation  $\theta$ , i.e.,

$$\theta = \int_0^a \phi(x) dx \quad (2.1)$$

It remains to determine a suitable integration length  $a$ , as discussed in the following.

It is assumed that for a beam member under a uniformly distributed load that the curvature changes in the same manner as the moment (Figure 2.11). The maximum curvature  $\phi_{\max}$  exists at the end of the beam and there exists a point of zero curvature at  $0.21L$ . Furthermore, we derive the average curvature for the parabolic distribution from the end of the beam to  $0.21L$  as,

$$\phi_{\text{avg}} = \frac{\int_0^{0.21L} \phi(x) dx}{0.21L} = 0.46\phi_{\max} \quad (2.2)$$

and where from Eqs. (2.1) and (2.2) we derive the approximate rotation for the member-end section as,

$$\theta = \int_0^{0.21L} \phi(x) dx = 0.46\phi_{\max} \times 0.21L = 0.09L\phi_{\max} \quad (2.3)$$

We thus obtain length  $0.09L$ , which we can use to multiply the maximum curvatures ( $\phi_{\max}$ ) for the member-end section provided by *Response*, in order to obtain an approximate rotation for the beam member-end section.

### Shear

The output data from *Response* for sectional analysis in shear includes a shear force-shear strain graph; however, a shear force-shear deformation graph is needed in order to calculate the post-elastic shear stiffness. Similar to the preceding method, the shear strain  $\gamma_s$  may be integrated over some length  $a$  in order to obtain the shear deformation,

$$\gamma_d = \int_0^a \gamma_s(x) dx \quad (2.4)$$

It remains to determine a suitable integration length  $a$ , as discussed in the following.

It is assumed that for a beam member under a uniformly distributed load that the shear strain changes in the same manner as the shear force (Figure 2.12). The maximum shear strain  $\gamma_{s,\max}$  exists at the end of the beam and there exists a point of zero shear strain at  $0.5L$ . Furthermore, we derive the average shear strain for the linear distribution from the end of the beam to  $0.5L$  as,

$$\gamma_{s,avg} = \frac{\int_0^{0.5L} \gamma_s(x) dx}{0.5L} = 0.5\gamma_{s,\max} \quad (2.5)$$

and where from Eqs. (2.4) and (2.5) we derive the approximate shear deformation for the member-end sections as,

$$\gamma_d = \int_0^{0.5L} \gamma_s(x) dx = 0.5\gamma_{s,\max} \times 0.5L = 0.25L\gamma_{s,\max} \quad (2.6)$$

We thus obtain length  $0.25L$ , which we can use to multiply the maximum shear strains ( $\gamma_{s,\max}$ ) for the member-end section provided by *Response*, in order to obtain an approximate shear deformation for a beam member-end section.



Columns have a constant shear force over their length (assuming no lateral loads), and thus, their entire length may be used as the integration length  $a$ .

### Axial Loads

The output data from *Response* for sectional analysis under axial load includes an axial force-axial strain graph; however, an axial force-axial deformation graph is needed in order to calculate the post-elastic axial stiffness. Since in most cases the axial force is constant for the entire member length, the axial strain is simply multiplied by the member length in order to obtain the axial deformation.

With the force-strain and moment-curvature data from *Response* and an approximation of the deformations and rotations associated with those strains and curvatures calculated, the force-deformation response of a member section subjected to bending moment, shear force or axial force can be obtained. To attain the post-elastic force-deformation response of a member section, the elastic deformations are simply subtracted from the total deformations.

## **2.5 Post-Elastic Stiffness and Force-Deformation Response**

Now that the sectional analysis and procedure for obtaining the post-elastic force-deformation response has been illustrated, the post-elastic sectional stiffness can be determined. As previously mentioned, the post-elastic stiffness is obtained by calculating the slope of the post-elastic force-deformation response at any particular point. The post-elastic stiffness is needed in order to calculate the stiffness degradation factors (Section 2.6) used later in the analysis procedure.

### **2.5.1 General Force-Deformation Response**

There are six possible force-deformation responses for reinforced concrete member-sections and they are dependent on the mode of loading applied and the reinforcement. The six different responses are: 1) under-reinforced for flexure 2) over-reinforced for flexure 3) shear with transverse reinforcement 4) shear without transverse reinforcement 5) tension axial force and 6) compression axial force. In this study all of these are approximated as either tri or bi-linear force-deformation responses as discussed in the following. Furthermore, it is assumed that a reinforced concrete member has an elastic response until cracking for members in tension, flexure and shear, and that for members in compression, it is assumed that the force-deformation response is elastic until 40% of the ultimate force is reached.

There exists a tri-linear general form of the total and post-elastic force-deformation response for bending of an under-reinforced section, shear for a section with transverse reinforcement and a section subjected to axial tension. All of these cases involve members experiencing cracking.

Figure 2.13 shows a general form of the tri-linear post-elastic force-deformation response.  $F_{cr} = M_{cr}, V_{cr},$  or  $P_{cr}$  is the bending, shearing, or axial tensile force at the point of cracking of concrete; i.e., flexural cracking in bending, diagonal cracking in shear and transverse cracking in tension.  $F_y = M_y, V_y,$  or  $P_y$  is the bending, shearing or axial tensile force at the point of yielding of the reinforcement; i.e., longitudinal reinforcement for bending and axial tension and transverse reinforcement for shear.  $F_{ult} = M_{ult}$  and  $V_{ult}$  is the bending and shearing force at the point of crushing of concrete, while  $F_{ult} = P_{ult}$  is the point at which the longitudinal reinforcement ruptures under axial tension. Correspondingly,  $D_y = \theta_y, \gamma_y, \delta_y$  and  $D_{ult} = \theta_{ult}, \gamma_{ult}, \delta_{ult}$  are the values of bending, shearing and axial tension post-elastic deformation at yielding of reinforcement and crushing of concrete (or rupture of longitudinal steel), respectively. The post-elastic stiffness is given by the slope of particular portions of the response, i.e.,  $dF/dD = R, T,$  or  $N_t$  for bending, shearing, and axial tension, respectively.

There exists two different values of post-elastic stiffness that remain constant through a particular range of loading. The values of the post-elastic stiffness for lines AB and BC are given by,

$$R, T \text{ or } N_t(AB) = \frac{F_y - F_{cr}}{D_y} \quad (2.7)$$

$$R, T \text{ or } N_t(BC) = \frac{F_{ult} - F_y}{D_{ult} - D_y} \quad (2.8)$$

Notice that at zero post-elastic deformation the graph is vertical up to the point  $F_{cr}$ , meaning that the post-elastic stiffness is infinite and the member-section is fully elastic. Just beyond this point, the member section begins to crack and there is a reduction in post-elastic stiffness and the member section is now partially plastic. The magnitude of the post-elastic stiffness is now a finite value between infinity (fully elastic) and zero. As the load increases, the post-elastic stiffness remains constant as the post-elastic deformation approaches  $D_y$ . At  $D_y$ , the reinforcement begins to yield and there is another reduction in post-elastic stiffness. The magnitude of the post-elastic stiffness decreases while the magnitude of the post-elastic degradation of the member-end increases. As the load increases, the post-elastic stiffness remains constant as the post-elastic deformation approaches  $D_{ult}$ . At  $D_{ult}$ , when the member-end has reached its ultimate capacity, its post-elastic stiffness

decreases to zero and the post-elastic stiffness is said to be fully degraded thereby initializing a section failure. Once a reinforced concrete section reaches its ultimate capacity due to the rupturing of reinforcement or crushing of concrete, the member section is damaged to the point that it can no longer carry load.

Figure 2.14 shows the *Response* data for an under-reinforced beam that has a 500x350mm cross section with a compressive strength and reinforcement ratio of 35 MPa and 1.31%, respectively. The data have been modified so that only plastic curvature is included. A polynomial curve was initially fit to the data to obtain a continuous function that could be used to obtain the slope of the graph by taking its 1st derivative; however, a polynomial curve did not fit well to the point at which the reinforcement begins to yield (shown by an arrow on the graph). Consequently, linear functions as just discussed were selected to represent the data: one from the beginning of the load history to the point at which post-elastic behaviour begin; one for the range of loading from initial cracking to initial yielding of the reinforcement; and another for the range of loading from initial yielding to the ultimate capacity of the member-section.

There also exists a bi-linear general form of the post-elastic force-deformation response for over-reinforced sections in flexure and sections subjected to axial compression (Figure 2.15). As previously mentioned, for sections subjected to axial compression, elastic behaviour governs until 40% of the ultimate compressive force has been reached at which point the section enters the post-elastic range. The post-elastic stiffness for line AB is given by,

$$N_c = \frac{F_{ult} - 0.4F_{ult}}{D_{ult}} \quad (2.9)$$

where  $F_{ult}$  is the ultimate compressive force of the concrete,  $0.4F_{ult}$  is the force at which post-elastic behaviour begins, and  $D_{ult}$  is the ultimate deformation at failure. At zero post-elastic deformation the slope of the graph is vertical and the member-section is fully elastic. At  $0.4F_{ult}$ , however, there is a reduction in stiffness and the member is then in the post-elastic range with a stiffness value between infinity and zero. The post-elastic stiffness remains constant until failure of the section.

## 2.5.2 Examples of Post-Elastic Force-Deformation Response and Post-Elastic Stiffness

The post-elastic force-deformation response for the six cases discussed earlier that can be represented by a tri-linear or bi-linear model are now shown. The post-elastic responses were obtained by converting the load-strain and moment-curvature data from *Response* to load-deformation and moment-rotation data and then subtracting the elastic deformations from the total deformations.

The following presents the six different post-elastic force-deformation responses possible. A 7500 mm long member with a 500x350 mm cross section and a compressive strength of 35 MPa is used for flexure and shear. For the under-reinforced case in flexure, the section has a reinforcement ratio of 1.04% whereas for the over-reinforced case the section has a reinforcement ratio of 3.06%. For shear, the under-reinforced section is used and has 10M closed stirrups spaced at 300 mm on centre for the case with transverse reinforcement. The same section is used albeit with the transverse reinforcement removed for the case of shear without transverse reinforcement. For axial compression and axial tension, a 3600 mm long column member having a 350x350 mm section with a compressive strength of 35 MPa is used. The section has a 2.1% reinforcement ratio. Note that for all cases the reinforcement properties are those for CSA G30.12 400 MPa reinforcing steel.

### 2.5.2.1 Post-Elastic Bending Stiffness

Figure 2.16 shows the post-elastic moment-rotation response for the under-reinforced cross section. The lines representing the tri-linear model are also shown. The section is subjected to bending moment only. Notice that there is no plastic deformation until the cracking moment  $M_{cr}$  is reached. Only after  $M_{cr}$  is reached does the section enter the post-elastic range. It is at this point that there is a reduction in post-elastic bending stiffness; i.e., from an infinite value when the section is fully elastic to the value given by Eq. (2.7), i.e.,

$$R_A = \frac{M_{yld} - M_{cr}}{\theta_{yld}} = \frac{308kN \cdot m - 30kN \cdot m}{0.0049rad} = 56735kN \cdot m$$

which is constant throughout the range of loading from  $M_{cr}$  to  $M_{yld}$ . Once the moment level reaches the yield moment  $M_{yld} = 308$  kN-m, there is another reduction in post-elastic stiffness to the value given by Eq. (2.8), i.e.,

$$R_B = \frac{M_{ult} - M_{yld}}{\theta_{ult} - \theta_{yld}} = \frac{347kN \cdot m - 308kN \cdot m}{0.0310rad - 0.0049rad} = 1494kN \cdot m$$

which is constant throughout the range of loading from  $M_{yld}$  to  $M_{ult}$ . The effect of the reinforcement yielding is apparent in the fact that the post-yielding stiffness  $R_B$  is only 2.6% of the post-cracking stiffness  $R_A$ . Once the moment level goes beyond  $M_{ult} = 347$  kN-m, the stiffness is said to be fully degraded and the section then has zero post-elastic bending stiffness.

Figure 2.17 shows the post-elastic moment-rotation response for the over-reinforced section. The lines representing the bi-linear model of the response are also shown. The section is subjected to bending moment only. Post-elastic behaviour begins once the bending moment reaches 40% of the ultimate moment resistance  $M_{ult} = 640$  kN-m. Once the section enters the post-elastic range the post-elastic bending stiffness is given by Eq. (2.9), i.e.,

$$R_A = \frac{M_{ult} - 0.4M_{ult}}{\theta_{ult}} = \frac{640kN \cdot m - 0.4(640kN \cdot m)}{0.0059rad} = 65084kN \cdot m$$

which is constant throughout the range of loading from  $0.4M_{ult}$  to  $M_{ult}$ .

### 2.5.2.2 Post-Elastic Shearing Stiffness

Figure 2.18 shows the post-elastic shear-shear deformation response of the cross section with transverse reinforcement. The lines representing the tri-linear model are also shown. The section is subjected to shear force only. The section does not enter the post-elastic range until the magnitude of the shear force has reached the cracking shear resistance  $V_{cr} = 174$  kN. The cracking discussed here is diagonal shear cracking. When the magnitude of the applied shear force is just beyond the cracking shear resistance, the section enters the post-elastic range and there is a reduction in post-elastic shear stiffness to the value given by Eq. (2.7), i.e.,

$$T_A = \frac{V_{yld} - V_{cr}}{\gamma_{yld}} = \frac{219kN - 174kN}{4.41mm} = 10.2kN / mm$$

which is constant throughout the range of loading from  $V_{cr}$  to  $V_{yld}$ . Once the magnitude of the shear force reaches the yield shear force  $V_{yld} = 219$  kN there is another reduction in post-elastic shear stiffness to the value given by Eq. (2.8), i.e.,

$$T_B = \frac{V_{ult} - V_{yld}}{\gamma_{ult} - \gamma_{yld}} = \frac{245kN - 219kN}{10.83mm - 4.41mm} = 4.05kN / mm$$

which is constant throughout the range of loading from  $V_{yld}$  to  $V_{ult}$ . Like in the case of bending moment, the effect of the transverse shear reinforcement yielding causes a large reduction in post-elastic shear stiffness whereby the post-yielding stiffness  $T_B$  is only 39% of the post-cracking stiffness  $T_A$ .

Figure 2.19 shows the post-elastic shear force-shear deformation response of the cross section without transverse reinforcement. The lines representing the bi-linear model are also shown. The section is subjected to shear force only. The section does not enter the post-elastic range until the magnitude of the shear force has reached the cracking shear resistance  $V_{cr} = 209$  kN. Once this occurs, the post-elastic shear stiffness reduces to zero. This is shown in the figure by the fact that the response is now represented by a flat line.

### 2.5.2.3 Post-Elastic Axial Tension Stiffness

Figure 2.20 shows the post-elastic axial force-axial deformation response for the cross section. The lines representing the tri-linear model are also shown. The section is subjected to axial tension only. The tri-linear model shown here is of the same form as under-reinforced sections in flexure and shear force for sections with transverse reinforcement. The section does not enter the post-elastic range until the concrete cracks due to an applied tensile force of  $P_{cr} = 277$  kN. Once this occurs there is a reduction in post-elastic axial stiffness to the value given by Eq. (2.7), i.e.,

$$N_{At} = \frac{P_{yld} - P_{cr}}{\delta_{yld}} = \frac{1680kN - 277kN}{6.8mm} = 206kN / mm$$

which is constant throughout the range of loading from  $P_{cr}$  to  $P_{yld}$ . Once the magnitude of the axial force reaches  $P_{yld} = 1680$  kN, there is another reduction in post-elastic axial tension stiffness to the value given by Eq. (2.8), i.e.,

$$N_{Bt} = \frac{P_{ult} - P_{yld}}{\delta_{ult} - \delta_{yld}} = \frac{2520kN - 1680kN}{288mm - 6.8mm} = 3kN / mm$$

which is constant throughout the range of loading from  $P_{yld}$  to  $P_{ult}$ . Again, yielding of the reinforcement causes a reduction in the post-yielding stiffness  $N_{Bt}$  to a value that is 1.5% of the post-cracking stiffness  $N_{At}$ .

#### 2.5.2.4 Post-Elastic Axial Compressive Stiffness

Figure 2.21 shows the post-elastic axial force-axial deformation response for the cross section. The lines representing the bi-linear model of the response are also shown. The section is subjected to axial compression only. The section enters the post-elastic range at 40% of the ultimate compressive force. Once this occurs there is a reduction in post-elastic axial stiffness to the value given by Eq. (2.9), i.e.,

$$N_c = \frac{P_{ult} - 0.4P_{ult}}{\delta_{ult}} = \frac{5780kN - 0.4(5780kN)}{5.29mm} = 656kN / mm$$

which is constant throughout the range of loading from  $0.4P_{ult}$  to  $P_{ult}$ .

Having fully developed the post-elastic force-deformation responses and the post-elastic sectional stiffness, the stiffness degradation factors can now be calculated as presented in the next section.

## 2.6 Stiffness Degradation Factors

Flexural stiffness degradation factors, are defined as the ratio of the rotation of a member-end to the combined rotation of the member-end and the connection due to a unit end-moment (Xu, 1994). In this study, stiffness degradation factors are taken as the ratio of elastic deformation to elastic plus plastic deformation (Xu *et al*, 2005), and are an indication of the extent of post-elastic behaviour of the member-end (Liu, 2007). Furthermore, the stiffness degradation factors are used to modify the elastic stiffness coefficients of the element stiffness matrix to account for post-elastic behaviour. Stiffness degradation factors  $r$ ,  $t$ , and  $n$  for bending, shearing, and axial force, respectively, range in value between unity and zero. What follows is the derivation of the stiffness degradation factors as given by Xu *et al* (2005) and Liu (2007).

### 2.6.1 Bending Stiffness Degradation Factor

Figure 2.22 shows the model used to derive the bending stiffness degradation factor. The member of length  $L$ , and flexural rigidity  $EI$  is pinned at its right end and able to rotate freely at its left end under

moment  $M$ , but unable to undergo shear or axial deformation. The elastic rotational deformation is  $\theta_e = ML/3EI$  and the post-elastic rotational deformation is  $\theta_p = M/R$ . The bending stiffness degradation factor is the ratio of elastic to elastic plus plastic deformation, i.e.,

$$r = \frac{\theta_e}{\theta_e + \theta_p} = \frac{\frac{ML}{3EI}}{\frac{ML}{3EI} + \frac{M}{R}} = \frac{1}{1 + \frac{3EI}{RL}} \quad (2.10)$$

When the post-elastic bending stiffness  $R = \infty$ , meaning that the member section is in the fully elastic range,  $r = 1$ , indicating that there is no post-elastic bending stiffness degradation. When the post-elastic bending stiffness  $R = 0$ , then the bending stiffness degradation factor  $r = 0$ , indicating that there is complete post-elastic bending stiffness degradation. For other values of post-elastic bending stiffness,  $r$  will vary between 1 and 0 to indicate varying degrees of post-elastic bending stiffness degradation.

Now that the bending stiffness degradation factor has been defined, another method is presented to give further credence in selecting 9% of the span length in Section 2.4 to use as an equivalent length for multiplying the maximum curvatures provided by *Response*.

A series of integration lengths represented as a percentage of the span length are used to calculate the rotation  $\theta$  of a reinforced concrete section according to Eq. (2.1). Using the rotations, the post-elastic bending stiffness is calculated as in Section 2.5, and, in turn, the bending stiffness degradation factors are found from Eq. (2.10). Table 2.1 shows the bending stiffness degradation factors (for the first constant stiffness region) and the percentage of the beam span length used to calculate the curvature for the beam of Figure 2.23. To determine what percentage of length to select in order to yield a value of degradation factor for the analysis, the ratio of post-cracking flexural stiffness to elastic flexural stiffness  $\mu$ , which is given by,

$$\mu = \frac{\frac{3EI_{eff}}{L}}{\frac{3EI_{gross}}{L}} \quad (2.11)$$

is compared to the  $r$  values in Table 2.1.



Since the degradation factor is a measure of the amount of post-elastic stiffness reduction, and for a section in bending it enters the post-elastic range once concrete cracks, this seems to provide a reasonable method for choosing an initial value for analysis. The post-cracking flexural stiffness is calculated by first calculating an effective moment of inertia  $I_{eff}$  (ACI 435R-04). The effective moment of inertia is dependent upon the moment level and is therefore calculated using the average moment between the cracking moment and yield moment as given by *Response* for the beam section of Figure 2.14.

The effective moment of inertia is given by,

$$I_{eff} = (I_g - I_{cr}) \left( \frac{M_{cr}}{M_a} \right)^3 + I_{cr} \quad (2.12)$$

where  $I_g$  is the moment of inertia for the gross section,  $M_{cr}$  is the cracking moment resistance given by *Response*,  $M_a$  is the average of the cracking moment and yield moment and  $I_{cr}$  is the fully cracked moment of inertia given by,

$$I_{cr} = \frac{1}{3} b(kd)^3 + nA_s d^2 (1-k)^2 + (n-1)A'_s (kd - d')^2 \quad (2.13)$$

where  $d$  is the depth from the top of the section to the tension reinforcement,  $d'$  is the depth to the compression reinforcement,  $A_s$  is the area of tension reinforcement,  $A'_s$  is the area of compression reinforcement and where,

$$kd = \frac{\left[ \sqrt{2dB \left(1 + \frac{rd'}{d}\right) + (1+r)^2} - (1+r) \right]}{B} \quad (2.14)$$

$B$  and  $r$  in Eq. (2.14) are given by,

$$B = \frac{b}{nA_s} \quad (2.15)$$

and

$$r = \frac{(n-1)A'_s}{nA_s} \quad (2.16)$$

respectively, where  $b$  is the width of the section and  $n$  is the ratio of Young's modulus of steel to Young's modulus of concrete.

Equation (2.11) reduces to the ratio of the moments of inertia for the cracked ( $I_{\text{eff}}$ ) and uncracked ( $I_{\text{gross}}$ ) member. For the beam of Figure 2.23,  $I_{\text{eff}} = 1677 \times 10^6 \text{ mm}^4$  and  $I_{\text{gross}} = 3646 \times 10^6 \text{ mm}^4$ , yielding a ratio  $\mu = 0.46$ . Interpolating this value from Table 2.1 indicates that 9% of the span length is indeed a suitable length to integrate the curvature over to obtain a rotation value  $\theta$  from Eq. (2.1). Appendix A shows similar calculations for other under-reinforced beams. It also shows that using 14% of the span length for columns with equal amounts of end-reinforcement as the integration length for curvature yields degradation factors approximately equal to the value of Eq. (2.11).

The bending stiffness degradation factors for the column member shown in Figure 2.4 are now calculated. The column member has a modulus of elasticity of 26540 MPa, a moment of inertia of  $1251 \times 10^6 \text{ mm}^4$ , and a length of 3600mm. The bending stiffness degradation factor for the first constant stiffness region (the range of loading from  $M_{\text{cr}}$  to  $M_{\text{yld}}$ ) is given by Eq. (2.10) and has a value of,

$$r_A = \frac{1}{1 + \frac{3EI}{R_A L}} = \frac{1}{1 + \frac{3(26540 \text{ Mpa})(1251 \times 10^6 \text{ mm}^4)}{(31897000 \text{ kN} \cdot \text{mm})(3600 \text{ mm})}} = 0.54$$

where  $R_A = 31897000 \text{ kN-mm}$  is the post-elastic bending stiffness of the member for the first constant stiffness region. Similarly, the bending stiffness degradation factor for the second constant stiffness region (the range of loading from  $M_{\text{yld}}$  to  $M_{\text{ult}}$ ) is,

$$r_B = \frac{1}{1 + \frac{3EI}{R_B L}} = \frac{1}{1 + \frac{3(26540 \text{ Mpa})(1251 \times 10^6 \text{ mm}^4)}{(374000 \text{ kN} \cdot \text{mm})(3600 \text{ mm})}} = 0.01$$

where  $R_B = 374000 \text{ kN-mm}$  is the post-elastic bending stiffness of the member for the second constant stiffness region. It thus shows that cracking of concrete in bending causes a  $(1-r_A \times 100) = 46\%$  reduction in post-elastic bending stiffness while yielding of the tensile reinforcement causes a  $(1-r_B \times 100) = 98\%$  reduction in post-elastic bending stiffness.

## 2.6.2 Shear Stiffness Degradation Factor

Figure 2.24 shows the model used to derive the shear stiffness degradation factor. The member is pinned at its right end and able to deform transversely only (no bending or axial deformation) at its left end. The elastic shear deformation due to shear force  $V$  at its left end is  $\gamma_e = VL^3/3EI$  and the post-elastic shear deformation is  $\gamma_p = V/T$ . The shear stiffness degradation factor is,

$$t = \frac{\gamma_e}{\gamma_e + \gamma_p} = \frac{\frac{VL^3}{3EI}}{\frac{VL^3}{3EI} + \frac{V}{T}} = \frac{1}{1 + \frac{3EI}{TL^3}} \quad (2.17)$$

When the post-elastic shearing stiffness  $T = \infty$ , meaning that the member-end is in the fully elastic range,  $t = 1$ , indicating that there is no post-elastic shear stiffness degradation. When the post-elastic stiffness  $T = 0$ , then the shear stiffness degradation factor  $t = 0$ , indicating that there is complete post-elastic shear stiffness degradation. For other values of post-elastic shearing stiffness,  $t$  will vary between 1 and 0 to indicate varying degrees of post-elastic shearing stiffness degradation.

The shearing stiffness degradation factors for the column member shown in Figure 2.4 are now calculated. Again, the column member has a modulus of elasticity of 26540 MPa, a moment of inertia of  $1251 \times 10^6 \text{ mm}^4$ , and a length of 3600mm. The shearing stiffness degradation factor for the first constant stiffness region (the range of loading from  $V_{cr}$  to  $V_{yld}$ ) is given by Eq. (2.17) and has a value of,

$$t_A = \frac{1}{1 + \frac{3EI}{T_A L^3}} = \frac{1}{1 + \frac{3(26540 \text{ Mpa})(1251 \times 10^6 \text{ mm}^4)}{(13.9 \text{ kN/mm})(3600 \text{ mm})^3}} = 0.87$$

where  $T_A = 13.9 \text{ kN/mm}$  is the post-elastic shearing stiffness of the member-section for the first constant stiffness region. Similarly, the shearing stiffness degradation factor for the second constant stiffness region (the range of loading from  $V_{yld}$  to  $V_{ult}$ ) is,

$$t_B = \frac{1}{1 + \frac{3EI}{T_B L^3}} = \frac{1}{1 + \frac{3(26540 \text{ Mpa})(1251 \times 10^6 \text{ mm}^4)}{(1.6 \text{ kN/mm})(3600 \text{ mm})^3}} = 0.43$$

where  $T_B = 1.6 \text{ kN/mm}$  is the post-elastic shearing stiffness of the member-section for the second constant stiffness region. It thus shows that diagonal cracking causes a  $(1-t_A \times 100) = 13\%$  reduction

in post-elastic shearing stiffness while yielding of the transverse reinforcement causes a  $(1-t_B \times 100) = 57\%$  reduction in post-elastic shearing stiffness. The effect of the reinforcement yielding is not as severe as in the case of flexural degradation (57% reduction compared to 98% reduction). This could be attributed to the fact that in shear there are other mechanisms of shear transfer such as aggregate interlock and dowel action, whereas in flexure the reinforcement alone is relied upon to form the moment resisting internal couple.

### 2.6.3 Axial Stiffness Degradation Factor

Figure 2.25 shows the model used to derive the axial stiffness degradation factor. The member is pinned at its right end and free to deform only axially (no bending or shear deformation) at its left end. The elastic axial deformation due to axial load  $P$  at its left end is  $\delta_e = PL/AE$  and the post-elastic axial deformation is  $\delta_p = P/N$ . The axial stiffness degradation factor is,

$$n = \frac{\delta_e}{\delta_e + \delta_p} = \frac{\frac{PL}{AE}}{\frac{PL}{AE} + \frac{P}{N}} = \frac{1}{1 + \frac{AE}{NL}} \quad (2.18)$$

When the post-elastic axial stiffness  $N = \infty$ , meaning that the member-end is in the fully elastic range,  $n = 1$ , indicating that there is no post-elastic axial stiffness degradation. When the post-elastic axial stiffness  $N = 0$ , then the axial stiffness degradation factor  $n = 0$ , indicating that there is complete post-elastic axial stiffness degradation. For other values of post-elastic axial stiffness,  $n$  will vary between 1 and 0 to indicate varying degrees of post-elastic axial stiffness degradation.

The axial stiffness degradation factors for both tension and compression of the column member shown in Figure 2.4 are now calculated. The column member has a modulus of elasticity of 26540 MPa, a cross sectional area of 122500mm<sup>2</sup> and a length of 3600mm. The axial stiffness degradation factor for the first constant stiffness region (the range of loading from  $P_{cr}$  to  $P_{yld}$ ) for axial tension is given by Eq. (2.18) and has a value,

$$n_{At} = \frac{1}{1 + \frac{AE}{N_{At}L}} = \frac{1}{1 + \frac{(122500mm^2)(26540Mpa)}{(206kN/mm)(3600mm)}} = 0.18$$

where  $N_{At} = 206 \text{ kN/mm}$  is the post-elastic axial stiffness of the member for the first constant stiffness region. Similarly, the axial stiffness degradation factor for the second constant stiffness region (the range of loading from  $P_{yld}$  to  $P_{ult}$ ) for axial tension is,

$$n_{Bt} = \frac{1}{1 + \frac{AE}{N_{Bt}L}} = \frac{1}{1 + \frac{(122500\text{mm}^2)(26540\text{Mpa})}{(3\text{kN/mm})(3600\text{mm})}} = 0.003$$

where  $N_{Bt} = 3 \text{ kN/mm}$  is the post-elastic axial stiffness of the member for the second constant stiffness region. Intuitively these results are reasonable. Once the concrete cracks the tensile force is carried by the longitudinal reinforcement only, and hence the reason there is a large reduction ( $1 - n_{At} \times 100 = 82\%$ ) in post-elastic axial tension stiffness. Once this longitudinal reinforcement yields the section is for all intents and purposes fully plastic and that is why the axial stiffness degradation factor is effectively zero.

The axial stiffness degradation factor for axial compression is also given by Eq. (2.10) and has a value of,

$$n_c = \frac{1}{1 + \frac{AE}{N_cL}} = \frac{1}{1 + \frac{(122500\text{mm}^2)(26540\text{Mpa})}{(656\text{kN/mm})(3600\text{mm})}} = 0.42$$

where  $N_c = 656 \text{ kN/mm}$  is the post-elastic axial stiffness of the member-section.

## 2.7 Member Stiffness Matrix

The analysis program is based on the displacement method of analysis whereby member-end forces are related to member-end deformations by an element stiffness matrix. This relation is defined by,

$$f = kd \tag{2.19}$$

where for the 6 local degrees of freedom (Figure 2.1),  $f = [f_1 \dots f_6]^T$  is the vector of member-end forces,  $d = [d_1 \dots d_6]^T$  is the vector of member-end displacements and  $k$  is the element stiffness matrix given by,

$$k = \begin{bmatrix} k_{11} & 0 & 0 & k_{14} & 0 & 0 \\ & k_{22} & k_{23} & 0 & k_{25} & k_{26} \\ & & k_{33} & 0 & k_{35} & k_{36} \\ & & & k_{44} & 0 & 0 \\ & Sym & & & k_{55} & k_{56} \\ & & & & & k_{66} \end{bmatrix} \quad (2.20)$$

The stiffness coefficients in Eq. (2.20) were first derived to account for geometric nonlinearity and shear deformation, and then extended to account for bending stiffness degradation based on the moment-rotation compatibility conditions accounting for axial force and shear deformation using a modified moment distribution method. The stiffness coefficients were then further extended to account for the combined effects of degraded bending and degraded shear stiffness, as well as the effects of degraded axial stiffness (Liu, 2007). With the exception of Eq. (2.22), whose derivation for this study is found in Appendix B, the following stiffness coefficients are taken directly from (Xu *et al.*, 2005) while detailed derivations are given in (Liu, 2007), i.e.,

$$k_{11} = k_{11}^a \chi_0 = k_{44} = -k_{14} = -k_{41} \quad (2.21a)$$

$$k_{22} = k_{22}^r \chi_1 = k_{55} = -k_{25} = -k_{52} \quad (2.21b)$$

$$k_{23} = k_{23}^r \chi_1 = k_{32} = -k_{35} = -k_{53} \quad (2.21c)$$

$$k_{26} = k_{26}^r \chi_1 = k_{62} = -k_{56} = -k_{65} \quad (2.21d)$$

$$k_{33} = k_{33}^r \chi_2 \quad (2.21e)$$

$$k_{36} = k_{36}^r \chi_3 = k_{63} \quad (2.21f)$$

$$k_{66} = k_{66}^r \chi_4 \quad (2.21g)$$

In Eq. (2.21a),  $k_{11}^a = AE/L$  is the elastic axial stiffness, and the factor,

$$\chi_0 = \frac{n_1 n_2}{n_1 + n_2 - n_1 n_2} \quad (2.22)$$

accounts for post-elastic axial stiffness degradation by incorporating the axial stiffness degradation factors  $n_i$  ( $i=1,2$ ). In Eqs. 2.21(b)-(g), the stiffness coefficients,

$$k_{22}^r = \frac{EI}{L^3\Omega} \left[ 3b\eta_1(1+c\eta_2)[6r_1r_2 + b\eta_1(1-c\eta_2)(r_1+r_2-2r_1r_2)] + P \frac{L^2\Omega}{EI} \right] \quad (2.23)$$

$$k_{23}^r = \frac{3b\eta_1 EI r_1 (1+c\eta_2)}{L^2\Omega} [b\eta_1(1-r_2)(1-c\eta_2) + 3r_2] \quad (2.24)$$

$$k_{26}^r = \frac{3b\eta_1 EI r_2 (1+c\eta_2)}{L^2\Omega} [b\eta_2(1-r_1)(1-c\eta_2) + 3r_1] \quad (2.25)$$

$$k_{33}^r = \frac{3r_1 b \eta_1 EI [b \eta_1 (1-r_2)(1-b^2 \eta_2^2) + 3r_2]}{L\Omega} \quad (2.26)$$

$$k_{36}^r = \frac{9bc\eta_1\eta_2 EI r_1 r_2}{L\Omega} \quad (2.27)$$

$$k_{66}^r = \frac{3r_2 b \eta_1 EI [b \eta_1 (1-r_1)(1-c^2 \eta_2^2) + 3r_1]}{L\Omega} \quad (2.28)$$

account for elastic bending stiffness and for post-elastic bending stiffness degradation by incorporating bending stiffness degradation factors  $r_i$  ( $i=1,2$ ), and the factors,

$$\chi_1 = \frac{t_1 t_2}{t_1 t_2 + 4\beta(t_1 + t_2 - 2t_1 t_2)} \quad (2.29)$$

$$\chi_2 = 1 - \left( \frac{b\eta_1 r_1}{4\Omega\beta} \right) \left( \frac{(1+c\eta_2)^2 [b\eta_1(1-r_2)(1-c\eta_2) + 3r_2]^2}{b\eta_1(1-r_2)(1-c^2\eta_2^2) + 3r_2} \right) (1-\chi_1) \quad (2.30)$$

$$\begin{aligned} \chi_3 = 1 - \left( \frac{b\eta_1(1+c\eta_2)^2}{12c\eta_2\Omega\beta} \right) [b\eta_1(1-r_1)(1-c\eta_2) + 3r_1] [b\eta_1(1-r_2)(1-c\eta_2) + 3r_2] \\ \times (1-\chi_1) \end{aligned} \quad (2.31)$$

$$\chi_4 = 1 - \left( \frac{b\eta_1 r_2}{4\Omega\beta} \right) \left( \frac{(1+c\eta_2)^2 [b\eta_1(1-r_1)(1-c\eta_2) + 3r_1]^2}{b\eta_1(1-r_1)(1-c^2\eta_2^2) + 3r_1} \right) (1-\chi_1) \quad (2.32)$$

account for post-elastic shear stiffness degradation by incorporating shear stiffness degradation factors  $t_i$  ( $i=1,2$ ).

The parameter  $P =$  axial force in Eq. (2.23), while in Eqs. (2.23) - (2.28) and Eqs. (2.30) - (2.32), the parameters,

$$b = \begin{cases} \frac{1 - \psi / \tan \psi}{\tan(\psi / 2) / (\psi / 2) - 1} & P \leq 0 \\ \frac{1 - \psi / \tanh \psi}{\tanh(\psi / 2) / (\psi / 2) - 1} & P > 0 \end{cases} \quad (2.33)$$

$$c = \begin{cases} \frac{\psi - \sin \psi}{\sin \psi - \psi \cos \psi} & P \leq 0 \\ \frac{\psi - \sinh \psi}{\sinh \psi - \psi \cosh \psi} & P > 0 \end{cases} \quad (2.34)$$

in which,

$$\psi = \begin{cases} L \sqrt{\frac{-P/EI}{1+P/GA}} & P \leq 0 \\ L \sqrt{\frac{P/EI}{1+P/GA}} & P > 0 \end{cases} \quad (2.35)$$

are geometrical stiffness coefficients used in both stability and geometrical nonlinear analysis, and the factors

$$\eta_1 = \left(1 + \frac{P}{GA}\right) \left(\frac{1 + \xi f_1}{1 + \xi f_2}\right) \quad (2.36)$$

$$\eta_2 = \frac{1 + \xi f_3}{1 + \xi f_1} \quad (2.37)$$

in which,

$$\xi = \frac{EI(1 + P/GA)}{GAL^2} \quad (2.38)$$

$$f_1 = \begin{cases} \psi^2 / (1 - \psi / \tan \psi) & P \leq 0 \\ -\psi^2 / (1 - \psi / \tanh \psi) & P > 0 \end{cases} \quad (2.39)$$

$$f_2 = \begin{cases} \psi^3 \tan(\psi / 2) / [\tan(\psi / 2) - \psi / 2] & P \leq 0 \\ -\psi^3 \tanh(\psi / 2) / [\tanh(\psi / 2) - \psi / 2] & P > 0 \end{cases} \quad (2.40)$$



$$f_3 = \begin{cases} \psi^2 / (1 - \psi / \sin \psi) & P \leq 0 \\ -\psi^2 / (1 - \psi / \sinh \psi) & P > 0 \end{cases} \quad (2.41)$$

account for the influence of shear deformation on elastic bending stiffness.

Lastly, in Eqs. (2.23) - (2.28) and Eqs. (2.30) - (2.32), the parameter

$$\Omega = 9r_1r_2 + 3r_2b\eta_1(1-r_1) + 3r_1b\eta_1(1-r_2) + b^2\eta_1^2(1-r_1)(1-r_2)(1-c^2\eta_2^2) \quad (2.42)$$

while in Eqs. (2.29) - (2.32), the parameter

$$\beta = \frac{L^3}{12EI} k_{22}^r \quad (2.43)$$

In the original derivation of the stiffness coefficients, the term  $A$  in Eqs. (2.35), (2.36), and (2.38) is given as  $A_s$  (the equivalent shear area). In this study, however, the shear force is assumed to act over the entire gross cross-sectional area when in the elastic range.

With an element stiffness matrix that accounts for geometric nonlinearity, shear deformation, and degraded post-elastic bending, shearing and axial stiffness of reinforced concrete, what is left to be done is to formulate an analysis procedure.

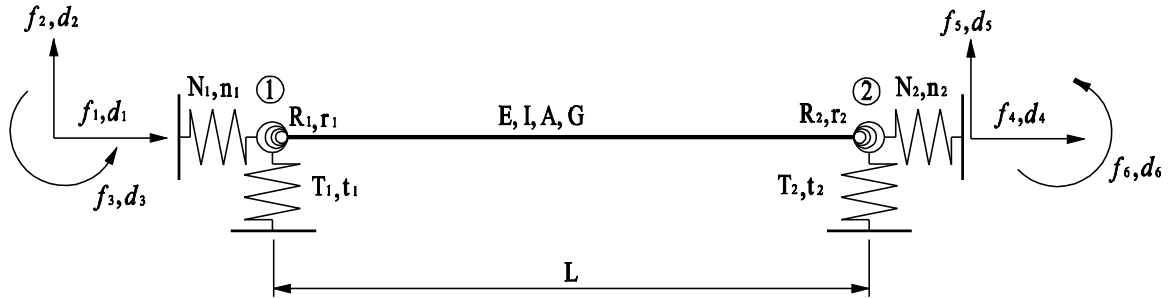


Figure 2.1: Beam-column analysis model (Xu *et al*, 2005)

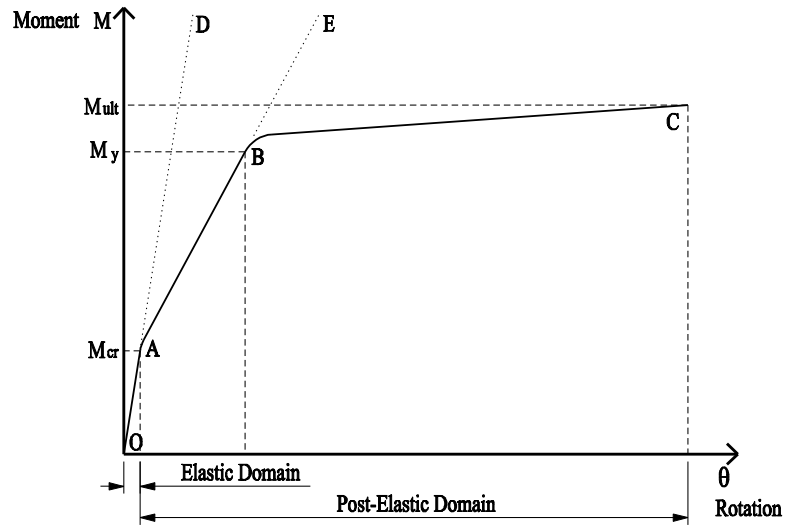


Figure 2.2: Typical moment-rotation response for an under-reinforced concrete section

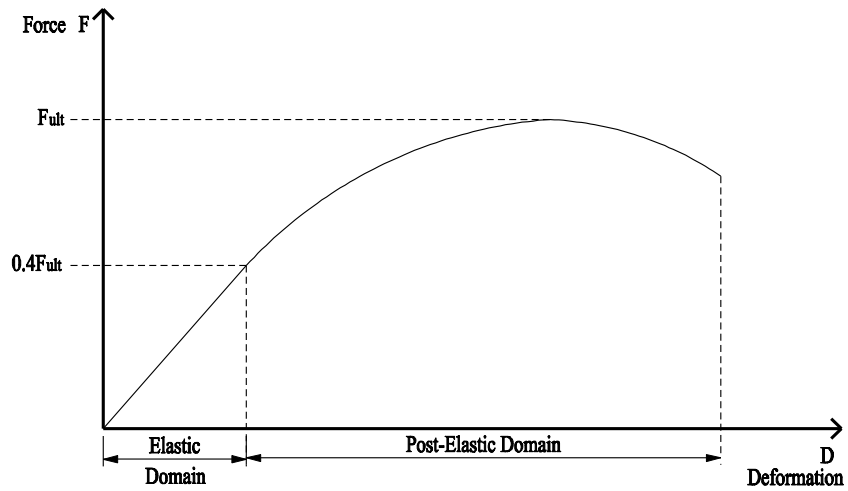


Figure 2.3: Typical force-deformation response for axial compression

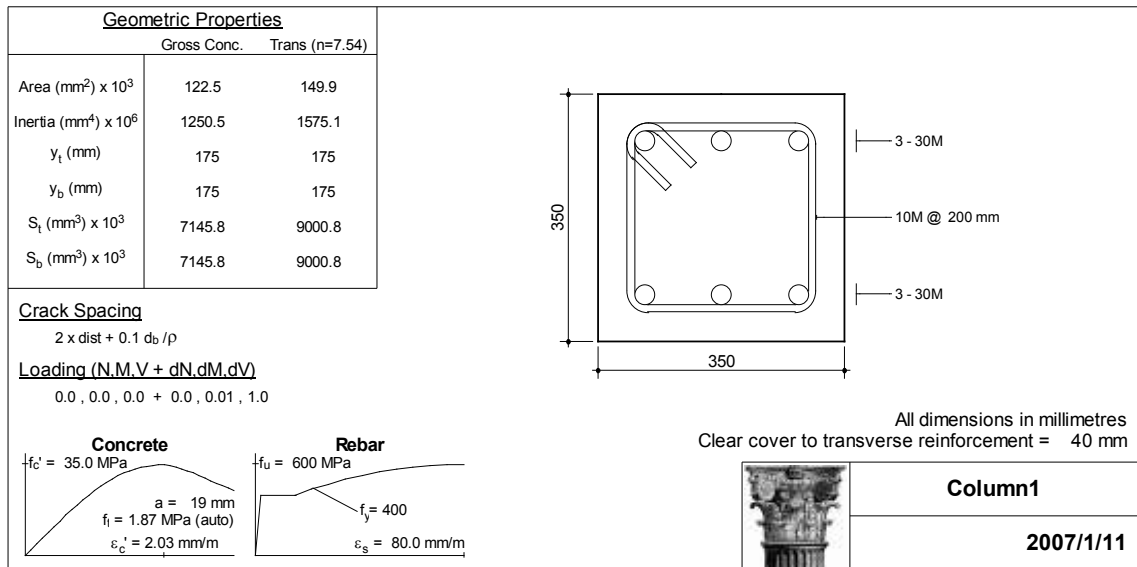


Figure 2.4: Summary of a reinforced concrete column section (*Response-2000*)

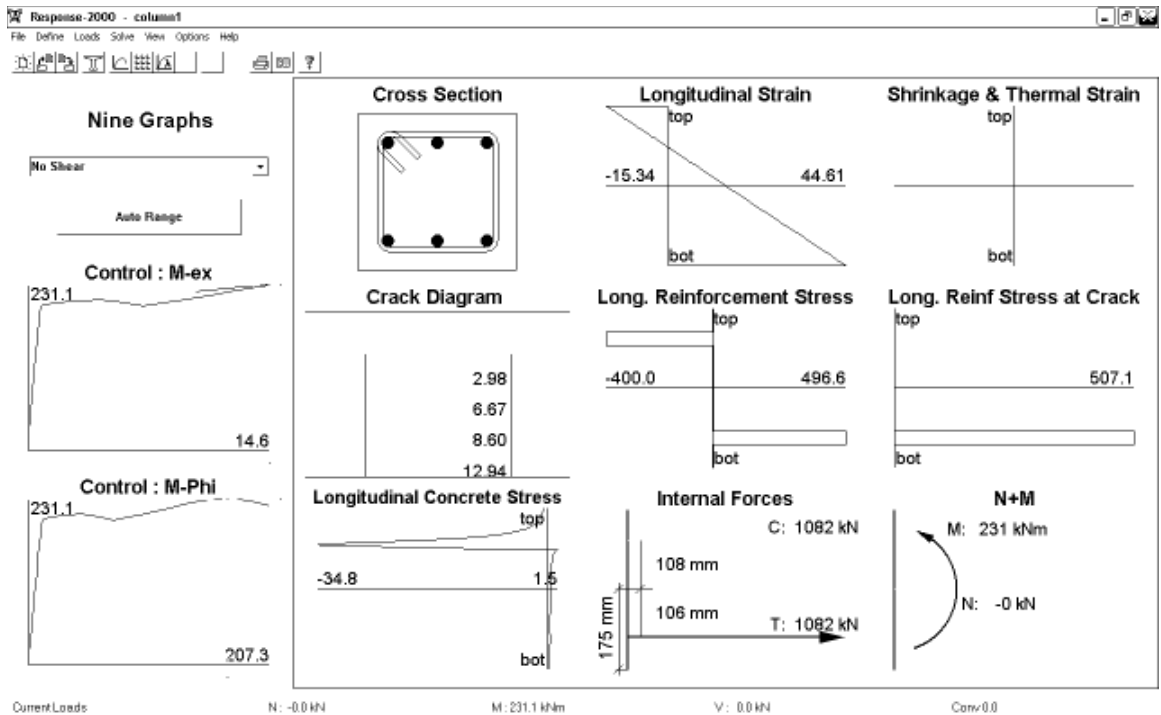


Figure 2.5: Sectional analysis in bending - output results (*Response-2000*)

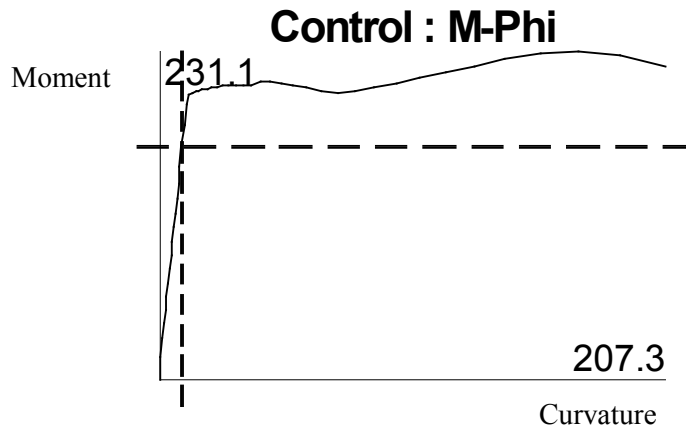


Figure 2.6: Moment-curvature control plot (*Response-2000*)

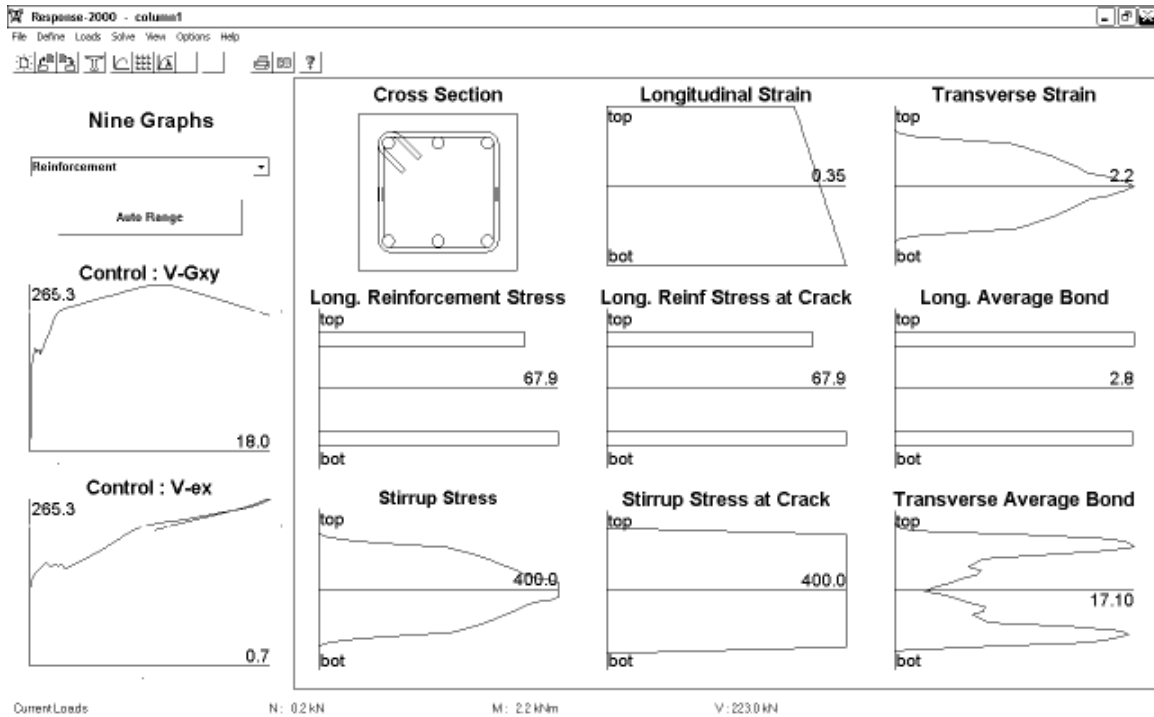


Figure 2.7: Sectional analysis in shear - output results (*Response-2000*)

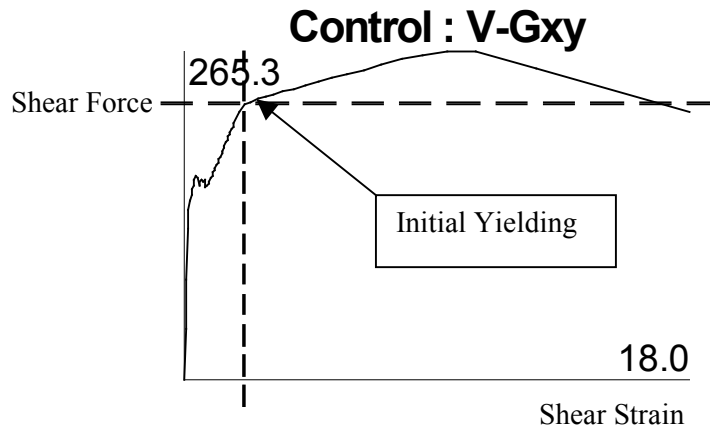


Figure 2.8: Shear force-shear strain control plot (*Response-2000*)

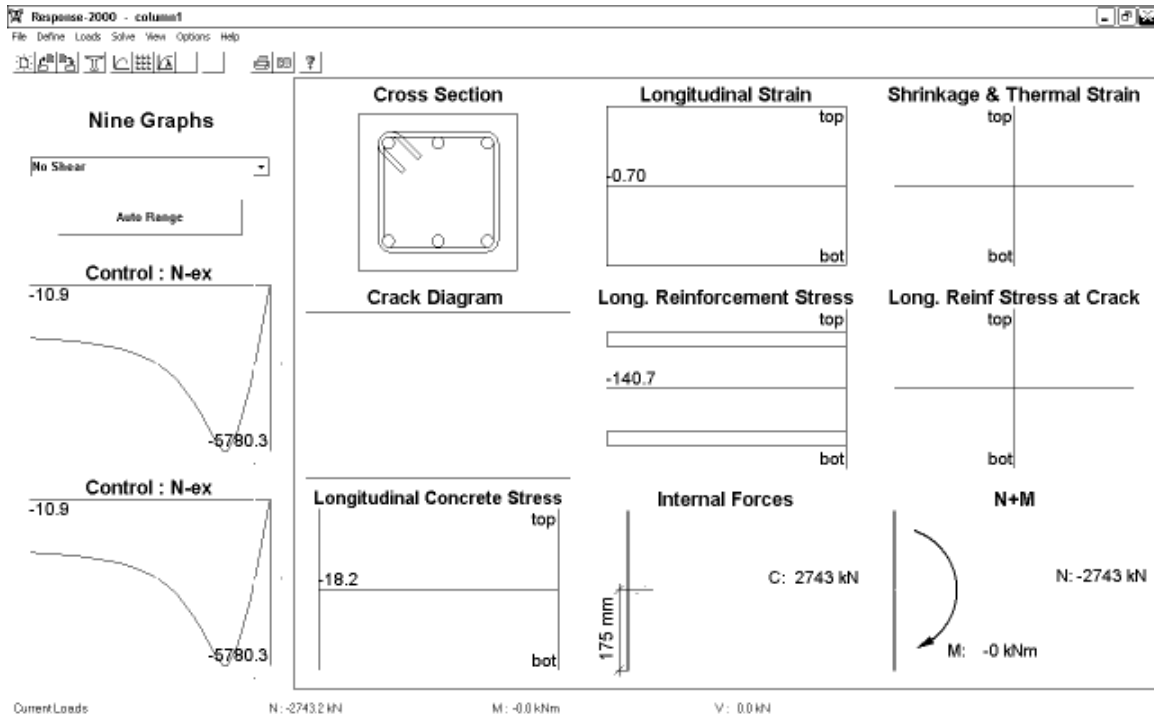


Figure 2.9: Sectional analysis in compression - output results (*Response-2000*)

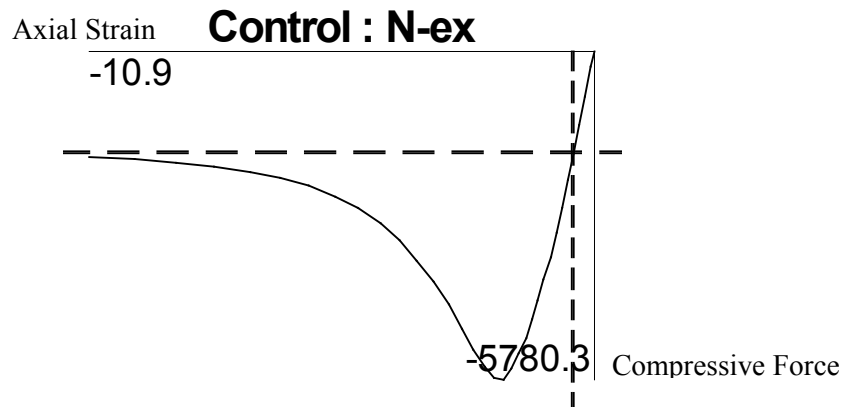


Figure 2.10: Compressive force-axial strain control plot (*Response-2000*)

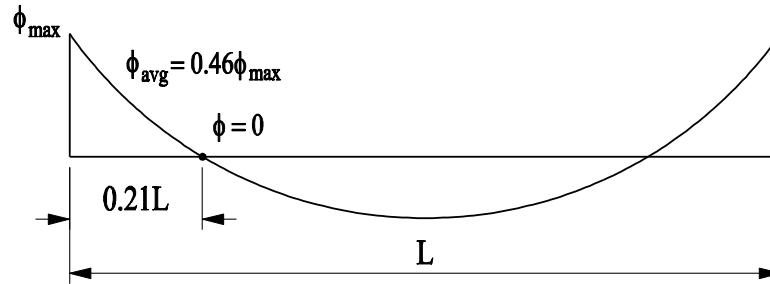


Figure 2.11: Curvature along a beam

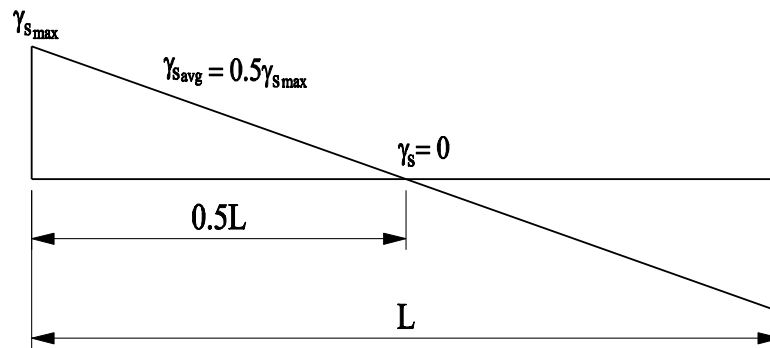


Figure 2.12: Shear strain along a beam

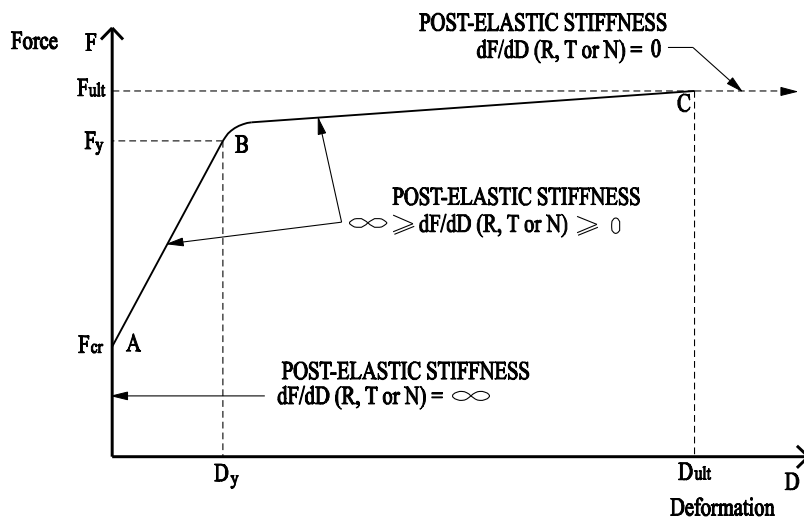


Figure 2.13: General post-elastic force-deformation response

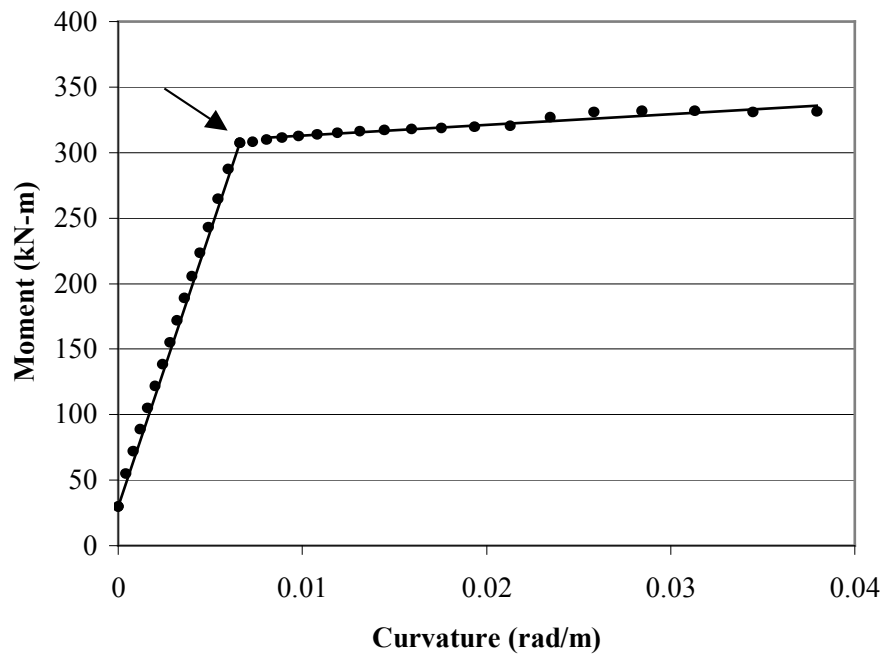


Figure 2.14: Post-elastic moment-curvature for a 500x350 mm section, 35 MPa,  $\rho = 1.31\%$

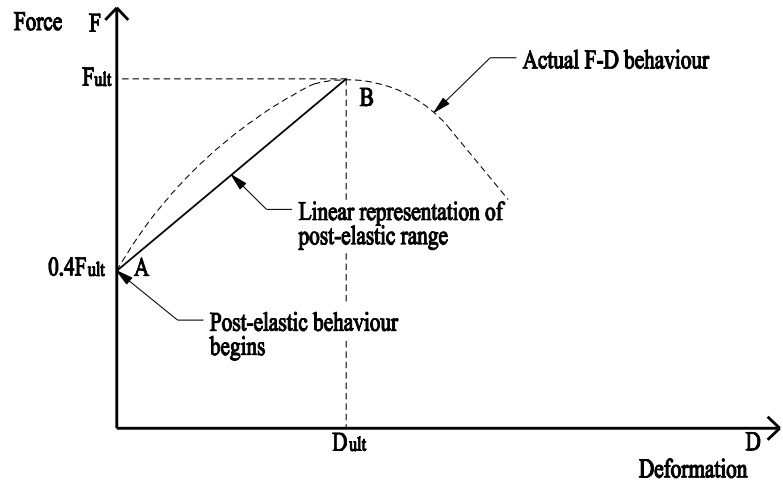


Figure 2.15: General post-elastic force-deformation response

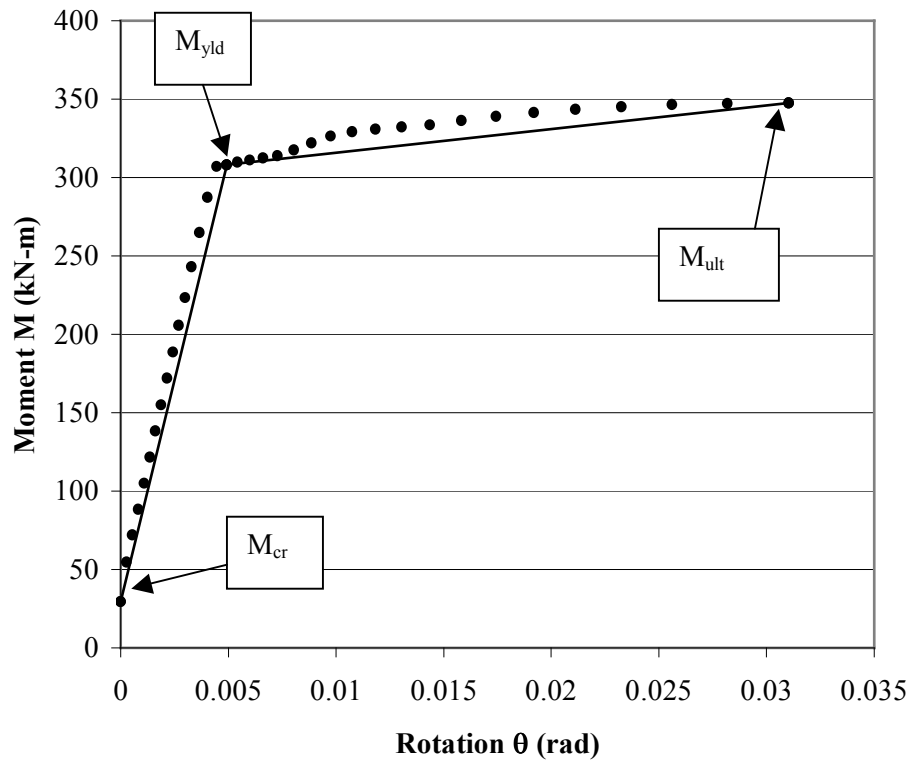


Figure 2.16: Post-elastic moment-rotation response for an under-reinforced section



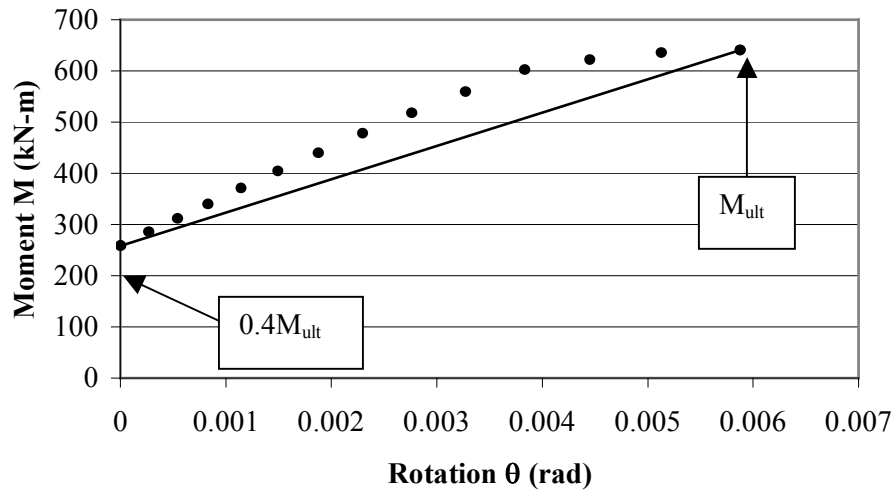


Figure 2.17: Post-elastic moment-rotation response for an over-reinforced section

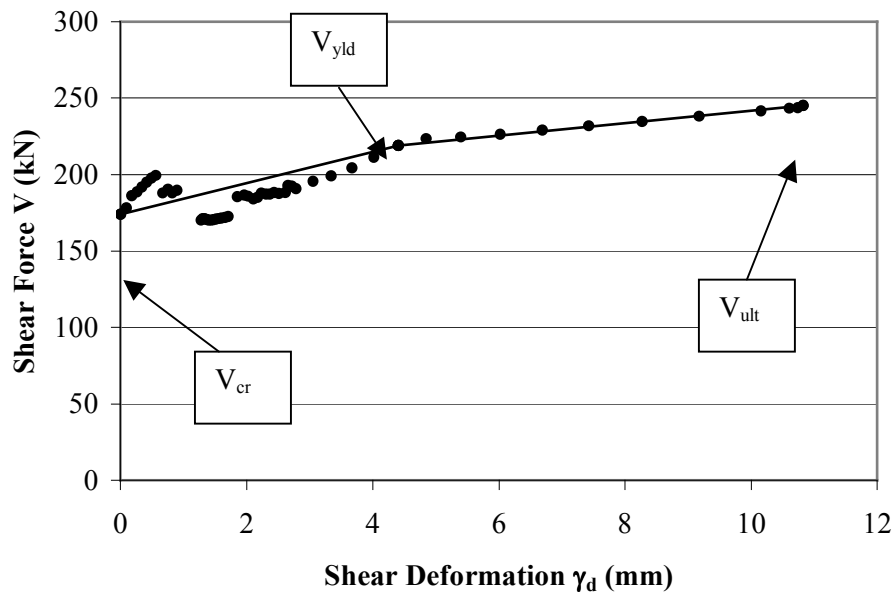
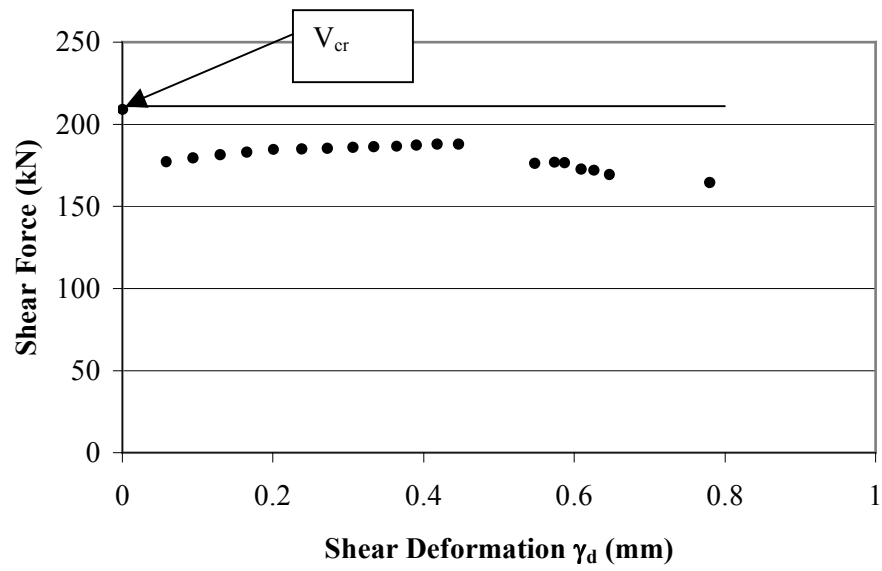
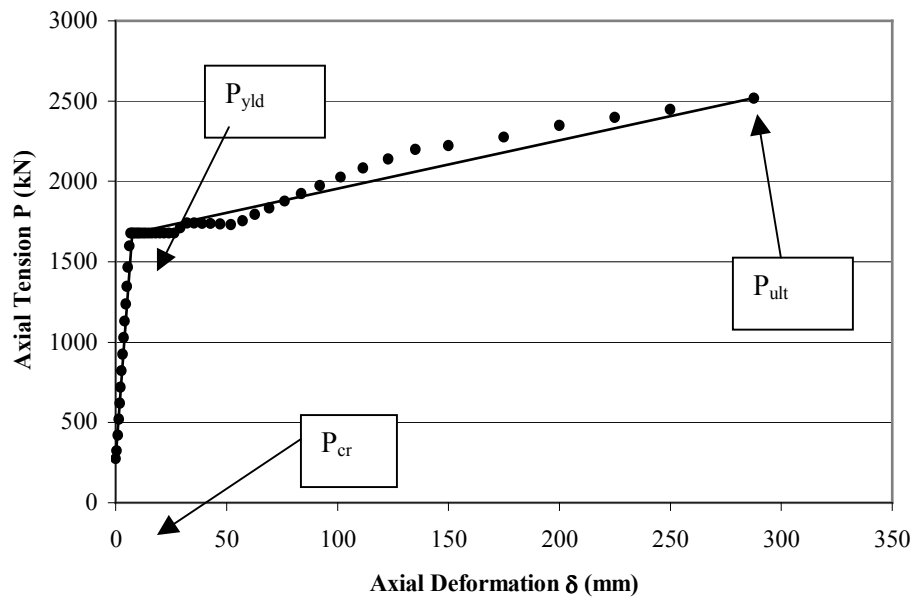


Figure 2.18: Post-elastic shear force-shear deformation response for a section with transverse reinforcement



**Figure 2.19: Post-elastic shear force-shear deformation response for a section without transverse reinforcement**



**Figure 2.20: Post-elastic axial tension-axial deformation**

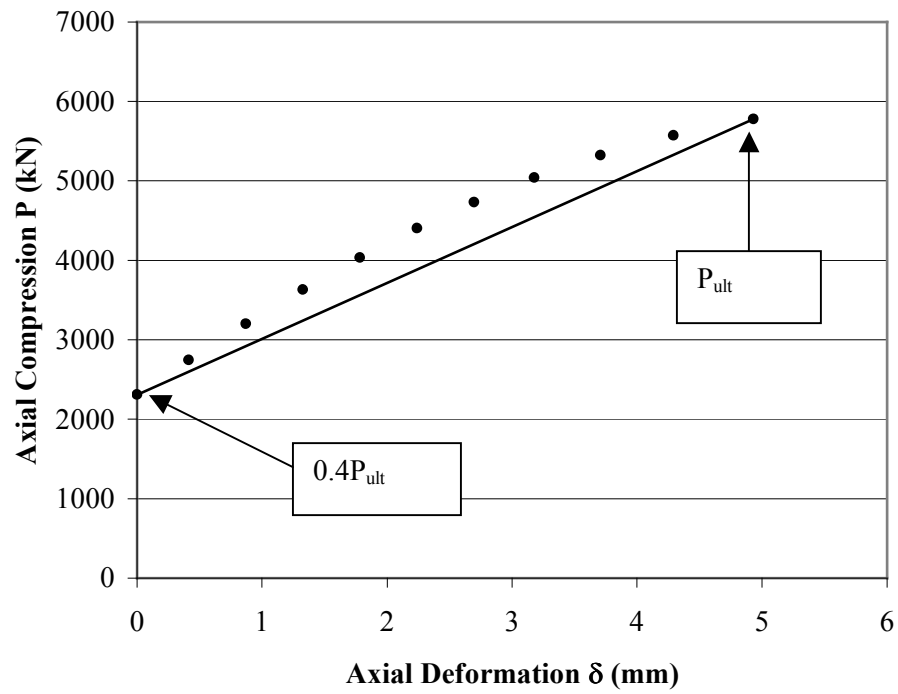


Figure 2.21: Post-elastic axial compression-axial deformation

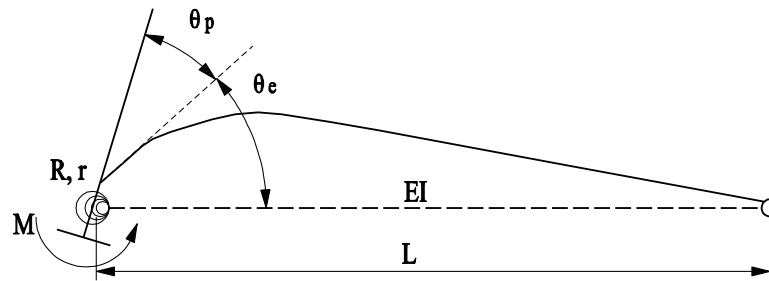
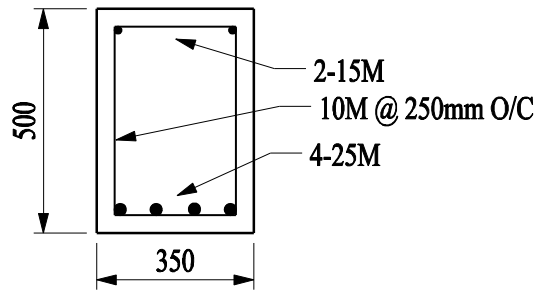


Figure 2.22: Model for bending stiffness degradation factor (Xu *et al*, 2005)

**Table 2.1: Degradation factors and curvature integration length**

% of Length	r
1	0.868
10	0.396
20	0.247
30	0.180
40	0.141
50	0.116
60	0.099
70	0.086
80	0.076
90	0.068
100	0.062



**Figure 2.23: Beam cross section**

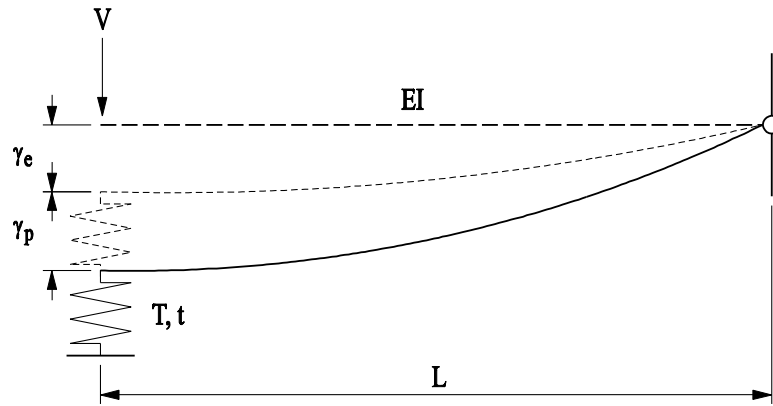


Figure 2.24: Model for shear stiffness degradation factor (Xu *et al*, 2005)

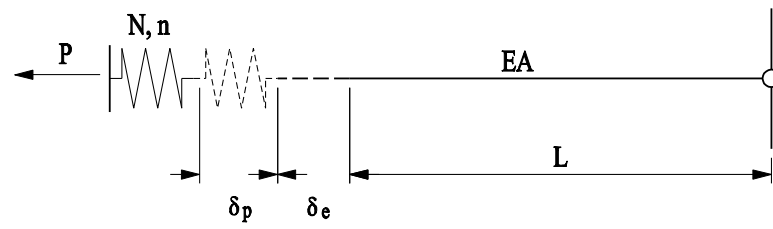


Figure 2.25: Model for axial stiffness degradation factor (Xu *et al*, 2005)

## Chapter 3

### Analysis Procedure

The analysis procedure for a reinforced concrete frame involves four distinct stages as outlined in Figure 3.1. Section 3.1 describes stage-zero elastic analysis which is performed on the structure up to the point that the structure no longer exhibits linear-elastic behaviour, i.e., when the first member-section enters the post-elastic range due to cracking of concrete. Section 3.2 presents stage-one inelastic incremental analysis, where, depending on the load level, the stiffness degradation factors are calculated and the degree of post-elastic stiffness degradation is tracked. Section 3.3 presents stage-two elastic-unloading analysis which is performed only after a member-section exceeds its ultimate load resistance and fails. Finally, Section 3.4 presents stage-three reloading inelastic analysis, which is similar to stage-two analysis in the sense that the stiffness degradation factors are calculated and the degree of post-elastic stiffness degradation is tracked. Stage-three reloading inelastic analysis, however, involves applying amplified debris loads on the structure due to members disengaging from the main structure and falling onto members below.

#### 3.1 Stage Zero Elastic Analysis

As discussed in Chapter 2, a structure's response to loads is linear-elastic until the first member-section cracks, i.e., flexural cracking due to bending moment or diagonal cracking due to shear force etc. The linear-elastic analysis procedure adopted by this study is based on the matrix displacement method of analysis in which the force-displacement relationship, e.g., (Sennett, 1994),

$$Ku = F \tag{3.1}$$

is solved for the vector of nodal displacements  $u$ , where  $K$  is the structural stiffness matrix and  $F$  is the vector of nodal loads.

The first step in the overall analysis procedure, which is also the first step in stage-zero elastic analysis, is to input all the necessary data required for a complete matrix displacement analysis. This is no different than any analysis conducted using a conventional software package. There is, however, additional force-deformation information that must be input into the program that is later used in the inelastic analysis and the formulation of the stiffness degradation factors.

The program first requires general information pertaining to the structure as a whole such as the number of members, nodes, supports and groups. A group consists of a number of members with common properties such as moment of inertia and modulus of elasticity. Specific node, group and member names are also required for identification purposes later on in the input process, as well as to be able to discern the output information.

Element (or member) connectivity is identified next whereby the start and end nodes for each member are input. The member-end restraints are also assigned here. Individual members can have a variety of end-restraints ranging from fully fixed to partially fixed to pin-ended or a combination thereof. For a partially fixed member-end an end-fixity factor  $r$  is input to define the degree of partial fixity, where the range of values is such that  $r = 1$  defines full end-fixity while  $r = 0$  applies for a pinned member-end.

Specific group information is input next and includes Young's modulus of elasticity, shear modulus, cross-sectional area and moment of inertia. These properties are based on the gross concrete section. As used in *Response* (Bentz, 2000), Young's modulus of elasticity (for normal density concrete) is herein calculated as (Collins & Mitchell, 1991),

$$E = 3320\sqrt{f'_c} + 6900 \text{ Mpa} \quad (3.2)$$

where  $f'_c$  is the concrete compressive strength. The shear modulus is given by (Hibbeler, 1994),

$$G = \frac{E}{2(1+\nu)} \quad (3.3)$$

where  $E$  is Young's modulus of elasticity and Poisson's ratio is taken as  $\nu = 0.20$ , the value commonly used in the design of concrete structures (Pillai, Kirk & Erki, 1999).

Nodal coordinates are input next, in addition to nodal support conditions which can be either fixed, free, pinned or on a roller support. Finally, the loads input for the structure can be any combination of nodal loads, member loads, temperature loads or support settlements.

As previously mentioned, in order to facilitate the inelastic analysis and the calculation of the stiffness degradation factors, force-deformation data is required. Using the force-strain or moment-curvature data from *Response* and approximating the deformations and rotations as discussed in Section 2.4, the required force-deformation data is obtained. As discussed in Section 2.5, depending on the force-deformation case being modeled, two or three sets of data points are sufficient to fully

represent the bilinear or trilinear force-deformation relationship of a member-section. That is, for the cases represented by a trilinear model, i.e. under-reinforced sections in flexure, reinforced sections in shear, and axially loaded sections in tension, data points that define the force and deformation at which initial cracking occurs, the reinforcement yields, and when the ultimate capacity of the section is exceeded are the only ones needed to develop the trilinear model.

For the cases represented by a bilinear model, i.e., over-reinforced sections in flexure, unreinforced (no stirrups) sections in shear and axially loaded sections in compression, data points that define the force and deformation at which post-elastic behaviour begins and when the ultimate capacity of the section is exceeded are the only ones needed to develop the bilinear model.

After all the pertinent input data is entered, the elastic analysis proceeds. The full design load acting on the structure is applied and Eq. (3.1) is solved for the nodal displacements, from which the member-end forces are obtained. The member-end forces from the elastic analysis are then scaled back such that one or more member-sections is at the point of entering the post-elastic range, i.e., due to cracking of concrete. The force magnitudes at which member-sections enter the post-elastic range are known from the previously entered *Response* data. The ratio by which the member-end forces are scaled back is retained as the total load factor level,  $\lambda_{j-1}$ , thus far in the analysis. The member-end forces at which the first member-section(s) enters the post-elastic range form the starting basis from which to commence an inelastic incremental analysis.

### 3.2 Stage One Inelastic Incremental Analysis

Once the first member-section(s) of the structure cracks, the response of the structure is no longer linear-elastic, and hence, a stage-one inelastic incremental analysis is required. The inelastic incremental analysis procedure begins at total load factor level,

$$\lambda_j = \lambda_{j-1} + \Delta\lambda^* \quad (3.4)$$

where  $\lambda_{j-1}$  is the total load factor level at which the response of the structure ceases to be linear-elastic and where  $\Delta\lambda^* < 1$  is an incremental load factor selected by the user. The total load factor level for subsequent load increments is,

$$\lambda = \lambda_{j-1} + \Sigma\Delta\lambda_i \quad (3.5)$$

where  $\Sigma\Delta\lambda_i$  is the sum of the incremental load factor levels up to increment  $i$ .



If, for example, an initial incremental load factor  $\Delta\lambda^* = 0.05$  is selected and the incremental analysis procedure begins at total load factor level  $\lambda = 0.3$ , then the total load factor level for increments 1, 2 and 3 is  $\lambda = 0.35, 0.40, \text{ and } 0.45$ , respectively, where 5% of the total load acting on the structure is applied at a time. The incremental analysis proceeds until either the target load level is reached, i.e.  $\lambda = 1$  (the full magnitude of the design loads) or a member-section failure occurs before that point.

The analysis procedure is incremental to facilitate determining precisely when the post-elastic stiffness of a member-section changes and thus Eq. (3.1) takes the new form,

$$K_i \Delta u_i = \Delta \lambda_i F \quad (3.6)$$

such that, now, the vector of incremental nodal displacements  $\Delta u_i$  is found for each load increment  $\Delta \lambda_i F$ , where  $K_i$  is the structural stiffness matrix and  $\Delta \lambda_i$  is the incremental scale factor for load increment  $i$ . Equation (3.6) is solved successively for  $\Delta u_i$  for each load increment and, then, the corresponding incremental local member-end forces  $\Delta f_i$  are given by,

$$\Delta f_i = \left( [k_e]_i^G \Delta u_i \right) [T] + [FEF]_i \quad (3.7)$$

where  $[k_e]_i^G$  is the element stiffness matrix for load increment  $i$  in global coordinates,  $[T]$  is a matrix that transforms the member-end forces from the global to local coordinate system, and  $[FEF]_i$  is the vector of fixed-end forces due to any member loads (if applicable).

Once the incremental nodal displacements and member-end forces are solved for, these values are then summed, respectively, for all load increments,

$$u = \Sigma \Delta u_i \quad (3.8)$$

$$f = \Sigma \Delta f_i \quad (3.9)$$

to obtain the accumulated nodal displacements  $u$  and member-end forces  $f$ .

If the analysis is either stage-one or stage-three inelastic analysis, the bending, shearing and axial stiffness degradation factors,  $r$ ,  $t$ , and  $n$ , respectively, are calculated.

Figure 3.2 shows the general form of the trilinear post-elastic force-deformation response used in this study. It represents the post-elastic force-deformation response for an under-reinforced section subject to flexure, a transversely reinforced section subject to shear or an axially loaded section in

tension. As discussed in Section 2.5, the other force-deformation cases are represented by a bilinear response. The degradation factors are calculated based on the magnitude of the member-end forces with respect to the graph. If the total member-end force  $f$  at load increment  $i$  is less than the cracking force  $f_{cr}$ , then the member-section is still in the elastic range and the degradation factor has a value of unity. If  $f$  at load increment  $i$  is between the cracking force  $f_{cr}$  and yielding force  $f_{yld}$  as shown in the figure, then the member-section is in the post-elastic range and the degradation factor for the first linear portion of the graph is calculated (a value between one and zero). If, on the other hand,  $f$  at load increment  $i$  is between the yielding force  $f_{yld}$  and the ultimate force  $f_{ult}$ , then the degradation factor for the second linear portion of the graph is calculated (a value between one and zero, but less than the previous value). As mentioned in Section 3.1, the cracking, yielding and ultimate member-section capacities are obtained from *Response* and included in the input file of the program developed by this study.

As discussed in Chapter 2, the element stiffness matrix is calculated for each member accounting for geometric nonlinearity and shear deformation. The stiffness degradation factors are used to modify the elastic stiffness coefficients in the element stiffness matrix to account for post-elastic behaviour. During stage-zero and stage-two elastic analysis, all degradation factors  $r$ ,  $t$  or  $n$  have a value of unity. In stage-one or stage-three inelastic analysis, however, the degradation factors may have values between one and zero which, from Section 2.7, are used to modify the stiffness coefficients.

Once a reinforced concrete member-section undergoes complete post-elastic stiffness degradation ( $f > f_{ult}$  and  $r$ ,  $t$ , or  $n = 0$ ), it is assumed that it loses all capacity to resist load (e.g., total flexural failure due to crushing of concrete in the compression zone and rupture of the steel in the tension zone) and the member is considered disengaged from the remaining structure. Once the degradation factors are calculated, a check is performed to determine whether any member-sections are completely degraded ( $r$ ,  $t$ , or  $n = 0$ ). If no member-section is yet fully degraded, the incremental analysis continues and the stiffness degradation factors are retained for later use in modifying the elastic stiffness coefficients in the element stiffness matrix. If a member-section does become fully degraded, the member is assumed to disengage from the structure at that section, the inelastic incremental analysis is terminated, and an elastic-unloading analysis is conducted as discussed in Section 3.3.

The program tracks the deterioration of post-elastic stiffness and determines when a material failure occurs. It also determines if a stability failure occurs by way of an Euler buckling check. The Euler buckling load is given by,

$$P_E = \frac{\pi^2 EI}{L^2} \quad (3.10)$$

while the critical buckling load, which takes into account the rotational end restraints of the member, is given by,

$$P_C = \frac{\pi^2 EI}{(kL)^2} \quad (3.11)$$

where  $EI$  is the flexural stiffness of the column and  $k$  is an effective length factor. The value of  $EI$  in Eq. (3.11) must take into account the effects of cracking, creep and the non-linearity of the stress-strain curve at the time of failure (MacGregor & Bartlett, 2000). CSA Standard A23.3-94 approximates the flexural stiffness as,

$$EI = \frac{0.2E_c I_g + E_s I_{st}}{1 + \beta_d} \quad (3.12)$$

where  $E_c$  is Young's modulus of elasticity of the concrete,  $I_g$  is the moment of inertia of the gross concrete section,  $E_s$  is Young's modulus of elasticity of the reinforcing steel and  $I_{st}$  is the moment of inertia of the reinforcing steel about the centroidal axis of the cross section. The denominator term, in which  $\beta_d$  is the ratio of the maximum factored axial dead load to the total factored axial load, represents the effect of creep due to sustained loads (MacGregor & Bartlett, 2000).

The advantage of using Eq. (3.12) is that it explicitly takes into account the contribution of the reinforcement to the flexural stiffness of the cross section; however, it is more time consuming to calculate. CSA A23.3-94 also gives a simpler method of approximating the flexural stiffness as,

$$EI = 0.25E_c I_g \quad (3.13)$$

Both equations represent lower bound values obtained from experiments; however, Eq. (3.12) is less conservative than Eq. (3.13) (Pillai, Kirk & Erki, 1999). It is felt that using Eq. (3.13) is warranted for this study due to the fact that only gross section properties are needed to calculate it

(thus making it easy to implement in an incremental analysis program) and because it is more conservative.

### 3.3 Stage Two Elastic-Unloading Analysis

After a member-section is subject to complete post-elastic stiffness degradation due to exceeding its ultimate load resistance and thus disengages from the structure, it is required to determine whether the associated member disengagement creates a local or global instability. A global instability means that part or all of the structure has collapsed to ground level, at which point the analysis fully terminates. A local instability means that part of the structure has disengaged from the main structure but not so as to cause collapse to ground level (e.g. a beam detaching from a joint at one end). If a local instability occurs, the analysis is continued by first conducting an elastic-unloading analysis.

A stage-two elastic-unloading analysis is required to determine the effects of the local instability on the remaining modified structure. As an example, a portal frame is shown in Figure 3.3 that has undergone a local instability, i.e. the right end of the beam has disengaged from the structure due to complete post-elastic stiffness degradation. The disengagement has not caused any portion of the structure to collapse to ground level, i.e. the columns remain erect and the beam now forms a cantilever. The member-end forces that exist at the end of the beam at the time of the disengagement immediately reduce to zero and thus the remaining structure experiences an abrupt change to its state of equilibrium. Stage-two elastic-unloading analysis models this.

The elastic-unloading analysis models this abrupt change by applying the member-end forces that existed at the beam-end at the time of the disengagement, to the beam-end, but in an opposite sense so that the net forces acting at the beam-end are zero. Figure 3.4 shows an axial force, shear force and bending moment at the beam-end at the instant before the disengagement. For the one-step elastic-unloading analysis the vector of nodal loads used for solving Eq. (3.1) consists of the axial force, shear force and bending moment acting at the beam-end but in an opposite sense. Figure 3.5 shows the nodal loads used in the elastic-unloading analysis. Notice that they are in the opposite sense to the member-end forces at the instant before the disengagement (Figure 3.4). Once the elastic-unloading analysis is complete, the before unloading member-end forces are added to the unloading member-end forces to obtain the after unloading member-end forces. The result is that the member-end forces at the free end of the beam are zero while the remaining structure is in a new state of equilibrium due

to the member-section failure. Although the member-sections of a structure may be at various degrees of post-elastic stiffness degradation at the time of a member-section failure, the unloading analysis is elastic, i.e., the stiffness degradation factors all have a value of unity, so as to simply obtain an approximate reaction to the member-section failure. The after unloading member-end forces and nodal displacements form the starting basis from which to continue with the inelastic analysis on the modified structure.

### 3.4 Stage Three Reloading Inelastic Analysis

Once an elastic-unloading analysis is complete, the incremental inelastic analysis resumes. The incremental analysis resumes at total load factor level  $\lambda_{j+1}$ , which is the total load factor level at which the member-section failure occurred to initiate the elastic-unloading analysis. The total load factor level for subsequent load increments is given by,

$$\lambda = \lambda_{j+1} + \Sigma \Delta \lambda_{(j+1)i} \quad (3.14)$$

where, again,  $\lambda_{j+1}$  is the total load factor level at which a member-section failure occurred to initiate an elastic-unloading analysis, and  $\Sigma \Delta \lambda_{(j+1)i}$  is the sum of the incremental load factor levels from after the elastic-unloading analysis to increment  $i$ .

The concept of debris loads and how they are applied in the program is now discussed. As stated in Section 3.2, a member-section subject to complete post-elastic bending, shearing, or axial stiffness degradation, is considered disengaged from the structure due to its inability to resist load. As discussed further in Section 3.3, a beam-member with one end subject to complete post-elastic stiffness degradation creates a local instability if the member-section failure does not cause collapse of the structure to ground level. A beam-member where both ends are subject to complete post-elastic stiffness degradation can also create a local instability if it falls onto the members below it without causing collapse to ground level.

Figure 3.6 shows a single bay, two storey structure. The ends of beam-member 1 have undergone complete post-elastic stiffness degradation such that they are no longer able to resist load and disengage from the structure. Beam-member 1 now falls down onto beam-member 2 below as an amplified debris load. Debris loads are assumed to act as uniformly distributed loads on the members below. Debris loads are comprised of the gravity load of the displaced member multiplied by a dynamic load amplification factor,

$$\alpha = \frac{\alpha^*}{1 - \lambda_{j+1}} \quad (3.15)$$

where  $\alpha^*$  is a dynamic load impact factor and the denominator term ensures that the full magnitude of the displaced gravity load is accounted for in the succeeding stages of the analysis (Liu, 2007). The dynamic load impact factor accounts for the fact that the load is no longer static. A large value of the dynamic load impact factor is indicative of a small amount of dynamic damping in the structure whereas a small value of the dynamic load impact factor is indicative of a large amount of dynamic damping. The debris load then, due to falling beam-member 1, is  $\alpha w_1$ , where  $w_1$  is the gravity load acting on beam-member 1. The load on beam member 2 below, which is the load that is applied to commence the reloading inelastic analysis, is equal to the full magnitude of the gravity load acting on member 2, plus the amplified debris load from falling member 1. Debris loads are discussed further in Chapter 4.

The load is incrementally applied and the stiffness degradation factors are calculated and the degree of post-elastic stiffness degradation is tracked. The analysis continues until either the full target load level is reached, i.e.  $\lambda = 1$ , or a progressive collapse to ground level occurs before that point. The incremental analysis stops and the results output once the target load level reaches unity during a stage-one or stage-three analysis. Output results are discussed in Chapter 4. Further aspects of the analysis procedure (Figure 3.7) are illustrated in the examples of Chapter 4.

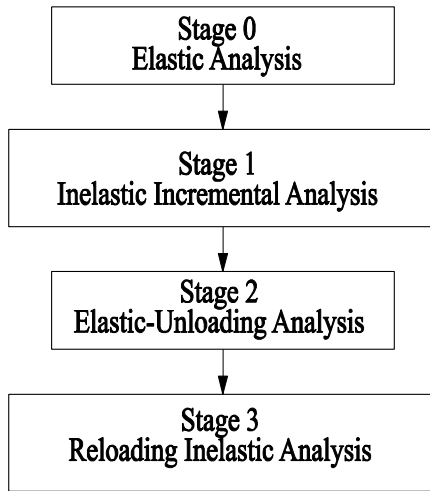


Figure 3.1: Four-stage analysis procedure

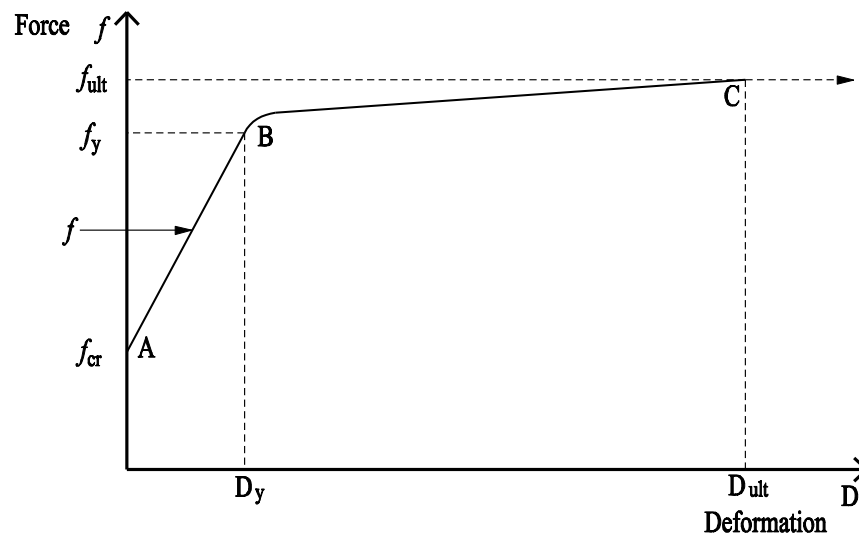
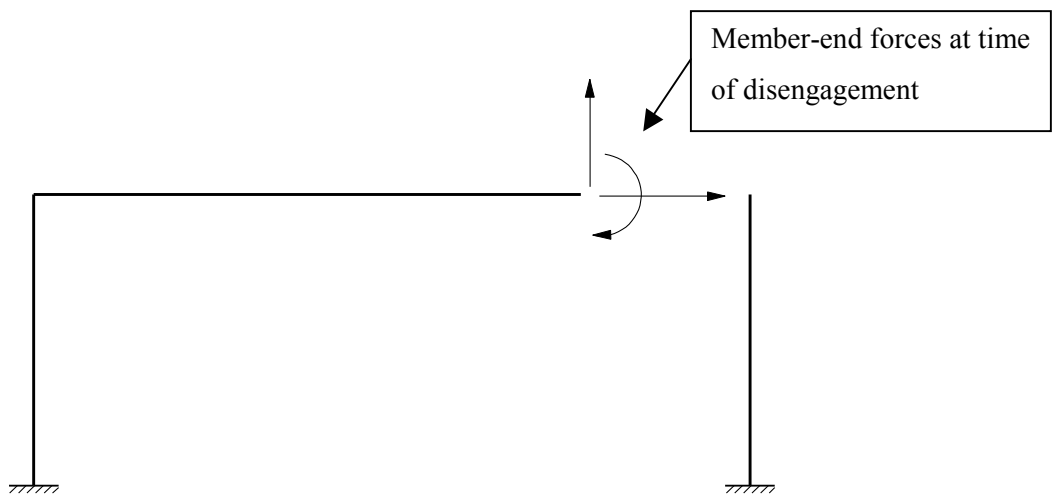


Figure 3.2: General trilinear post-elastic force-deformation response



**Figure 3.3: Local instability**



**Figure 3.4: Member-end forces at time of disengagement**

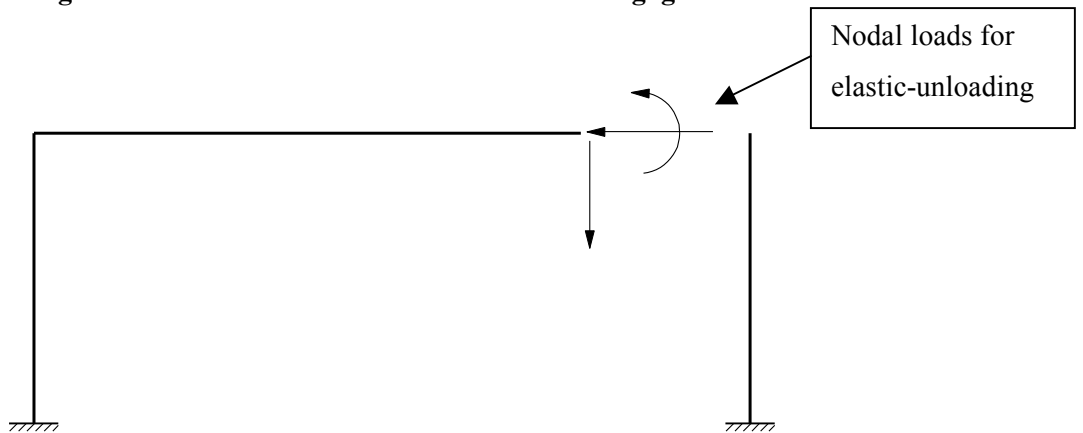


**Figure 3.5: Elastic-unloading nodal loads**



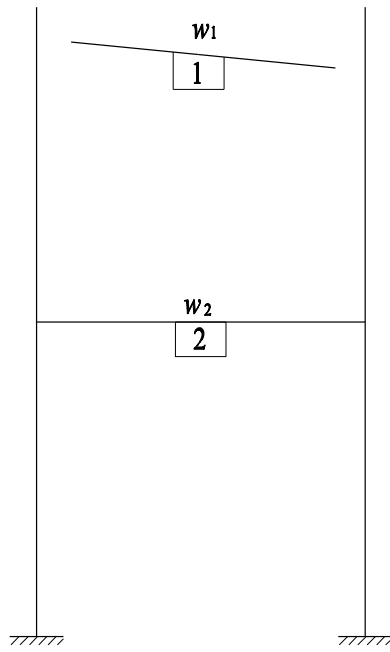


**Figure 3.6: Falling debris load**

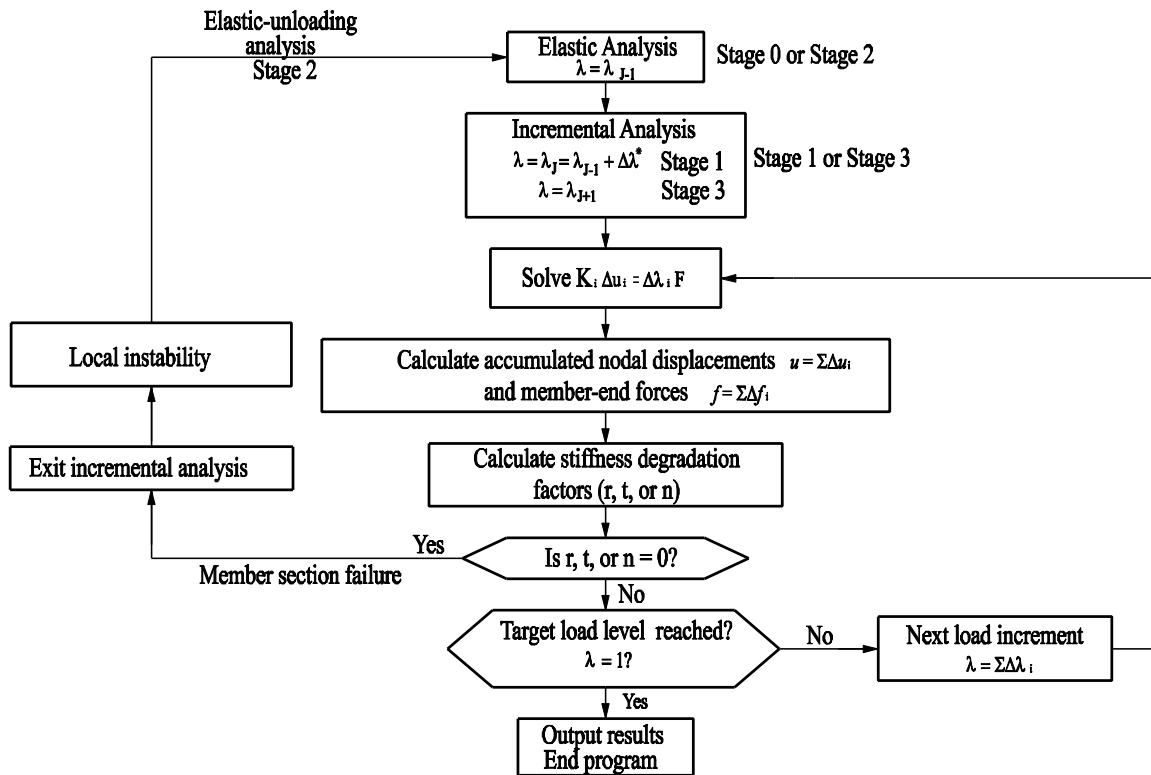


Figure 3.7: Analysis procedure

## **Chapter 4**

### **Example Problems**

The computer program developed by this study for the nonlinear analysis of reinforced concrete frames subject to normal and abnormal loads is demonstrated in this chapter through a series of example problems. The first is a simple portal frame used to illustrate the features of the analysis procedure and the various outputs from the program. The second example is a 2 bay-2 storey frame, used to illustrate the analysis procedure for a common building frame. The final example concerns the same 2 bay-2 storey frame with, however, some initial damage assumed to be caused by some abnormal loading event, and serves to illustrate the program's capability to conduct a progressive collapse analysis. To begin, the principles underlying the design of the reinforced concrete frames are explained. Then, the output data provided by the analysis computer program is described.

#### **4.1 Reinforced Concrete Frame Design**

The loads acting on the reinforced concrete frames are established in accordance with Part 4 of the 1995 National Building Code of Canada (NRCC, 1995). The use and occupancy of the frames is assumed to be an office area above the first storey and, thus, has a minimum specified live load of 2.4 kPa. Climatic information is taken from the region of Waterloo, Ontario, which has a ground snow and rain load of 1.8 and 0.4 kPa, respectively. The 1/100 hourly wind pressure is 0.42 kPa. Seismic loads are not accounted for.

The reinforced concrete frames are designed according to CSA A23.3-94 - Design of Concrete Structures (CSA, 1994). Limit States Design is used and all resistances and loads are appropriately factored. The slab thickness of the frames is 250 mm and the frame dimensions are based on typical dimensions from examples in the Concrete Design Handbook (CAC, 1995). An elastic analysis was performed on the frames with the aforementioned factored loads in order to determine the design forces for member-sections. Refer to Appendix C for the detailed designs of the frames presented in this chapter.

Note that although the initial frame designs account for both factored wind and gravity loads acting on the structure, their subsequent post-elastic incremental analysis accounts only for factored gravity loads due to the unlikely scenario that full gravity and full wind load will simultaneously act on the structure when it is subjected to some abnormal loading event.



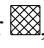
## 4.2 Analysis Program Outputs

The developed program can output a wide variety of information; however, there is specific information that is significant to this study. The output information is presented in the following and includes stiffness degradation factors, member-section failure warnings, percent degradation, member-end forces, nodal displacements, and member-end post-elastic deformation.

As the incremental analysis progresses, different member-sections enter the post-elastic range. It is therefore desirable to know the magnitude of post-elastic stiffness degradation at any particular point in the load history, and not just at the end of the analysis. The program records the load factor level and magnitude of the respective stiffness degradation factor for each member-section. One may then determine the load factor level at which post-elastic behaviour begins or when reinforcement starts to yield, etc., for any member-section.

The program also records the load at which a member-section attains complete post-elastic stiffness degradation and fails, and is assumed disengaged from the structure. The program stops the incremental analysis and records the load factor level at which the member-section failure occurs. At this point, as described in Chapter 3, an elastic-unloading analysis is conducted. After the elastic-unloading analysis, the incremental analysis continues until either the full load level has been applied to the structure, or progressive collapse failure has occurred at a lower loading level. At the end of the analysis procedure, the program outputs the member-end forces, nodal displacements and member-end post-elastic deformations in a single output file.

To better understand the forthcoming analysis examples, a series of symbols are employed to designate various degrees of post-elastic behaviour. Figure 4.1 shows the generalized trilinear post-elastic force-deformation response, as used in this study, along with the symbols. Bending, shearing and axial stiffness degradation due to cracking of concrete is represented by a circle, inverted triangle or square, respectively ( $\bigcirc, \nabla, \square$ ). These symbols are shown at the point on the response at which cracking occurs ( $F_{cr}$ ). Bending, shearing and axial stiffness degradation due to yielding of reinforcement is represented by a hatched circle, inverted triangle or square, respectively ( $\textcircled{hatched}, \nabla\text{hatched}, \square\text{hatched}$ ). These symbols are shown on the graph at the point at which yielding of the reinforcement occurs ( $F_{yld}$ ). If a section has fully degraded post-elastic stiffness, the same symbols are used with cross-hatching to indicate that the member-section has failed; i.e., bending, shearing, or axial stiffness

degradation is then represented by , , or , respectively. These symbols are shown on the graph at the end of the loading history.

If there is only partial stiffness degradation, the magnitude of the degradation is inscribed in the symbol and is given by,

$$\text{Percent Degradation} = (1 - r, t, \text{ or } n)100 \quad (4.1)$$

If, for example, a member-section has a bending stiffness degradation factor value of  $r = 0.24$ , then that member-section is considered to be  $(1.0 - 0.24)100 = 76\%$  degraded. The following examples show how these symbols are used in representing the inelastic behaviour of members of a reinforced concrete structure.

### 4.3 Portal Frame

Figure 4.2 shows the geometry and loading of a simple portal frame while Figure 4.3 shows the node and member numbering used for reference. The frame's centre-to-centre height and width are 3600 mm and 7500 mm, respectively. The loading consists of an 83.6 N/mm uniformly distributed load. The column cross sections (Figure 4.4) are 450x450 mm and have a reinforcement ratio of 2.02% with 10M closed stirrups spaced at 250 mm on centre. The beam cross sections (Figure 4.5) are 500x450 mm and have a tension reinforcement ratio of 1.07%, a compression reinforcement ratio of 0.2% and 10M closed stirrups spaced at 150 mm on centre. For positive moment regions along the beam, the reinforcement is as shown in Figure 4.5 whereas for negative moment regions along the beam, the reinforcement is as shown in Figure 4.5 but rotated 180 degrees so that the tension reinforcement (3-30M bars) is at the top of the section. The concrete compressive strength is 35MPa. The tributary width of the frame is 7500 mm, where the concrete slab is assumed to act as a one-way slab. The portal frame has fixed supports at its base. This simple portal frame example serves well to demonstrate the features of the analysis procedure. More redundant frames are dealt with in the other examples.

#### 4.3.1 Post-Elastic Bending Stiffness Degradation

The frame is analyzed to account for degraded post-elastic bending stiffness only. The load is incrementally increased and the program determines when a member-section reaches the post-elastic range. For this example, the load increment factor is set to 0.2% of the total load. Such a small increment factor enables the deterioration of post-elastic stiffness to be precisely tracked.

Figure 4.6 and Figure 4.7 show the post-elastic moment-rotation responses of the beam and column sections, respectively. These figures enable visualization of the response of each section relative to the stage of the analysis. The points at which the sectional stiffness changes are indicated along with the corresponding moment magnitudes. The beam has a cracking moment resistance of 37 kN-m, a yield moment resistance of 324 kN-m and an ultimate moment resistance of 367 kN-m. The column has a cracking moment resistance of 36 kN-m, a yield moment resistance of 462 kN-m and an ultimate moment resistance of 569 kN-m. With regard to the beam's post-elastic moment-rotation response (Figure 4.6), the post-elastic stiffness is infinite up to the point of initial cracking of concrete at moment  $M_{cr} = 37$  kN-m, as indicated by the vertical line at  $\theta = 0$ . At this point there is a reduction in post-elastic stiffness to some lesser value, as indicated by the reduced slope of the response. This stiffness then remains constant until yielding of the reinforcement occurs at moment  $M_{yld} = 324$  kN-m. At this point there is another reduction in post-elastic stiffness, as indicated by a second reduction in the slope of the response. This stiffness then remains constant until the ultimate moment capacity of the section is reached due to crushing of concrete in the compression zone of the cross section at moment  $M_{ult} = 367$  kN-m. The column behaves in an analogous way.

Figure 4.8 to Figure 4.18 show the degradation of post-elastic bending stiffness throughout the load history up to the target load level (load factor level  $\lambda = 1.0$ ). All moment diagrams are plotted on the tension side. At load factor level  $\lambda = 0.124$ , two member-sections enter the post-elastic range due to cracking of concrete in the tension zone of the cross-section, indicated by the circles in Figure 4.8. The amount of partial post-elastic stiffness degradation is inscribed in the circles: column member-sections 1-3 (member 1, node 3) and 2-5 are each 42% degraded (i.e., from Eq. (4.1), their bending stiffness degradation factor  $r = 0.58$ ). The bending moment diagram at the load factor level  $\lambda = 0.124$  is shown in Figure 4.9. Notice that the magnitude of the bending moment for the columns at the location they join the beams is 36.3 kN-m. This moment just surpasses the magnitude of the column's cracking moment resistance (36.0 kN-m) and hence why the columns at these two points enter the post-elastic range. On the column's moment-rotation response (Figure 4.7), the column-section is at the point marked  $M_{cr}$ . Prior to this point, the entire moment-rotation response was elastic (following the vertical line at post-elastic rotation  $\theta = 0$  on the response). Now that the moment in the column-section has reached  $M_{cr}$ , there is a reduction in post-elastic bending stiffness and the column-section follows the response of the reduced slope between  $M_{cr}$  ( $\theta = 0$ ) and  $M_{yld}$  ( $\theta = 0.005$ ).

On the other hand, the beam's cracking moment resistance is slightly larger (37.0 kN-m), which is why the beam is not yet in the post-elastic range. At the very next load step, however, the beam moments surpass the beam's cracking moment resistance, thereby entering the post-elastic range. Figure 4.10 shows that at load factor level  $\lambda = 0.126$ , the midspan section of the beam enters the post-elastic range due to cracking of concrete. Beam-members 3-4 and 4-4 are each 58% degraded (i.e.,  $r = 0.42$ ). Figure 4.11 shows the bending moment diagram at load factor level  $\lambda = 0.126$ . Notice that the moment at midspan is 37.1 kN-m. This moment just surpasses the cracking moment resistance of the beam (37.0 kN-m) and hence why the beam-section has entered the post-elastic range. On the beam's post-elastic moment-rotation response (Figure 4.6) the beam-section moment =  $M_{cr}$ . Prior to this point, the entire moment-rotation response was elastic (following the vertical line at post-elastic rotation  $\theta = 0$  on the response). Now that the moment in the beam-section has reached  $M_{cr}$ , there is a reduction in post-elastic stiffness and the beam-section follows the response of the reduced slope between  $M_{cr}$  ( $\theta = 0$ ) and  $M_{yld}$  ( $\theta = 0.005$ ).

Figure 4.12 and Figure 4.13 show the frame response at load factor level  $\lambda = 0.128$ . The end-sections 3-3 and 4-5 of the beam enter the post-elastic range at this point. The moment magnitude at the ends of the beam is 37.6 kN-m, which just surpasses the cracking moment resistance of the beam. The beam end-sections are 58% degraded ( $r = 0.42$ ).

As shown in Figure 4.14, at load factor level  $\lambda = 0.266$ , the base of the columns enter the post-elastic range and attain 42% degradation ( $r = 0.58$ ). From Figure 4.15, the moment at the base of the columns is 36.2 kN-m which just surpasses the cracking moment resistance of the column (36 kN-m). Also notice that the midspan beam moment (83.2 kN-m) is larger than the end moments (73.1 kN-m).

As both the beam and columns follow the same constant slope portion of their respective post-elastic moment-rotation response, there is no change to the structure's degree of post-elastic bending stiffness until load factor level  $\lambda = 0.984$  is reached. Yielding of the tension reinforcement at the midspan of the beam occurs at this point, which causes further reduction in post-elastic bending stiffness there. Figure 4.16 shows that once yielding occurs (indicated by the hatched circle), the midspan section of the beam becomes 99% degraded ( $r = 0.01$ ). Figure 4.17 shows the bending moment diagram at load factor level  $\lambda = 0.984$ . The magnitude of the midspan moment is 324 kN-m, the yield moment resistance of the beam as shown in the beam post-elastic moment-rotation response (Figure 4.6). On this response, the beam-section moment at midspan =  $M_{yld}$ . Once this moment is reached, there is a reduction in post-elastic bending stiffness as is evident from the reduced slope of

the response in Figure 4.6. The beam-section now follows the response of the reduced slope between  $M_{yld}$  ( $\theta = 0.005$ ) and  $M_{ult}$  ( $\theta = 0.041$ ).

Between the load factor level  $\lambda = 0.984$  and the target load level  $\lambda = 1.0$  (the full factored design load), there is little change in the forces for the frame members, as can be seen by comparing Figure 4.17 and Figure 4.18, and no change in the degree of post-elastic bending stiffness degradation. At the target load level then, the frame remains intact with some degree of post-elastic bending stiffness degradation at each member-section and with the reinforcement yielding at the beam midspan, as shown in Figure 4.16. The column-sections are each 42% degraded ( $r = 0.58$ ) while the beam end-sections are each 58% degraded ( $r = 0.42$ ). The midspan of the beam is 99% degraded ( $r = 0.01$ ).

The user may increase the load on the structure beyond the target load level ( $\lambda = 1.0$ ) until a failure state is reached. Continuing the analysis shows that at load factor level  $\lambda = 1.12$  the beam end-sections become 99% degraded ( $r = 0.01$ ) as shown in Figure 4.19. The accompanying bending moment diagram (Figure 4.20) shows that the moments at the ends of the beam have a magnitude of 324 kN-m, which is equal to the yield moment resistance of the beam. At 12% beyond the target load level, the end moments increase in magnitude by a value of 62 kN-m while the midspan moment increases by only 3 kN-m (the bending moments are distributed more to the ends of the beam because the midspan of the beam is yielding and the stiffness there is vastly reduced). In fact, as can be seen from the beam's post-elastic moment-rotation response in Figure 4.6, there is very little increase in midspan bending moment for a large increase in rotation.

With the tension reinforcement now yielding in the beam in both the positive and negative moment regions, the loading level is further increased. At load factor level  $\lambda = 1.25$  the midspan and ends of the beam simultaneously reach their ultimate moment resistance and fail due to crushing of concrete in the compression zone (designated by the cross-hatch symbol in Figure 4.21). This is associated with a bending stiffness degradation factor of  $r = 0$ , indicating that there is no post-elastic bending stiffness and complete degradation has occurred. The bending moments in the beam (Figure 4.22) have a magnitude of 367 kN-m, which is equal to the ultimate bending moment resistance of the beam as shown in Figure 4.6. The larger of the end moments in the two columns have a magnitude of 367 kN-m; however, the column-sections still remain within the first constant stiffness region of their post-elastic moment-rotation response as shown in Figure 4.7 (between  $M_{cr}$  ( $\theta = 0.005$ ) and  $M_{yld}$  ( $\theta = 0.061$ )).



Once the beam member-sections fail due to crushing of concrete in the compression zone, they are also assumed to be unable to resist shear and axial forces and the member-section is for all intents and purposes disengaged from the structure. The entire beam at this point is therefore unable to carry load and the frame has effectively failed. Thus, the analysis shows that as the load further increases and the frame's post-elastic bending stiffness continues to deteriorate, the frame may be loaded up to 1.25 times its factored design load level before structural failure occurs due to crushing of concrete in the compression zone of the cross-sections at the ends and midspan of the beam.

### 4.3.2 Post-Elastic Shear Stiffness Degradation

The frame is analyzed to account for degraded post-elastic shear stiffness only. The load is incrementally increased and the program determines when a member-section reaches the post-elastic range. Figure 4.23 and Figure 4.24 show the post-elastic shear force-shear deformation response of the beam and column sections, respectively. The points at which the sectional stiffness changes are indicated along with the corresponding shear force magnitudes. The beam has a cracking shear resistance of 224 kN, a yield shear resistance of 346 kN and an ultimate shear resistance of 391 kN. The column has a cracking shear resistance of 202 kN, a yield shear resistance of 307 kN and an ultimate shear resistance of 377 kN.

Similar to the moment-rotation response discussed in Section 4.3.1, there exists an infinite amount of post-elastic shear stiffness (indicated by the vertical slope of the response at  $\tau = 0$ ) up to the point of initial cracking of concrete of the beam at shear force  $V_{cr} = 224$  kN (Figure 4.23). The cracking discussed here, however, is not flexural cracking due to bending, but is instead diagonal cracking due to shear. Once the cracking shear resistance is reached, there is a reduction in post-elastic shear stiffness to some lesser value, as indicated by the reduced slope of the response. The stiffness then remains constant until the transverse reinforcement yields at shear force  $V_{yld} = 346$  kN. At this point there is another reduction in post-elastic stiffness as indicated by a second reduction in the slope of the response. This stiffness then remains constant until the ultimate shear capacity of the section is reached due to crushing of concrete in the principal compressive direction at shear force  $V_{ult} = 391$  kN. The column behaves in an analogous way.

Figure 4.25 to Figure 4.31 show the degradation of post-elastic shear stiffness throughout the load history up to the target load level (load factor level  $\lambda = 1.0$ ). At load factor level  $\lambda = 0.716$ , the ends of the beam (member-sections 3-3 and 4-5) enter the post-elastic range due to diagonal shear

cracking, indicated by the inverted triangles in Figure 4.25. The amount of partial post-elastic stiffness degradation is inscribed in the triangles: beam member-sections 3-3 and 4-5 are each 24% degraded (i.e., from Eq. (4.1), their shear stiffness degradation factor  $t = 0.76$ ). The shear force diagram at load factor level  $\lambda = 0.716$  is shown in Figure 4.26. The shear force at the ends of the beam is 224 kN which is equal to the cracking shear resistance of the beam and hence why the beam end-sections enter the post-elastic range. On the beam post-elastic force-deformation response (Figure 4.23) the beam end-sections are at the point marked  $V_{cr}$ . Prior to this point, the force-deformation response has been entirely elastic and has followed the vertical line at  $\gamma_d = 0$ . Now that the shear force in the beam-sections has reached  $V_{cr}$ , there is a reduction in post-elastic shear stiffness and the beam-sections follow the response of the reduced slope between  $V_{cr}$  ( $\gamma_d = 0$ ) and  $V_{yld}$  ( $\gamma_d = 5.3$  mm). The shear force in the columns is a constant 87.5 kN which is not close to the 202 kN cracking shear resistance of the column and is why it remains in the elastic range.

As the beam follows the constant slope portion of its post-elastic force-deformation response, there is no change to the structure's degree of post-elastic shear stiffness between the load factor level  $\lambda = 0.716$  and the target load level ( $\lambda = 1.0$ ). The magnitude of the shear forces increase however, as can be seen by comparing Figure 4.26 and Figure 4.27. The beam-end shear force is 314 kN while the columns have a constant shear force of 122 kN. At the target load level then, the frame remains intact while only beam member-sections 3-3 and 4-5 exhibit any post-elastic shear stiffness degradation. All other member-sections remain in the elastic range.

As in the case of degraded bending stiffness from the previous example, the user may increase the load on the structure beyond the target load level ( $\lambda = 1.0$ ) until a failure state is reached. Continuing the analysis shows that at load factor level  $\lambda = 1.10$  the transverse reinforcement at the ends of the beam yields, indicated in Figure 4.28 by the hatched inverted triangles. The beam end-sections are 45% degraded ( $t = 0.55$ ). The accompanying shear force diagram (Figure 4.29) indicates that the shear force at the ends of the beam is 346 kN which is equal to the yield shear resistance of the beam. With regard to the beam's post-elastic force-deformation response (Figure 4.23), the beam end-sections are at the point marked  $V_{yld}$ . There is another reduction in post-elastic shear stiffness and the beam end-sections follow the response of the reduced slope between  $V_{yld}$  ( $\gamma_d = 5.3$  mm) and  $V_{ult}$  ( $\gamma_d = 10.4$  mm). The shear force in the columns is 135 kN which is still below the cracking shear resistance of the columns (202 kN) and is why they remain in the elastic range.

With the transverse reinforcement at the ends of the beam yielding, the loading level is further increased. At load factor level  $\lambda = 1.25$  the ends of the beam reach their ultimate shear resistance and fail due to crushing of concrete in the diagonal compression struts (designated by the cross-hatched symbol in Figure 4.30). This is associated with a shear stiffness degradation factor of  $t = 0$ , indicating that there is no post-elastic shear stiffness and complete degradation has occurred. The shear force in the ends of the beam has a magnitude of 391 kN (Figure 4.31) which is equal to the ultimate shear resistance of the beam as shown in Figure 4.23. The column shear force is equal to 153 kN, which is below the column's cracking shear resistance and therefore remains in the elastic range of response.

Once the beam member-sections fail due to crushing of concrete in the diagonal compression struts, they are also assumed to be unable to resist bending moment and axial force and the member-sections are further assumed to disengage from the structure. The beam at this point is unable to carry any more additional load and the frame has effectively failed. Thus, the analysis shows that as the load further increases and the frame's post-elastic shear stiffness continues to deteriorate, the frame may be loaded up to 1.25 times its factored design load level before structural failure occurs due to crushing of concrete in the compression struts at the ends of the beam. Note that the beam fails in shear at the same load factor ( $\lambda = 1.25$ ) as the beam fails in bending, when each type of degradation is applied separately.

### **4.3.3 Post-Elastic Axial Stiffness Degradation**

The frame is analyzed to account for degraded post-elastic axial stiffness only. The load is incrementally increased and the program determines when a member-section reaches the post-elastic range. For this analysis, only post-elastic axial degradation of columns is accounted for. This is due to the fact that beams will develop small axial forces (relative to the columns) and not experience any post-elastic axial stiffness degradation. The axial forces in the beams are, however, accounted for through the use of stability functions in the bending and shearing elastic stiffness coefficients of the element stiffness matrix as discussed in Section 2.7. It should also be noted that buckling is explicitly checked for in the analysis; however, the critical buckling load for the column of this example is quite high ( $P_c = 17,265$  kN). Buckling does not, therefore, preclude material failure of the column as will be shown.

Figure 4.32 shows the post-elastic axial compressive force-axial deformation response of the column-section. Figure 4.32 shows that there exists an infinite amount of post-elastic axial stiffness

(indicated by the vertical slope of the response at  $\delta = 0$ ) up to the point at which elastic behaviour ceases (40% of the ultimate compressive force as discussed in Section 2.5.1). Once the compressive force reaches 40% of the ultimate compressive resistance of the column does the column-section enter the post-elastic range. This occurs at a compressive force of 3830 kN as indicated in Figure 4.32. Once the compressive force reaches 3830 kN, there is a reduction in post-elastic axial stiffness as indicated by the reduced slope of the response. The post-elastic axial stiffness then remains constant as the column-section follows the response of the reduced slope between  $0.4P_{ult}$  ( $\delta = 0$ ) and  $P_{ult}$  ( $\delta = 4.93$  mm).

Figure 4.33 shows the frame at load factor level  $\lambda = 1.0$ . The compressive force in the columns is 345 kN which is only a fraction of the 3830 kN compressive force needed in order for the column-sections to enter the post-elastic range. Since at load factor level  $\lambda = 1.0$  the structure is fully in the elastic range, the analysis continues beyond the target load level. Figure 4.34 shows the frame at load factor level  $\lambda = 12.35$ . The compressive force in the columns is 3830 kN and the column-sections enter the post-elastic range, indicated in Figure 4.34 by the squares at the column ends. The amount of partial post-elastic axial stiffness degradation is inscribed in the squares: column-sections are each 56% degraded (i.e., from Eq. (4.1), their axial stiffness degradation factor  $n = 0.44$ ). If the load factor level is increased further, the column-sections become fully degraded and reach their ultimate compressive resistance at load factor level  $\lambda = 30.6$ , indicated in Figure 4.35 by the cross-hatched squares. The compressive force in the columns is 9575 kN which is equal to the ultimate compressive resistance of the column as shown in Figure 4.32. Once the column-sections fail due to crushing of concrete, they are also assumed to be unable to resist bending moment and shear force and the column-sections are for all intents and purposes disengaged from the structure. The columns at this point are unable to carry any more additional load and the frame has therefore failed.

Although the analysis shows that the frame may be loaded up to 30.6 times its factored design load level before structural failure occurs due to crushing of concrete, it must be understood that this analysis strictly involves degraded post-elastic axial stiffness only. That is to say, if post-elastic bending or shearing stiffness degradation was accounted for, the frame would have failed at a much lower load level as shown in Figure 4.21 and Figure 4.30. The bending moment at the midspan of the beam at load factor level  $\lambda = 30.6$ , for example, is 8990 kN-m, which greatly exceeds the beam's ultimate moment resistance of 367 kN-m as discussed in Section 4.3.1. This example does illustrate,

however, that post-elastic axial stiffness degradation for reinforced concrete columns is not a major contributor to the eventual failure of the frame at an abnormal load level.

The preceding example of Section 4.3 was used to illustrate the analysis procedure and output results on a simple frame. The analysis procedure is now presented on a larger system, with more structural redundancy.

#### **4.4 2 Bay - 2 Storey Frame**

Figure 4.36 shows the geometry and loading of a 2 bay-2 storey reinforced concrete frame while Figure 4.37 shows the node and member numbering used for reference. The frame's centre-to-centre width is 3750 mm in the shorter bay and 7500 mm in the larger bay. All columns are 3600 mm high. The loading consists of a 60.6 N/mm and 56.4 N/mm uniformly distributed load on the first and second storey, respectively. The beam cross sections (Figure 4.38) are 500x350 mm with a tension reinforcement ratio of 1.04%, a compression reinforcement ratio of 0.26% and 10M closed stirrups spaced at 250 mm on centre. For positive moment regions along the beam, the reinforcement is as shown in Figure 4.38 whereas for negative moment regions along the beam, the reinforcement is as shown in Figure 4.38 but rotated 180 degrees so that the tension reinforcement (4-25M) is at the top of the section. The column cross sections (Figure 4.39) are 350x350 mm with a reinforcement ratio of 2.1% and 10M closed stirrups spaced at 200mm on centre. There are fourteen total members (six column members and eight beam members). The tributary width of the frame is 5000 mm where the concrete slab transferring load to the frame is assumed to act as a one-way slab. The frame has fixed supports at its base.

##### **4.4.1 Post-Elastic Bending Stiffness Degradation**

The frame is analyzed to account for degraded post-elastic bending stiffness only. The load increment is set to 1% of the total design load. The load is incrementally increased and the program determines when a member-section reaches the post-elastic range. The post-elastic force-deformation response of the frame member-sections is not given here, as it is similar to the response of the member-sections used in Section 4.3, but may be found in Appendix D. The beam cracking moment resistance is 30 kN-m, the yield moment resistance 308 kN-m ( $\theta_{yld} = 0.0044$  rad) and the ultimate moment resistance 331 kN-m ( $\theta_{ult} = 0.0228$  rad). The column cracking moment resistance is 16 kN-

m, the yield moment resistance 201 kN-m ( $\theta_{yld} = 0.0064$  rad) and the ultimate moment resistance 231 kN-m ( $\theta_{ult} = 0.0861$  rad).

Figure 4.40 shows the results of the analysis at the target load factor level  $\lambda = 1.0$ . The circles at the ends of the members are consistent with the symbols developed in Section 4.2 for degraded post-elastic bending stiffness due to cracking of concrete. The amount of partial post-elastic stiffness degradation is inscribed in the circles. Almost all member-sections experience some degree of post-elastic bending stiffness degradation by the time the target load level is reached, except for column 1 member-sections and member-sections 7-5, 8-5, 11-9, 11-10 and 12-10. All beam sections that experience post-elastic bending stiffness degradation are each 55% degraded ( $r = 0.45$ ), while all column sections that experience post-elastic bending stiffness degradation are each 46% degraded ( $r = 0.54$ ). Figure 4.40 also shows the load factor levels at which the member-sections first enter the post-elastic range. Several members (6-8, 6-13, 9-6, 13-11), for example, are first to enter the post-elastic range simultaneously at load factor level  $\lambda = 0.15$ . As the load factor level increases, other member-sections at some point along the load history enter the post-elastic range. Member 7-4 is the last member-section to enter the post-elastic range (at load factor level  $\lambda = 0.65$ ) before the target load level is reached. Between  $\lambda = 0.65$  and  $\lambda = 1.0$  there is no change in the degree of post-elastic bending stiffness degradation for any of the member-sections, albeit the bending moments certainly increase.

These results show that initial flexural cracking has a significant effect on the flexural bending stiffness of the member-sections. Once initial flexural cracking occurs (when the member-end moment reaches the cracking moment resistance) there is an immediate reduction in post-elastic bending stiffness. The new reduced level of post-elastic bending stiffness remains constant until yielding of the reinforcement occurs. For several column and beam members, an average of 50% reduction of post-elastic bending stiffness exists at only 15% of the target load level. Figure 4.40 shows that members 6-8 and 6-13 have bending stiffness degradation factors of  $r = 0.54$  (46% degraded). When these degradation factor values are used in modifying the  $k_{33}$  term in the element stiffness matrix of Eq. (2.20) for example, it translates into a 56% reduction in the elastic stiffness coefficient. That is to say, if we compare the  $k_{33}$  term given by Eq. (2.21e) for the cracked ( $r_1 = r_2 = 0.54$ ) and uncracked ( $r_1 = r_2 = 1.0$ ) fully elastic state, we find that there is a 56% reduction in its value. Again, this occurs at just 15% of the target load level.

The bending moment diagram plotted on the tension side of the frame is shown in Figure 4.41 at load factor level  $\lambda = 1.0$ . Any member-section for which post-elastic bending stiffness degradation is indicated will have a moment magnitude which exceeds its cracking moment resistance (30 kN-m for beams, 16 kN-m for columns). Column 1 shows no post-elastic bending stiffness degradation in Figure 4.40. Accordingly, the bending moment diagram indicates that its end moments are 15 kN-m. Beam members 7-5, 8-5, 11-10, and 12-10 also show no post-elastic bending stiffness degradation. Their bending moments are 14, 14, 2, and 2 kN-m, respectively, which is below the cracking threshold for beams. The largest bending moments at the target load level exist in the lower and upper beams of the larger bay at the interior column (members 9-6 and 13-11) and have magnitude 253 kN-m and 239 kN-m, respectively.

At the target load level then, the frame remains intact with some degree of post-elastic bending stiffness degradation at most member-sections. The user may increase the load on the structure beyond the target load level ( $\lambda = 1.0$ ) until a failure state is reached. Continuing the analysis shows that at load factor level  $\lambda = 1.51$  member-section 13-11 becomes 100% degraded ( $r = 0.0$ ) as shown in Figure 4.42. The load factor levels shown beside the degradation symbols indicate when a member-section's post-elastic bending stiffness changes between the target load level  $\lambda = 1.0$  and  $\lambda = 1.51$ . That is to say, the load factor level is shown if at the target load level a member-section was fully elastic or cracked, and now, beyond the target load level a member-section is cracked or yielding. Several members that at the target load level were still fully in the elastic range, now experience post-elastic bending stiffness degradation. Member-sections 1-1, 11-9, 1-4, 7-5, and 8-5 enter the post-elastic range due to flexural cracking at load factor levels 1.03, 1.03, 1.06, 1.39, and 1.39, respectively. Column member-sections 1-1 and 1-4 have bending stiffness degradation factors  $r = 0.54$  while the other beam member-sections have degradation factors  $r = 0.45$ .

Several other member-sections that previously entered the post-elastic range due to flexural cracking, now undergo further bending stiffness degradation due to yielding of their tension reinforcement. Beam member-sections 9-6, 13-11, 9-7, 10-7, 13-12, 14-12, and 10-8 yield at load factor levels 1.23, 1.30, 1.36, 1.36, 1.36, 1.36, and 1.49, respectively. These member-sections are now each 98% degraded ( $r = 0.02$ ). Column member-section 6-13 yields at load factor level 1.46 and is 99% degraded ( $r = 0.01$ ).

The frame exhibits considerable ductility. Several member-sections continue to resist bending moment and deform after their reinforcement yields. Member-section 9-6, which is the first to yield

at load factor level 1.23 and  $M = 308$  kN-m, remains intact at load factor level 1.51. This shows that the load on the structure may be increased by  $100(1.51-1.23) = 28\%$  beyond the point of initial yielding of the member-section, while maintaining its ability to resist moment. Its member-end post-elastic deformation at load factor level 1.23 is  $\theta = 0.0044$  rad. The post-elastic deformation increases to  $\theta = 0.0183$  rad for an increase in load of only 28%. The post-elastic deformation from yielding to the end of the analysis (an increase in load of 28%) is 3.1 times larger than the post-elastic deformation from cracking ( $\lambda = 0.15$ ) up to yielding ( $\lambda = 1.23$ ) (an increase in load of 108%). Member-sections 9-7, 10-7, 13-12 and 14-12 that yield at load factor level 1.36, continue to resist bending moment and deform for at least an increase of  $100(1.51-1.36) = 15\%$  of load. They could perhaps deform more, but are unable to because another member-section reaches its ultimate capacity, thereby ending the inelastic analysis. Member-section 13-11, which yields at load factor level 1.30, can resist moment and deform for an additional increase of  $100(1.51-1.30) = 21\%$  of the load before it reaches its ultimate capacity (at load factor level  $\lambda = 1.51$ ) and effectively disengages from the structure. Its member-end post-elastic deformation at load factor level 1.30 is  $\theta = 0.0044$  rad. At load factor level 1.51 its post-elastic deformation is  $\theta = 0.0228$  rad, which is 4.2 times larger than the post-elastic deformation from the time post-elastic behaviour began ( $\lambda = 0.15$ ) up to yielding ( $\lambda = 1.30$ ).

The bending moment diagram for the frame at load factor level  $\lambda = 1.51$  is shown in Figure 4.43. The beam's ultimate moment resistance is 331 kN-m and the figure shows that member-section 13-11 is the first member-section to reach this point. Member-section 13-11 exceeds its ultimate moment resistance and fails due to crushing of concrete in the compression zone of the cross section. The member-section at this point is 100% degraded ( $r = 0.0$ ). At the target load level, the largest end-moment in the frame was located at member 9-6 (Figure 4.41). This was also the first member-section to yield. As a consequence of this member-section yielding first, the moment distribution in the frame was altered due to the vastly reduced bending stiffness at this particular section. Member-section 13-11 was the second section to yield in the frame. This too caused the bending moments in subsequent loading increments to redistribute due to the reduced bending stiffness. As more members began to yield and cause the moments to redistribute, member-section 13-11 was consequently the first to reach its ultimate moment resistance.

A concrete section is unable to maintain its ultimate moment capacity once it is subject to complete post-elastic bending stiffness degradation. There is some further deformation, however, but this



occurs through a decreasing load. This study ignores the unloading phenomenon and considers the point at which the section reaches its ultimate moment resistance the end of its post-elastic force-deformation response.

As previously stated, member-section 13-11 reaches the end of its post-elastic force-deformation response at load factor level  $\lambda = 1.51$  and effectively disengages from the structure. At this point the structure experiences an unloading phenomenon whereby the restraint provided by the member-end forces at 13-11 and joint 11 is lost. The member-end forces at 13-11 consist of a 331 kN-m counter-clockwise moment, a 336 kN upward shear force and a 104 kN compressive force. The member-end forces acting on joint 11 from member 13-11 are equal in magnitude but opposite in sense. To account for this loss of restraint at joint 11, an elastic-unloading analysis is performed. This is done in the program by applying the opposite sense of the forces that exist at 13-11 to 13-11 and applying the opposite sense of the forces that exist at joint 11 to joint 11 (Figure 4.44). This effectively negates the contributions of these forces to the overall equilibrium of the structure. For the elastic-unloading analysis then, member 13-11 would have a 331 kN-m *clockwise* moment, a 336 kN *downward* shear force, and a 104 kN *tensile* force applied to it. The forces applied to joint 11 would be opposite in sense.

The elastic-unloading analysis assumes elastic behaviour and uses the gross section properties of the members. The elastic-unloading analysis provides a measure of the response of the structure due to the loss of restraint at some member-end(s). The results of the elastic-unloading analysis are shown in the bending moment diagram of Figure 4.45.

Notice first that the bending moment at 13-11 is -331 kN-m, which is equal to the concentrated moment applied there as part of the load vector for the elastic-unloading analysis. Referring back to Figure 4.43 shows that the bending moment prior to unloading was +331 kN-m such that the net result after unloading is that there is zero member-end moment at 13-11. Such is the case for shear force and axial force also. The net effect produces zero member-end forces at the detached member-section as is expected for what is now the free end of a cantilever. The resulting unloading (or loss of restraint of 13-11) has relatively little effect on the smaller bay when compared to that for the larger bay. The larger bay (whose top-most member is now a cantilever) has large bending moments in the columns and beams, the largest of which is 2579 kN-m. To determine what effect the unloading has on the overall structure and its post-elastic bending stiffness, the before unloading member-end

moments are added to the elastic-unloading member-end moments to obtain the after unloading member-end moments. The results are shown in Figure 4.46.

Figure 4.46 shows that losing the restraint of member-section 13-11 at load factor level  $\lambda = 1.51$  results in the complete destruction of the larger bay. The cross-hatched circles, shown in Figure 4.46 are indicative of complete post-elastic bending stiffness degradation as discussed in Section 4.2. The smaller bay is only partially destroyed, yet enough to cause collapse to ground level. Figure 4.46 shows member-section 13-11 detached from the structure to symbolize that no forces exist there and that it provides no restraint to the gravity loads acting on the member. Comparing Figure 4.42 to Figure 4.46 shows the increase in post-elastic bending stiffness degradation due to the loss of member-section 13-11. All member-sections in the larger bay, which at load factor level 1.51 were either in a cracked state or yielding, are now completely degraded. Furthermore, while at load factor level 1.51 there were several member-sections yet to enter the post-elastic range, all member-sections for the entire structure now experience some degree of post-elastic bending stiffness degradation.

Figure 4.47 shows the bending moment diagram for the frame after the elastic-unloading. All bending moments in the larger bay associated with a cross-hatched circle exceed that member-section's ultimate moment resistance. This is also true for columns 1 and 2. In the case of the beams, the ultimate moment resistance is 331 kN-m and in the case of the columns it is 231 kN-m.

The bending moments for column member-sections 4-9 and 5-11 and for beam member-sections 11-9 and 12-11 are below those member-section's respective cracking moment resistance (16 kN-m for columns and 30 kN-m for beams), yet Figure 4.46 shows that they are all in the post-elastic range. This occurs because a member-section cannot regain post-elastic stiffness. That is to say, beam member-section 11-9 for example, entered the post-elastic range at load factor level 1.03. This was because the moment reached the cracking moment resistance and caused the concrete to crack in the tension zone of the cross section. The subsequent unloading caused the magnitude of the bending moment at 11-9 to reduce to 2 kN-m as shown in Figure 4.47, which is below the cracking moment resistance. Once a member-section cracks, however, and reduces its post-elastic bending stiffness, it cannot "uncrack" and regain that stiffness, even if the moment magnitude falls to a value in the elastic range.

If no global instability (total or partial collapse to ground level) had occurred, then the inelastic analysis would continue by further increasing the load level. This is shown in Section 4.5. In this particular case, because a global instability has occurred, the analysis ends. Thus, the analysis shows

that as the load further increases and the frame's post-elastic bending stiffness continues to deteriorate, the frame may be loaded up to 1.51 times its gravity load level before a member-section failure causes complete collapse of the frame to ground level.

#### 4.4.2 Post-Elastic Shear Stiffness Degradation

The frame is analyzed to account for degraded post-elastic shear stiffness only. The load increment is set to 1% of the total design load. The load is incrementally increased and the program determines when a member-section reaches the post-elastic range. The post-elastic force-deformation response of the frame member-sections for shear can be found in Appendix D. The beam has a cracking shear resistance of 174 kN, a yield shear resistance of 239 kN ( $\tau_{\text{yld,short}} = 2.42$  mm,  $\tau_{\text{yld,long}} = 4.84$  mm), and an ultimate shear resistance of 263 kN ( $\tau_{\text{ult,short}} = 5.04$  mm,  $\tau_{\text{ult,long}} = 10.09$  mm). The column has a cracking shear resistance of 122 kN, a yield shear resistance of 223 kN ( $\tau_{\text{yld}} = 7.29$  mm) and an ultimate shear resistance of 265 kN ( $\tau_{\text{ult}} = 33.40$  mm).

Figure 4.48 shows the results of the analysis at the target load level  $\lambda = 1.0$ . The inverted triangles are consistent with the symbols developed in Section 4.2 for degraded post-elastic shear stiffness due to cracking of concrete. Inscribed in the triangles is the percent degradation of the member-sections. At the target load level, only four member-sections have entered the post-elastic range. Beam member-sections 9-6, 13-11, 10-8 and 14-13 first enter the post-elastic range at load factor levels  $\lambda = 0.73, 0.76, 0.81$  and  $0.89$ , respectively. All of these beam sections are each 29% degraded ( $t = 0.71$ ). Between load factor level  $0.89$  and  $1.0$  there is no change in the degree of post-elastic shear stiffness degradation for any of the member-sections.

Contrary to post-elastic bending stiffness degradation, where member-sections entered the post-elastic range at low load levels, post-elastic shear stiffness degradation does not occur until a high load level is reached. In this case, the first instance does not occur until 73% of the target load level is reached. This is attributed to the high cracking shear resistance of the beams (174 kN). Once cracking does occur, however, there is an immediate reduction in post-elastic shear stiffness. The new reduced level of post-elastic shear stiffness is assumed to remain constant until yielding of the transverse reinforcement occurs. Cracking causes the beam sections to experience a 29% reduction in post-elastic shear stiffness ( $t = 0.71$ ). When this degradation factor value is used in modifying the  $k_{22}$  term in the element stiffness matrix of Eq. (2.20) for example, where one end of the beam has  $t = 1.0$ , it translates into a 62% reduction in the elastic stiffness coefficient. That is to say, if we compare the

$k_{22}$  term given by Eq. (2.21b) for the cracked ( $t = 0.71$ ) and uncracked ( $t = 1.0$ ) fully elastic state, we find that there is a 62% reduction in its value. This shows that diagonal shear cracking has a significant effect on the stiffness of the member.

The shear force diagram of the frame is shown in Figure 4.49 at load factor level  $\lambda = 1.0$ . Any member-section for which post-elastic shear stiffness degradation is indicated will have a shear magnitude that exceeds the member-section's shear cracking resistance. The shear forces in members 9-6, 13-11, 10-8, and 14-13 are 238, 227, 216 and 196 kN, respectively, which are greater than the 174 kN cracking shear resistance of the beam. No other beam-section has a shear force greater than this and is why no other beam-sections enter the post-elastic range. No shear forces have exceeded the column's cracking shear resistance of 122 kN.

At the target load level then, the frame remains intact with some degree of post-elastic shearing stiffness degradation at a few member-sections. The user may increase the load on the structure beyond the target load level ( $\lambda = 1.0$ ) until a failure state is reached. Continuing the analysis shows that at load factor level  $\lambda = 1.12$  member-section 9-6 becomes 100% degraded ( $t = 0.0$ ) as shown in Figure 4.50. Two new degradation symbols are now used: the hatched triangle represents a member-section in which the transverse reinforcement is yielding, while the cross-hatched triangle represents a member-section that has surpassed its ultimate shear resistance and is fully degraded. The load factor levels shown beside the degradation symbols indicate when a member-section's post-elastic shearing stiffness changes between the target load level  $\lambda = 1.0$  and  $\lambda = 1.12$ . That is to say, the load factor level is shown if at the target load level a member-section was fully elastic or cracked, and now, beyond the target load level, a member-section is cracked or yielding.

Increasing the load factor level to 1.12 does not cause any new member-sections to enter the post-elastic range. However, several of the member-sections which previously entered the post-elastic range now undergo further post-elastic shear stiffness degradation. Beam member-sections 9-6, 13-11 and 10-8 have their transverse reinforcement yield at load factor levels  $\lambda = 1.01$ , 1.06, and 1.10, respectively. These member-sections are now each 55% degraded ( $t = 0.45$ ).

When accounting for post-elastic shear stiffness degradation only, the frame does exhibit some ductility, but not as much as when accounting for degraded post-elastic bending stiffness only. Several member-sections continue to resist shear force and deform after their transverse reinforcement yields. Member-section 9-6 is the first to yield at load factor level 1.01 and  $V = 239$

kN and remains intact until failing at  $\lambda = 1.12$ . This shows that the load on the structure may be increased by  $100(1.12-1.01) = 11\%$  beyond the point of initial yielding of the member-section, while maintaining its ability to resist shear. Its member-end post-elastic deformation at load factor level 1.01 is  $\tau = 4.8$  mm. The post-elastic deformation increases to  $\tau = 10.1$  mm for an increase in load of only 11%. The post-elastic deformation from yielding to failure (an increase in load of 11%) is 1.1 times the post-elastic deformation from cracking ( $\lambda = 0.73$ ) to yielding ( $\lambda = 1.01$ ) (an increase in load of 28%). This ductility is associated with an increase in shear resistance of 24 kN, which is 10% of the yield shear resistance. Members 13-11 and 10-8 also yield; however, a local instability occurs elsewhere before they experience any significant post-elastic deformation.

The shear force diagram at load factor level  $\lambda = 1.12$  is shown in Figure 4.51. The beam's ultimate shear resistance is 263 kN and Figure 4.51 shows that member-section 9-6 is the first member-section to reach this point. Member-section 9-6 reaches its ultimate shear resistance and fails due to crushing of concrete along the compression diagonals (principal compressive stress exceeds the maximum compressive stress of the concrete). The member-section at this point is 100% degraded ( $t = 0.0$ ). Unlike with post-elastic bending stiffness degradation, yielding of the shear reinforcement at the ends of the beams does not cause any redistribution of shear force. Maximum shear is located at the ends of the beams while the minimum shear is located near the midspan.

The structure now experiences an unloading phenomenon whereby the restraint provided by the member-end forces at 9-6 and joint 6 is lost. This occurs because it is assumed that the member disengages from the structure once it reaches the end of its post-elastic force-deformation response. The member-end forces at 9-6 at the time of failure consist of a 302 kN-m counter-clockwise moment, a 264 kN upward shear force and a 49 kN tensile force. The member-end forces acting on joint 6 from member 9-6 are equal in magnitude but opposite in sense. To account for the loss of restraint at joint 6, an elastic-unloading analysis is performed. Similar to the unloading analysis in Section 4.4.1, to simulate the loss of restraint at 9-6 and joint 6, the forces that exist there are applied there but in the opposite sense (Figure 4.52). This negates the contribution of these forces to the overall equilibrium of the structure. For the elastic-unloading analysis then, member 9-6 would have a 302 kN-m *clockwise* moment, a 264 kN *downward* shear force and a 49 kN *compressive* force applied to it. The forces applied to joint 6 would be opposite in sense.

Notice at the time of failure in shear for member-section 9-6 that the bending moment is still below the beam's ultimate moment resistance ( $M_f = 302 < M_{ult} = 331$  kNm). This shows that when only

post-elastic shear stiffness degradation is taken into account, the beam's shear resistance governs the amount of overloading the structure can withstand. When only post-elastic bending stiffness degradation is accounted for (Section 4.4.1), the load on the structure can be increased to 151% of its design load before a member-section failure occurs, resulting in the complete collapse of the frame. When only post-elastic shear stiffness degradation is accounted for, the load on the structure can be increased to only 112% of its design load before a member-section failure occurs. Whether this causes complete collapse of the structure is forthcoming; however, up to now it is clear that post-elastic shear stiffness degradation governs the structure's first member-section failure.

The results of the elastic unloading analysis are shown in the shear force diagram of Figure 4.53. Comparing the magnitude of the shear force at member-section 9-6 in Figure 4.51 and Figure 4.53 shows that the net shear force at the now free end of the beam is zero. The net moment and axial force are also zero. If the figures are compared further still, it is clear that the elastic-unloading creates large shear forces in the columns. Columns 3 and 6, for example, have shear forces of 299 and 250 kN, respectively. To determine what effect the unloading has on the overall structure and its post-elastic shear stiffness, the before unloading member-end shear forces are added to the elastic unloading member-end shear forces to obtain the after unloading member-end shear forces. The results are shown in Figure 4.54.

Figure 4.54 shows that losing the restraint of member-section 9-6 at load factor level  $\lambda = 1.12$  results in significant, albeit not complete destruction of the frame. Both ends of columns 3 and 6 are completely degraded, as is member 10-8. This causes members 3, 6, 9, and 10 to collapse to ground level leaving the smaller bay standing and the top-most members of the larger bay cantilevering from the smaller bay. Comparing Figure 4.50 and Figure 4.54 shows the increase in post-elastic shear stiffness degradation due to the loss of member-section 9-6. Where previously no member-sections in the smaller bay had entered the post-elastic range, several member-sections now exhibit some degree of degradation. Both ends of columns 1, 2, 3, and 5 are each 13% degraded ( $t = 0.87$ ). Additionally, member 11-9 is 62% degraded ( $t = 0.38$ ).

Figure 4.55 shows the shear force diagram for the frame after the elastic-unloading. All shear forces in the frame associated with a cross-hatched triangle exceed that member-section's ultimate shear resistance (263 kN for beams, 265 kN for columns). Columns 1, 2, 4, and 5, which are each 13% degraded, have shear force magnitudes that surpass their cracking shear resistance of 122 kN.

The shear force at member-section 9-6 (now a cantilever due to its disengagement) is zero, as discussed earlier.

Since the frame partially collapses to ground level, a global instability occurs, and the analysis ends. The analysis thus shows that when considering only degraded post-elastic shear stiffness, the frame may be loaded up to 1.12 times its gravity load level before a member-section failure causes partial collapse of the frame to ground level. In addition, it can now be conclusively stated that shear governs the frame's ability to resist load beyond the target load level. The frame fails at load factor level 1.12 when considering only degraded post-elastic shear stiffness (whereby the moment level at  $\lambda = 1.12$  at the critical section is still below the ultimate moment resistance of the beam) whereas the frame fails at load factor level 1.51 when considering only degraded post-elastic bending stiffness.

#### **4.4.3 Post-Elastic Axial Stiffness Degradation**

The frame is analyzed to account for degraded post-elastic axial stiffness only. The load increment is set to 1% of the total design load. The load is incrementally increased and the program determines when a member-section reaches the post-elastic range. The post-elastic force-deformation response for axial tension can be found in Appendix D. Similar to Section 4.3.3, only axial degradation for columns is accounted for here. The column has a cracking compressive resistance of 2312 kN and an ultimate compressive resistance of 5780 kN ( $\delta_{ult} = 4.93$  mm). Buckling is explicitly checked for in the analysis; however, the critical buckling load for the columns of this example is quite high ( $P_c = 6,316$  kN), and buckling does not preclude material failure as will be shown.

Figure 4.56 shows the axial load for each column (a negative sign indicating compression) at the target load factor level  $\lambda = 1.0$ . The highest axial force is in column 2 and has a magnitude of 755 kN. Since this is well below the cracking compressive resistance of the column, column 2 and the other columns remain in the elastic range.

At the target load factor level the frame remains intact and no member-sections are subject to post-elastic axial stiffness degradation; therefore, the load factor level increases until a failure state is reached. The first member-section failure occurs at load factor level  $\lambda = 7.92$  (Figure 4.57). As discussed in Section 4.2, the open square represents a member-section entering the post-elastic range due to microcracking in the concrete. The cross-hatched square represents a member-section that has surpassed its ultimate compressive resistance and is fully degraded. The load factor level at which a member-section enters the post-elastic range is beside the square.

The first member-sections to enter the post-elastic range are 2-2 and 2-6 and do so simultaneously (since the axial force throughout the length of a column is the same) at load factor level  $\lambda = 3.07$ . These member-sections become 56% degraded ( $n = 0.44$ ). As discussed in Section 2.2, the reduction in post-elastic axial stiffness is due to microcracking in the concrete whereby the force-deformation response becomes nonlinear at approximately 40% of the ultimate compressive force. When these stiffness degradation factor values are used in modifying the  $k_{11}$  term in the element stiffness matrix of Eq. (2.20) (where  $n_1 = n_2 = 0.44$ ) for example, it translates into a 72% reduction in the elastic stiffness coefficient. That is to say, if we compare the  $k_{11}$  term given by Eq. (2.21a) for the cracked ( $n_1 = n_2 = 0.44$ ) and uncracked ( $n_1 = n_2 = 1.0$ ) fully elastic state, we find that there is a 72% reduction in its value. This shows that microcracking in compression has a significant effect on the member-section's axial stiffness.

The analysis continues, since at load factor level  $\lambda = 3.07$  the frame is still intact, and column member-sections 3-3, 3-8, 5-6 and 5-11 enter the post elastic range at load factor levels  $\lambda = 5.6, 5.6, 6.35$  and  $6.35$ , respectively. These sections are each 56% degraded ( $n = 0.44$ ).

At load factor level  $\lambda = 7.92$  column member-sections 2-2 and 2-6 reach their ultimate compressive resistance (5780 kN) and become fully degraded ( $n = 0.0$ ). The member-sections of column 2 fail due to crushing of concrete. At this point the member-sections are assumed to be no longer able to resist load. The structure experiences an unloading phenomenon, similar to when member-section failures occurred for degraded post-elastic bending and shear stiffness. The restraint provided by the member-end forces at 2-6 and joint 6 is lost and consequently an elastic-unloading analysis is performed to model this loss of restraint.

The results of the elastic-unloading analysis show that the member-sections of column 1 fail due to reaching their ultimate compressive resistance (Figure 4.58). Column 3, however, remains erect and theoretically able to carry the compressive loads transferred from columns 1 and 2 which now have no load carrying capacity. This is theoretically possible because the analysis accounts for degraded post-elastic axial stiffness only, such that the bending and shear stiffness of the column-sections is fully elastic. Since no global instability occurs, a second elastic-unloading analysis is performed. The results show that the member-sections of column 3 also fail due to reaching their ultimate compressive resistance (Figure 4.59). Although the analysis is presented in a step-wise fashion, the actual physical failure of the lower three columns is immediate, once column 2 fails at load factor level  $\lambda = 7.92$ .



Since the frame collapses to ground level, a global instability occurs and the analysis ends. Thus, the analysis shows that when considering degraded post-elastic axial stiffness only, the frame may be theoretically loaded up to 7.92 times its gravity load level before a member-section failure causes complete collapse of the frame to ground level. These results are quite unrealistic, however, due to the fact that the moment and shear forces at many member-sections at load factor level  $\lambda = 7.92$  are extremely high. The bending moment and shear force in member-section 9-6 at the time of axial failure, for example, (which is the same member-section that caused failure of the frame due to degraded shear stiffness) are 2157 kN-m and 1871 kN, respectively. These force magnitudes are many times larger than the actual moment and shear resistance of member-section 9-6. A failure in member-section 9-6 would have occurred (if bending or shear degradation was accounted for) well before load factor level  $\lambda = 7.92$  was ever reached.

Even at load factor level  $\lambda = 3.07$ , which is the load factor level that column 2 enters the post-elastic range, the moments and shears in many member-sections are quite large. The moment and shear force in 9-6 at this load factor level are 885 kN-m and 735 kN, respectively. These values are still large enough that a member-section failure would have occurred at an earlier load increment if bending or shear degradation was accounted for. This shows that post-elastic axial stiffness degradation has little effect on the analysis of the structure because a large enough axial force cannot realistically occur for post-elastic axial stiffness degradation to occur.

The critical buckling load for the columns of this frame is obtained from Eq. (3.11) and has a value of 6,316 kN, which is larger than the ultimate compressive resistance and hence why buckling is not a concern for this example. The value given here is an underestimate of the actual buckling load because a  $k$  value of 1 is used in Eq. (3.11). For perfectly stiff end restraints a  $k$  value of 0.67 is given in Fig. N10.15.2 of CSA A23.3-94, which would lead to a critical buckling load of 14,070 kN. In actuality there is some degree of partial end restraint at the ends of the column, giving rise to a higher  $k$  value than 0.67, in which the critical buckling load would fall between the two values given here. These values then, present a lower and upper bound, respectively. In fact, if an analysis is run with degraded bending stiffness (not done in this case) then the bending stiffness degradation factors at the ends of the columns could be used to account for the degree of end restraint. In either case, since the ultimate compressive resistance of the column is below the lower bound of the critical buckling load, the frame is subject to a material failure and not a stability failure.

## 4.5 2 Bay-2 Storey Frame with Initial Damage

The same frame as in Section 4.4 is now analyzed assuming it has been subjected to some abnormal loading event such that upper exterior column 6 is damaged. The damaged column is assumed to break away from the structure so as not to create a debris load on the remaining structure below (Figure 4.60). The frame is analyzed to account for degraded post-elastic bending stiffness only. The load increment is set to 1% of the total load. The load is incrementally increased and the program determines when a member-section enters the post-elastic range.

The post-elastic force-deformation response of the columns is the same as in Section 4.4; however, an additional post-elastic force-deformation response must be accounted for in the beams. For the undamaged two-bay two-storey frame subjected to uniformly distributed loads across all bays, negative moment regions (tension on top) in the beams are expected at their ends and positive moment regions are expected at their midspan. This is how the frame was originally designed, i.e., for normal bending. In the negative moment regions the tension reinforcement is placed at the top of the cross section and in positive moment regions the tension reinforcement is placed at the bottom of the cross section. As the following example will show, however, the removal of a main supporting member can cause load reversals in the beams such that the tension reinforcement acts as compression reinforcement and the compression reinforcement acts as tension reinforcement. This load reversal causes a completely different post-elastic force-deformation response of the cross section. The columns, on the other hand, have symmetric amounts of reinforcement in their cross section and therefore do not have a different post-elastic force-deformation response under reverse bending.

Figure 4.38 shows the cross section of the beams in the frame. The beams are designed for normal bending where, for positive moment regions (tension on the bottom), the beam cross sections in the program are oriented as shown in Figure 4.38. For negative moment regions, the same beam cross section is used in the program, except it is rotated 180° so that the tension reinforcement (4-25M bars) is located at the top of the cross section. If this cross section is subjected to reverse bending, what was originally intended to be the compression reinforcement (added for the sole purpose of anchoring the stirrups) will act as tension reinforcement. That is to say, the 2-15M bars would be in tension and the 4-25M bars would be in compression. The post-elastic moment-rotation response for the cross section under normal and reverse bending is shown in Figure 4.61.

Under normal bending the cross section's cracking moment resistance, yield moment resistance and ultimate moment resistance are 30, 308 and 331 kN-m, respectively. Under reverse bending, however, the cross section's cracking moment resistance, yield moment resistance and ultimate moment resistance are 30, 66, and 96 kN-m, respectively. The cracking moment resistance is the same regardless of the type of bending because it depends on the concrete's tensile resistance and not the reinforcement. The yield moment resistance in reverse bending is substantially less than in normal bending. This is because with the 2-15M bars acting as tension reinforcement there is only a 0.26% reinforcement ratio compared to a 1.31% reinforcement ratio when the 4-25M bars act as tension reinforcement. The ultimate moment capacity is also substantially less. This is due to the fact that the tension force in the 2-15M bars cannot balance the compressive force in the concrete and 4-25M bars. The section fails due to the 2-15M bars rupturing. Plotted on the same scale, Figure 4.61 shows that the section is many times more ductile in reverse bending. A trilinear representation of the reverse bending post-elastic moment-rotation response is used to calculate the post-elastic bending stiffness and degradation factors used in the analysis. The analysis is adapted so that the appropriate value of post-elastic bending stiffness is used in calculating the degradation factors depending on the type of bending that the beam cross section experiences.

As the load factor level increases, various member-sections enter the post-elastic range. At load factor level  $\lambda = 0.22$  member 13-11 reaches its ultimate moment capacity (Figure 4.62). Member 13-11 (which acts as the fixed end of a cantilever) is subjected to a negative moment such that tension is experienced at the top of the section. This member-section was designed for a negative moment and hence it undergoes normal bending for which its ultimate moment resistance is 331kN-m. Figure 4.63 shows the bending moment diagram (plotted on the tension side) at load factor level  $\lambda = 0.22$ . The moment diagram shows member-section 13-11 having a 331 kN-m moment with tension at the top of its cross section.

Notice in Figure 4.62 that member-sections 13-12 and 14-12 are yielding and are each 99% degraded ( $r = 0.01$ ). These member-sections were designed for normal bending where tension is at the bottom of the cross section and the moment distribution along the beam looks similar to that of Figure 4.41. As a consequence of column 6 breaking away due to an abnormal loading event, member-sections 13-12 and 14-12 experience a tension force along their entire top side, i.e., as for a cantilever beam. Member-sections 13-12 and 14-12 thereby experience reverse bending and their reverse bending post-elastic moment-rotation response governs. The yield moment resistance is no

longer 308 kN-m but is instead only 66 kN-m. The moment diagram in Figure 4.63 shows that member-sections 13-12 and 14-12 are subjected to a moment of 83 kN-m which is beyond the yield moment resistance of the beam in reverse bending. Member-sections 11-10 and 12-10 are also subjected to reverse bending. Their end-moments are 71 kN-m which also exceeds the beam's yield moment resistance in reverse bending and is why they are shown as yielding and 99% degraded.

Member-section 11-9 which is 89% degraded ( $r = 0.11$ ) was designed for a negative moment where tension should be at the top of the section. The moment diagram shows that member-section 11-9 is subjected to a 60 kN-m moment with tension on the bottom of the cross section. Member-section 11-9 is therefore subjected to reverse bending and its reverse bending post-elastic moment-rotation response governs. Member-section 11-9 exceeds its cracking moment resistance of 30 kN-m and enters the post-elastic range at load factor level  $\lambda = 0.13$ . Member-section 7-4 is also subjected to reverse bending, however, its member-end moment is below the cracking moment resistance and that is why it remains in the elastic range. All other member-sections that have entered the post-elastic range have done so under normal bending and their percent degradation and the load factor at which they entered the post-elastic range are shown in Figure 4.62.

The foregoing demonstrates that at a very low load level (22% of the target load) several members in the structure will yield if reverse bending is caused due to the loss of a critical member.

Since member-section 13-11 reaches its ultimate moment resistance it is assumed to be no longer able to carry load and members 13 and 14 are assumed to disengage from the structure. An elastic-unloading analysis is performed whereby the member-end forces that existed at section 13-11 are applied to the remaining structure, but in an opposite sense (Figure 4.64) so as to model the loss of restraint due to members 13 and 14 disengaging from the structure. The results of the elastic-unloading analysis are shown in Figure 4.65.

The elastic-unloading results are added to the before unloading results to obtain the after elastic unloading results (Figure 4.66 and Figure 4.67). Only member-section 2-6, that previously was in the elastic range, now enters the post-elastic range as a result of the elastic-unloading. Figure 4.66 shows some member-sections in the post-elastic range even though their moment magnitudes after elastic-unloading are below their respective cracking moment resistance. This is attributed to the fact that members cannot regain post-elastic stiffness.

Beam members 13 and 14 now fall onto beam members 9 and 10 as debris loading. The debris load is assumed to be uniformly distributed on the members below. The magnitude of the debris load is the full intensity of the load on members 13 and 14 multiplied by a load amplification factor given by Eq. (3.15).

For a specified dynamic load impact factor of  $\alpha^* = 2$  and the load factor level at which the debris loading occurs at ( $\lambda = 0.22$ ), the load amplification factor  $\alpha = 2/(1-0.22) = 2.56$ . The debris load is then  $2.56(w_{13,14}) = 2.56(56.4 \text{ N/mm}) = 144.4 \text{ N/mm}$ . The debris load is added to the gravity load already acting on members 9 and 10 such that the full intensity of load acting on members 9 and 10 is  $144.4 \text{ N/mm} + w_{9,10} = 144.4 \text{ N/mm} + 60.6 \text{ N/mm} = 205.2 \text{ N/mm}$  (Figure 4.68). The after unloading member-end forces are the starting basis from which to apply the loads in Figure 4.68 for the reloading stage of the analysis (stage three). The inelastic incremental analysis now continues from load factor level  $\lambda = 0.22$ .

The next member-section failure occurs at load factor level  $\lambda = 0.55$  (Figure 4.69). Several member-sections who previously were yet to enter the post-elastic range now do so. The load factor levels at which this occurs are indicated in Figure 4.69. Member-sections 9-7 and 10-7 reach their ultimate moment capacity in normal bending and fail due to crushing of concrete in the compression zone of their cross section. The bending moment diagram at load factor level  $\lambda = 0.55$  is shown in Figure 4.70. Figure 4.70 shows member-sections 9-7 and 10-7 having moment magnitudes of 331 kN-m which is equal to the ultimate moment resistance of the section. Member-sections 7-5 and 8-5 at the time of the first member-section failure were not in the post-elastic range, but now enter the post-elastic range at load factor level  $\lambda = 0.46$ . As the moment diagram shows, however, these member-sections are in reverse bending (tension at the top of the cross section) and exceed their cracking moment resistance. Hence, they are each 89% degraded ( $r = 0.11$ ).

With member-sections 9-7 and 10-7 failed, an elastic-unloading analysis is performed. The member-end forces that existed at 9-7 and 10-7 are applied there but in an opposite sense so as to model the loss of restraint on the structure (Figure 4.71). These forces consist of a 49 kN tensile force, a 24 kN shear force and a 331 kN-m bending moment. Because member-sections 9-7 and 10-7 failed and are assumed to be no longer able to carry load (essentially breaking apart) there are now two separate structures as shown in Figure 4.71. The before elastic-unloading forces (Figure 4.70) are added to the elastic-unloading forces (Figure 4.72) and the results are shown in Figure 4.73. Figure 4.73 shows that member-sections 7-4, 8-6, 9-6, 10-8, 3-3, and 3-8 exceed their ultimate

moment capacity as a result of the unloading. The bending moment diagram for after elastic-unloading (Figure 4.74) shows that every member-section that failed, except for member 7-4, did so by reaching its ultimate moment capacity in normal bending. Member-section 7-4, however, which has moment magnitude 106 kN-m, exceeds its ultimate moment capacity (96 kN-m) in reverse bending (with tension at the bottom of the cross section). Member-sections 7-5 and 8-5 have moment magnitude 89 kN-m are yielding and are each 99% degraded. They have exceeded their yield moment capacity (66 kN-m) in reverse bending also.

As a result of column 6 being destroyed by an abnormal loading event the entire right bay and the first floor of the left bay collapse to ground level (Figure 4.75). This occurs at load factor level  $\lambda = 0.55$  which is slightly over half of the full design load intensity. This indicates that the structure does not have enough residual load carrying capacity to prevent a progressive collapse if, as considered here, column 6 is destroyed.

It is interesting to note that the load reversals in members 7 and 8 were responsible for these two members collapsing to ground level. Removal of column 6 causes the collapse of the entire right bay of the structure. Each member-section failure in the right bay, however, was due to that section exceeding its ultimate moment capacity in normal bending. If member-section 7-4 were designed for the effects of reverse bending and had even slightly more moment resistance, then the first floor in the left bay (members 7 and 8) would remain standing, albeit as a cantilever.

A final point about the dynamic load impact factor must be made. It is difficult to select a value for the dynamic load impact factor as it reflects the amount of dynamic damping in the structure. That is to say, a small value of the dynamic load impact factor indicates a large amount of dynamic damping while a large value of the dynamic load impact factor indicates a small amount of dynamic damping. A factor of 2 was used in this example because it was known previously to cause a progressive collapse of the structure (at load factor level  $\lambda = 0.55$ ) before the target load level is reached. Using different values of the dynamic load impact factor such as 1.25, 1.5, 4 or 8, for example, causes a progressive collapse to occur at load factor levels  $\lambda = 0.70, 0.67, 0.43$  and  $0.34$ , respectively. In fact, if the dynamic load impact factor had a value of unity, a progressive collapse would occur at load factor level  $\lambda = 0.79$ . If the dynamic load impact factor has a value of unity, however, that would indicate that the debris loads do not have any velocity and are statically applied. Thus, it is not necessary to select a value of the dynamic load impact factor that accurately reflects the amount of dynamic damping in a structure because it is sufficient to show, as has been done here, that

progressive collapse occurs regardless of the amount of dynamic damping. This is because the two-bay two-storey structure has little structural redundancy.

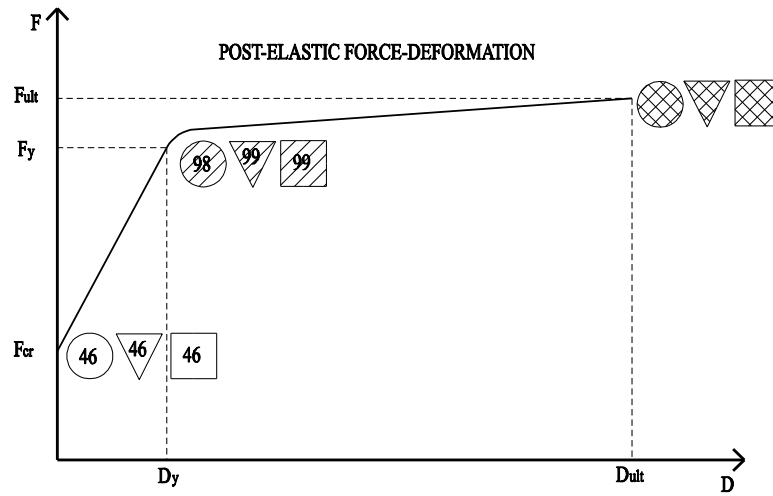


Figure 4.1: Symbol legend

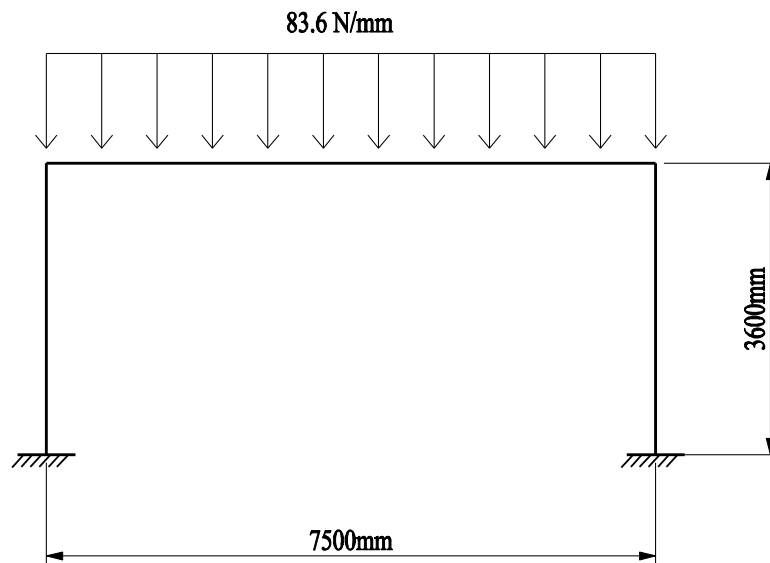
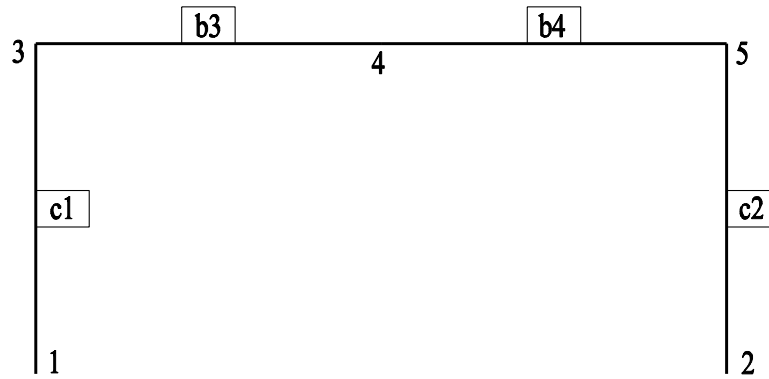
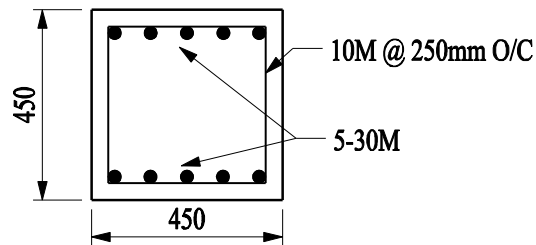


Figure 4.2: Portal frame geometry and loading



**Figure 4.3: Portal frame analysis model**



**Figure 4.4: Column cross section**

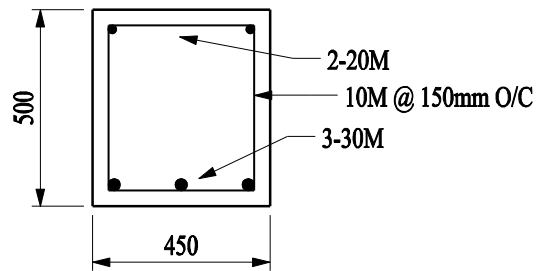


**Figure 4.5: Beam cross section**



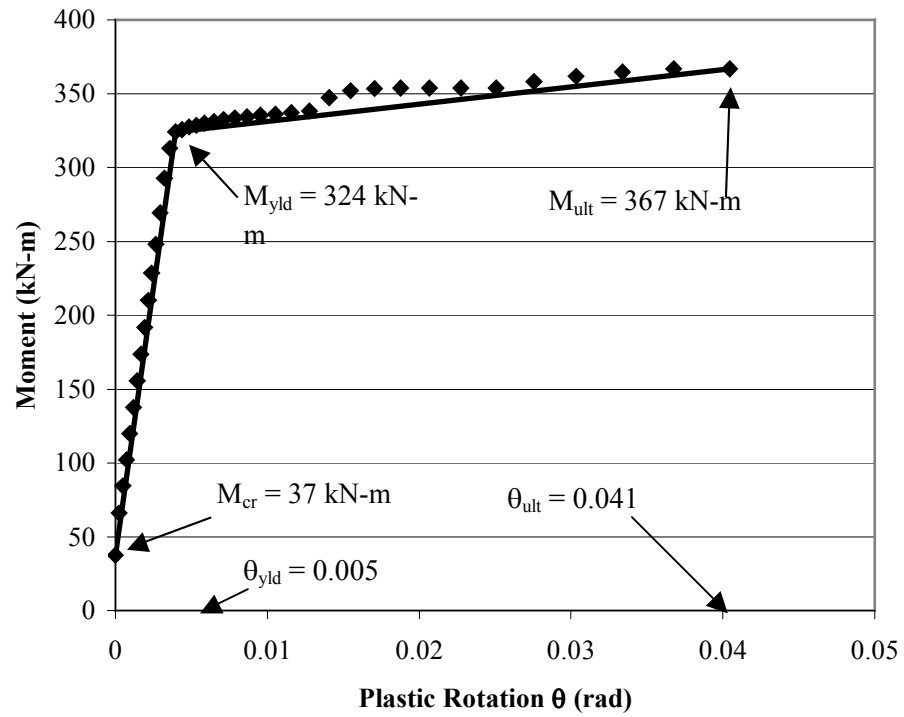


Figure 4.6: Beam post-elastic moment-rotation graph

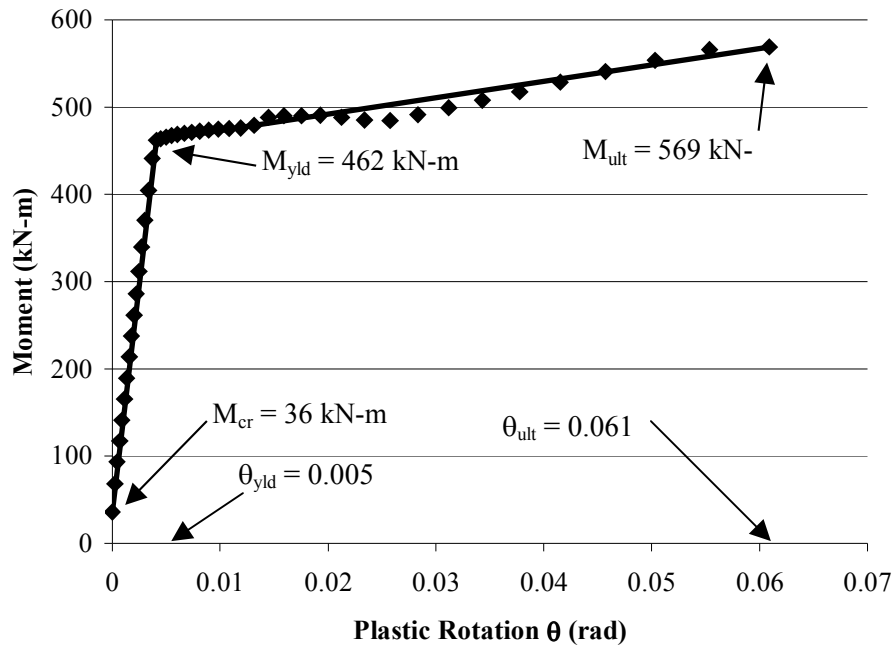


Figure 4.7: Column post-elastic moment-rotation graph



Figure 4.8: Load factor  $\lambda = 0.124$

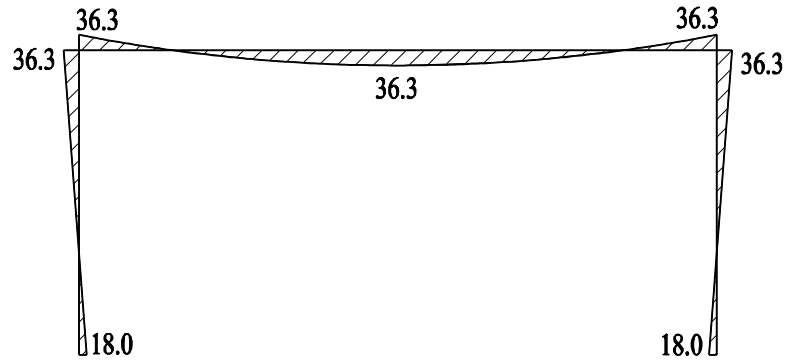


Figure 4.9: Bending moment diagram (kN-m)  $\lambda = 0.124$

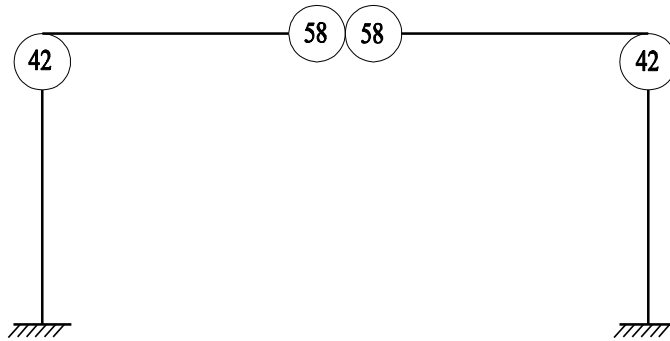


Figure 4.10: Load factor  $\lambda = 0.126$

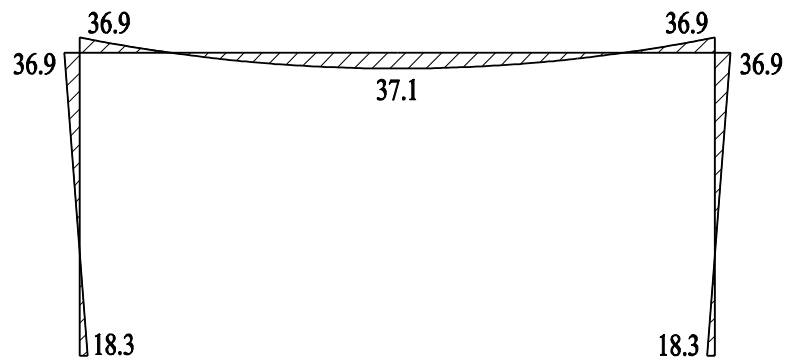


Figure 4.11: Bending moment diagram (kN-m)  $\lambda = 0.126$

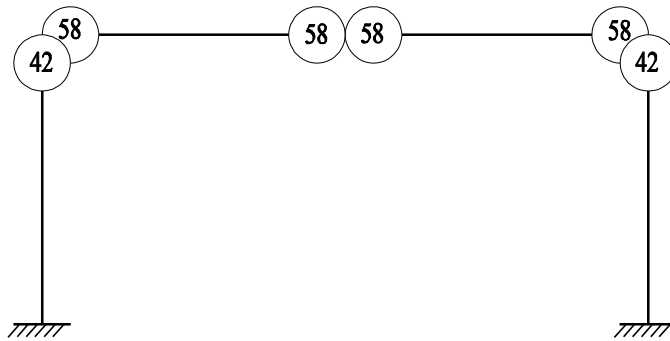


Figure 4.12: Load factor  $\lambda = 0.128$

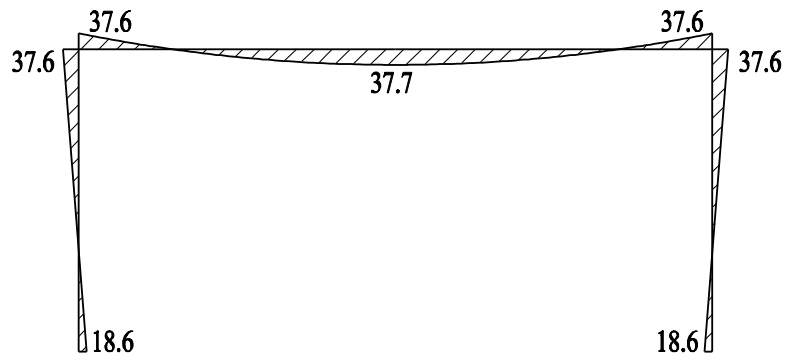


Figure 4.13: Bending moment diagram (kN-m)  $\lambda = 0.128$

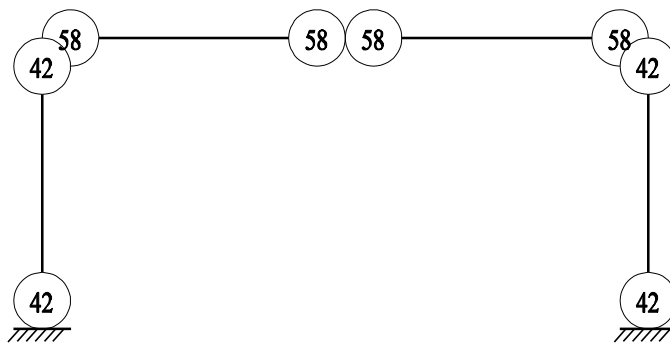


Figure 4.14: Load factor  $\lambda = 0.266$

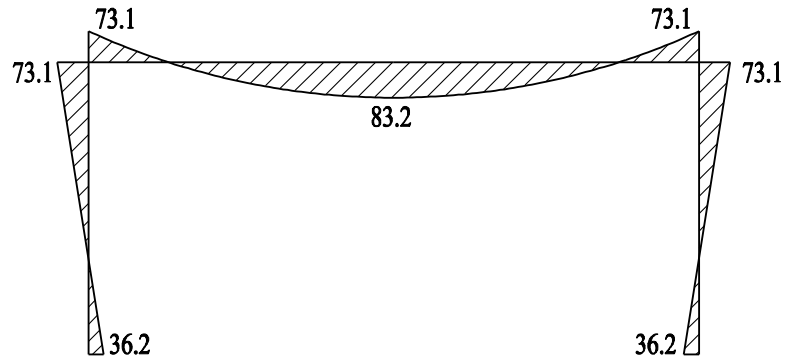


Figure 4.15: Bending moment diagram (kN-m)  $\lambda = 0.266$

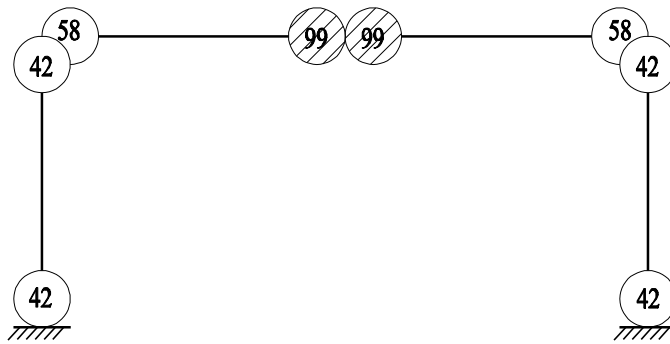


Figure 4.16: Load factor  $\lambda = 0.984$

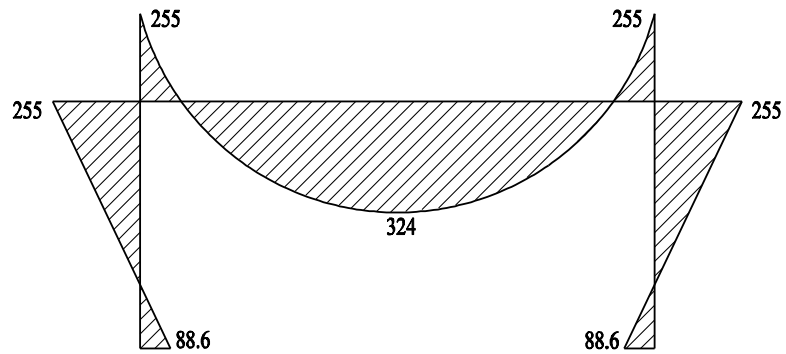


Figure 4.17: Bending moment diagram (kN-m)  $\lambda = 0.984$

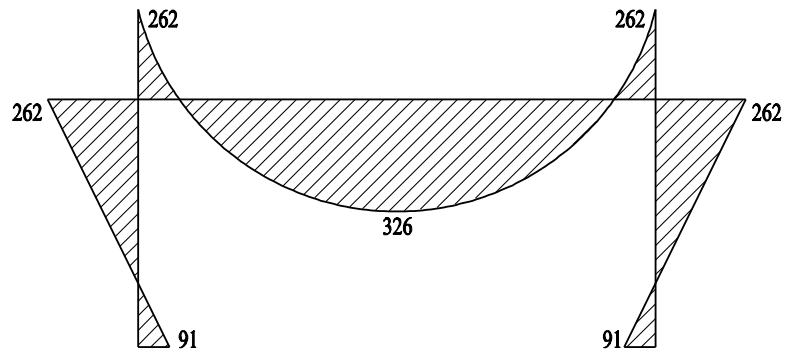


Figure 4.18: Bending moment diagram (kN-m)  $\lambda = 1.00$

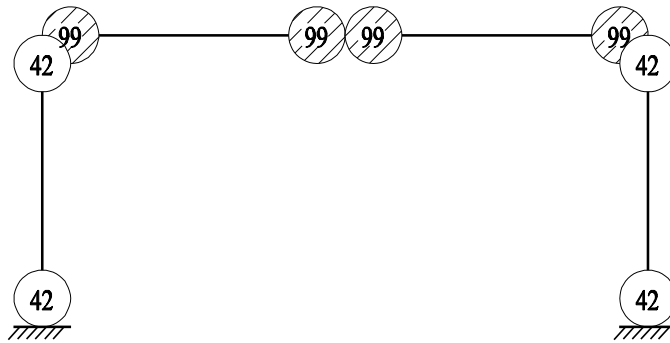


Figure 4.19: Load factor  $\lambda = 1.12$

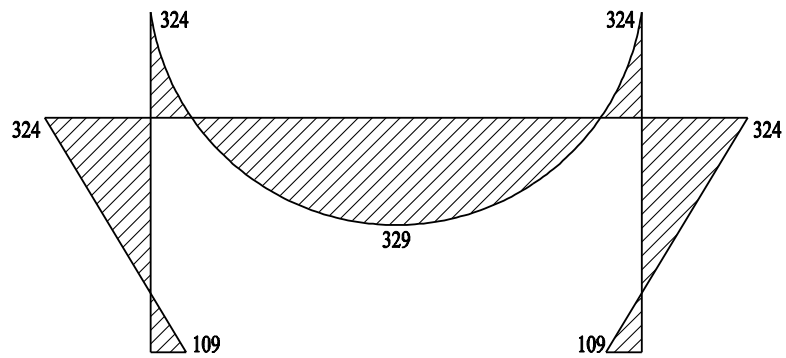


Figure 4.20: Bending moment diagram (kN-m)  $\lambda = 1.12$

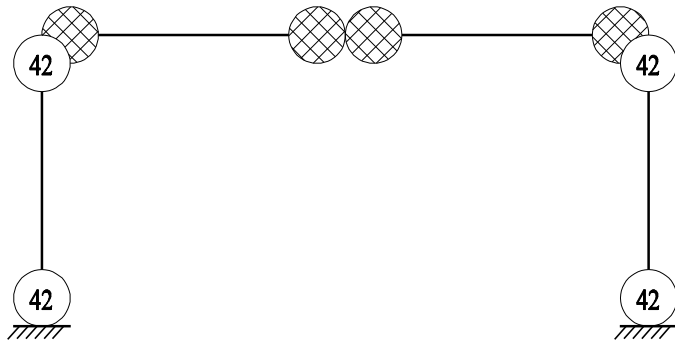


Figure 4.21: Load factor  $\lambda = 1.25$

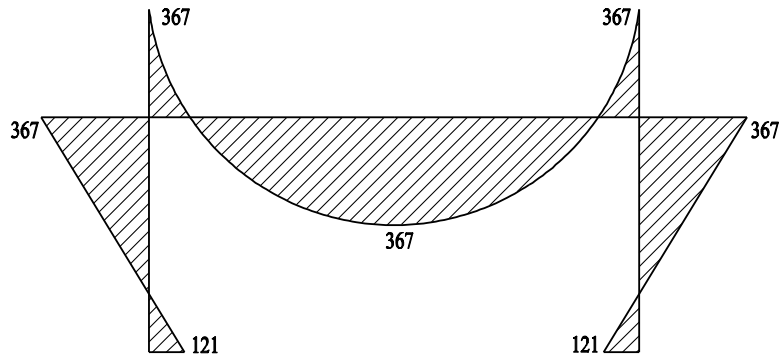
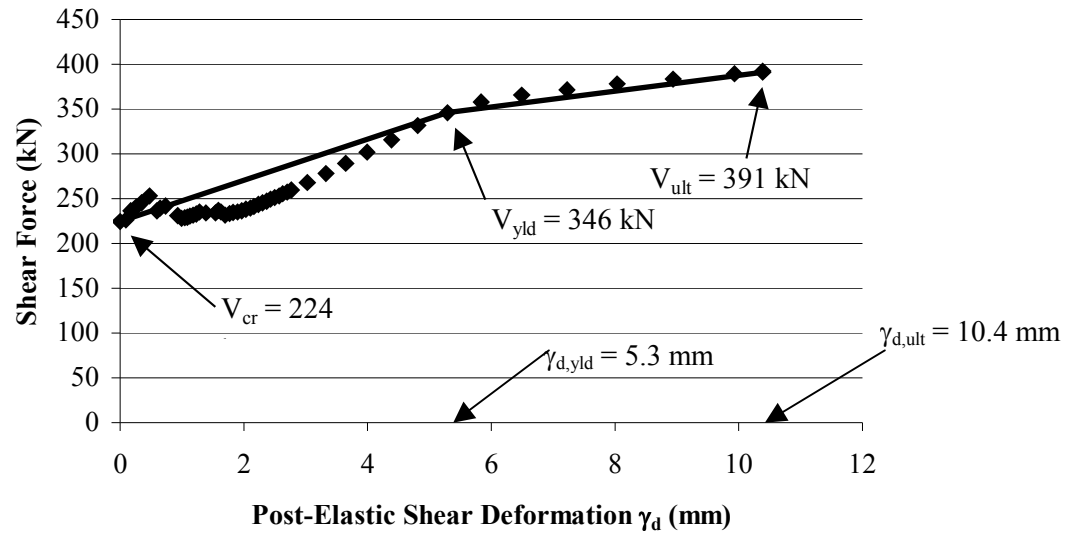


Figure 4.22: Bending moment diagram (kN-m)  $\lambda = 1.25$



**Figure 4.23: Beam post-elastic shear force-shear deformation response**



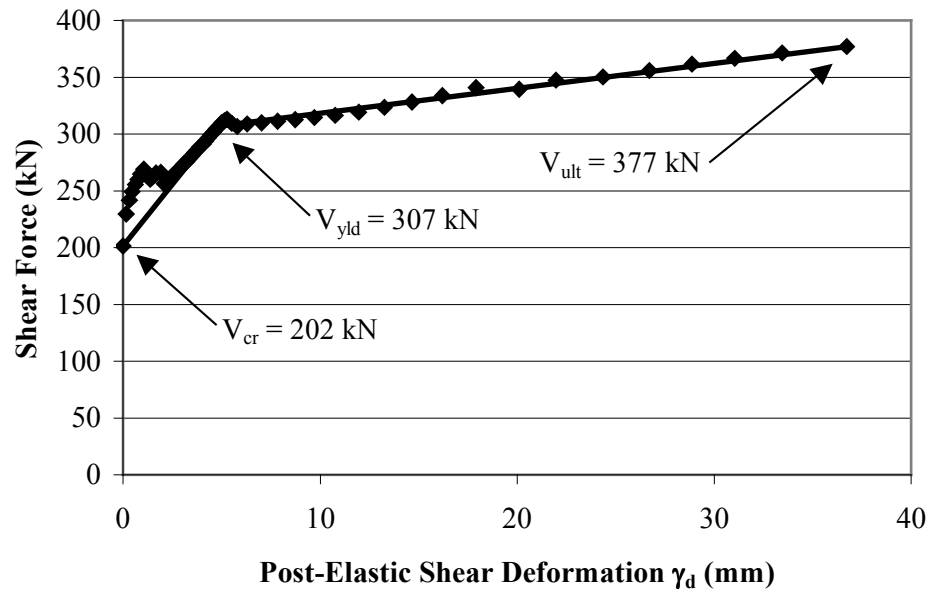


Figure 4.24: Column post-elastic shear force-shear deformation response



Figure 4.25: Load factor  $\lambda = 0.716$

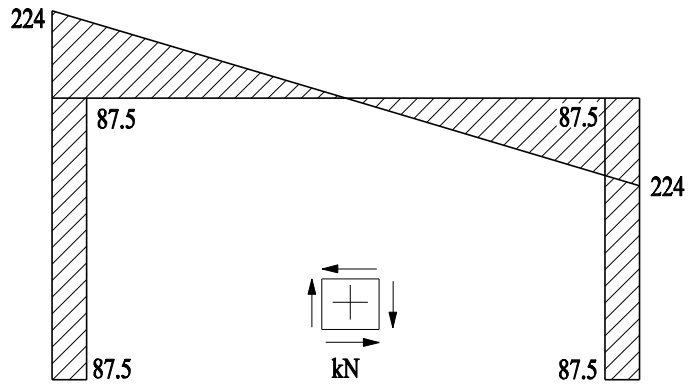


Figure 4.26: Shear diagram  $\lambda = 0.716$

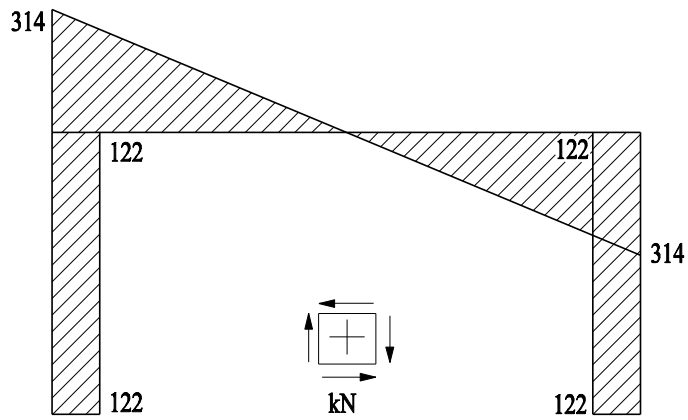


Figure 4.27: Shear diagram  $\lambda = 1.0$



Figure 4.28: Load factor  $\lambda = 1.10$

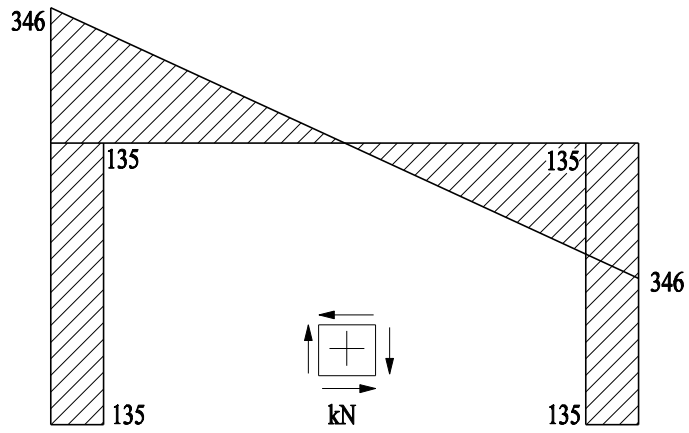


Figure 4.29: Shear diagram  $\lambda = 1.10$



Figure 4.30: Load factor  $\lambda = 1.25$

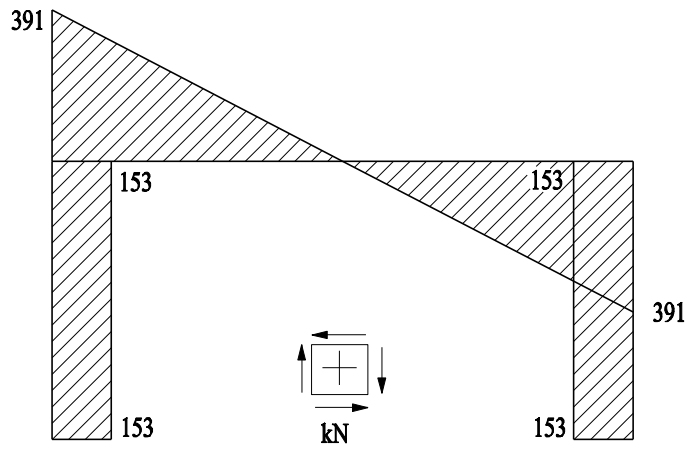


Figure 4.31: Shear diagram  $\lambda = 1.25$

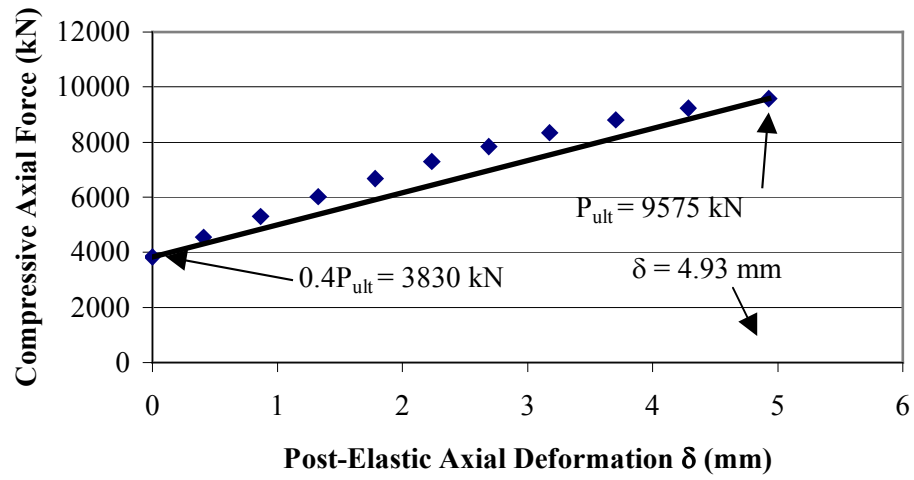


Figure 4.32: Column post-elastic compression-axial deformation graph

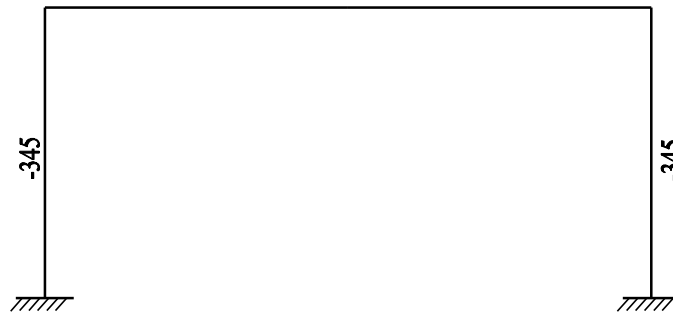


Figure 4.33: Load factor  $\lambda = 1.0$

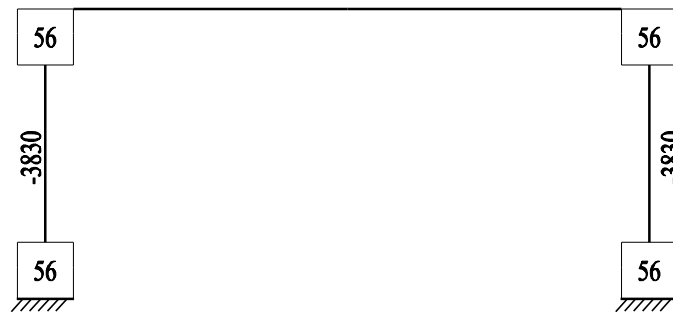


Figure 4.34: Load factor  $\lambda = 12.35$



Figure 4.35: Load factor  $\lambda = 30.6$

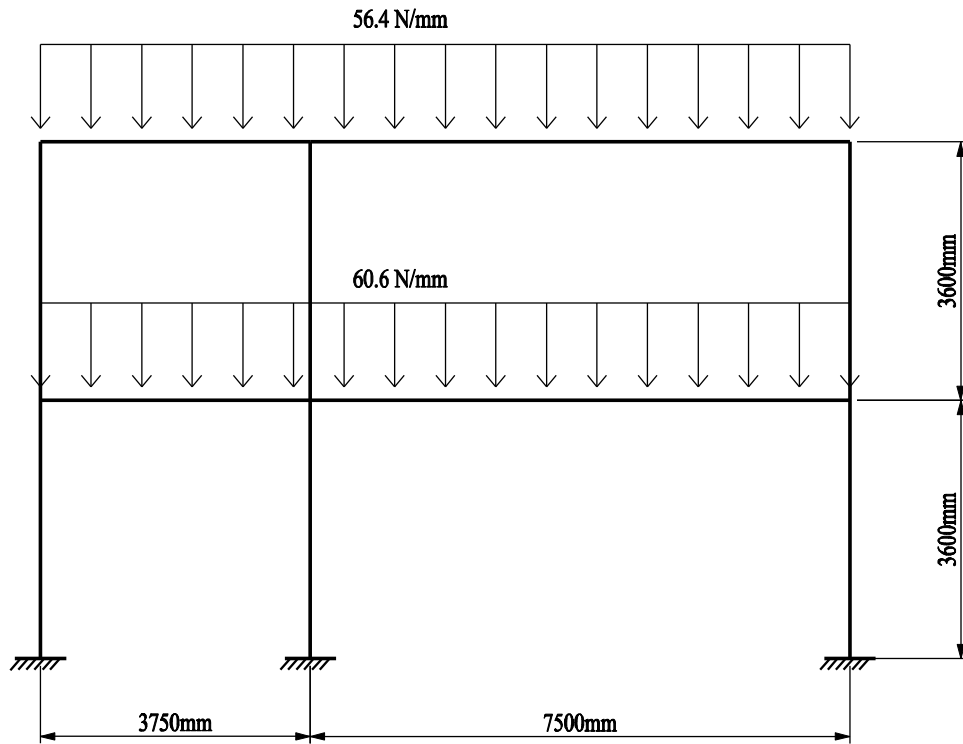


Figure 4.36: Frame geometry and loading

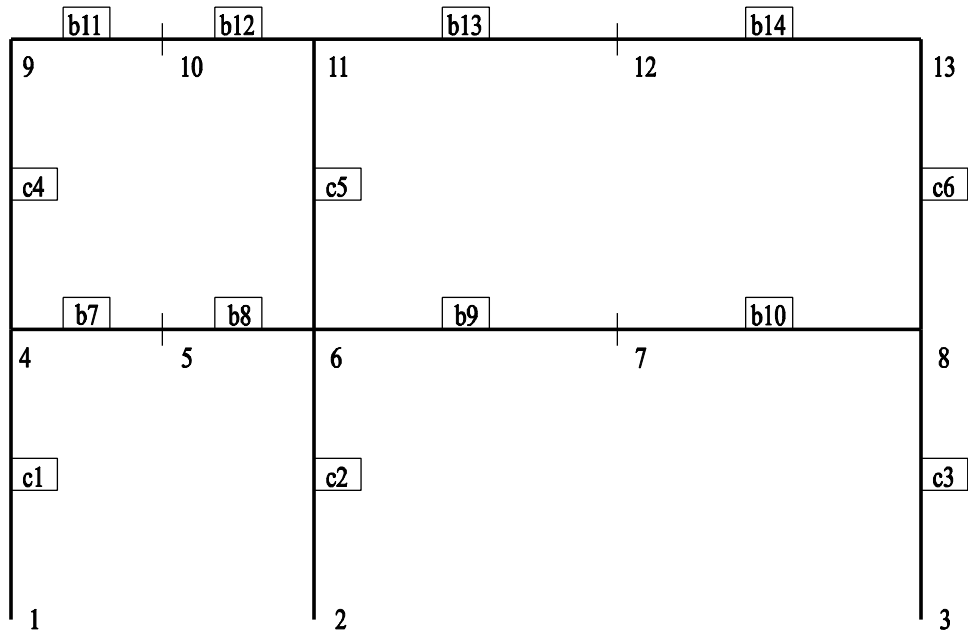


Figure 4.37: Node and member numbering

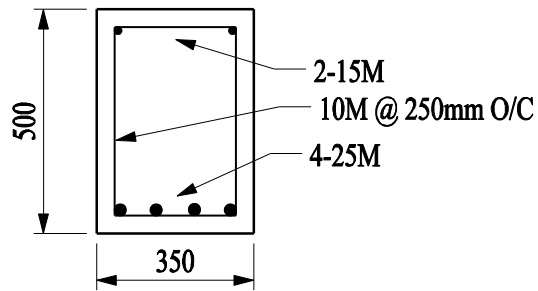


Figure 4.38: Beam cross-section

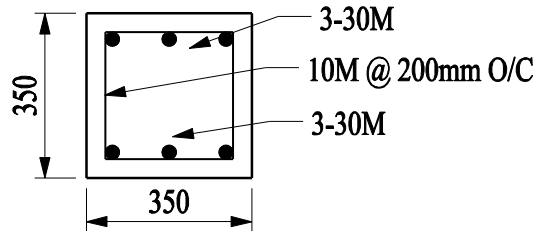


Figure 4.39: Column cross-section

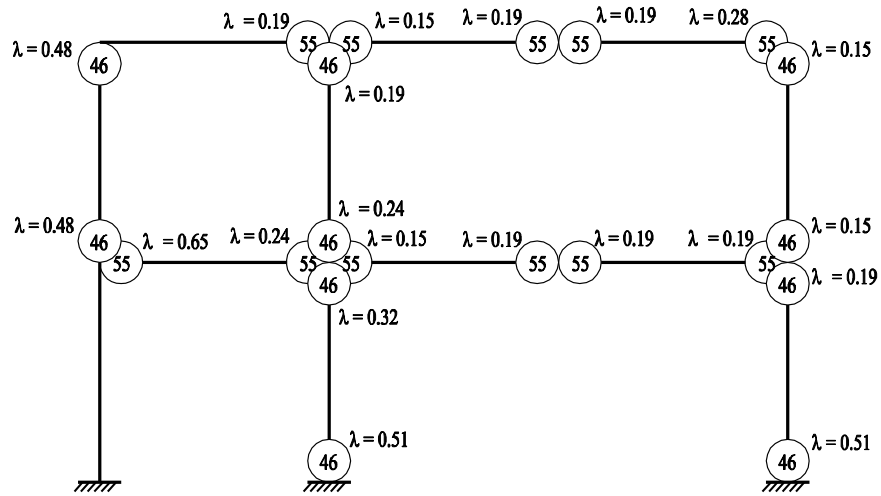


Figure 4.40: Load factor  $\lambda = 1.0$

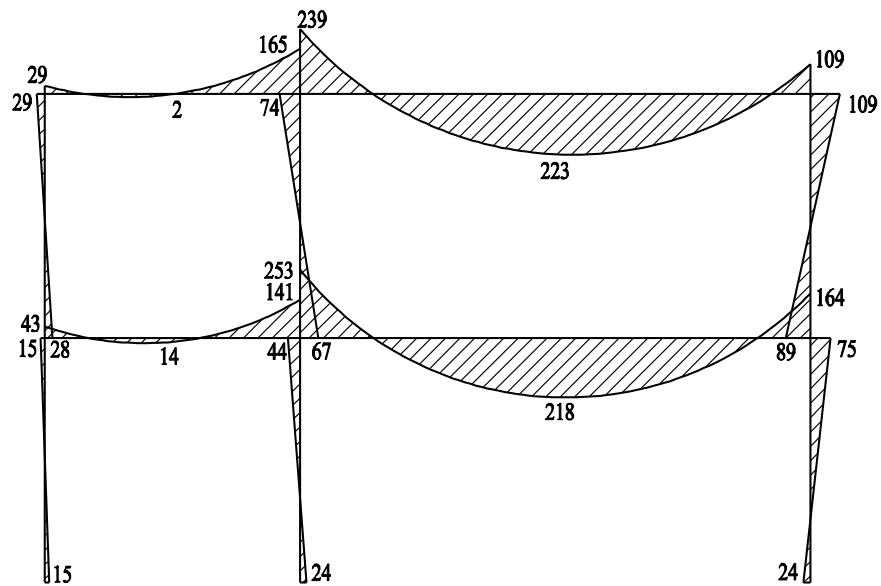


Figure 4.41: Bending moment diagram (kN-m)  $\lambda = 1.0$

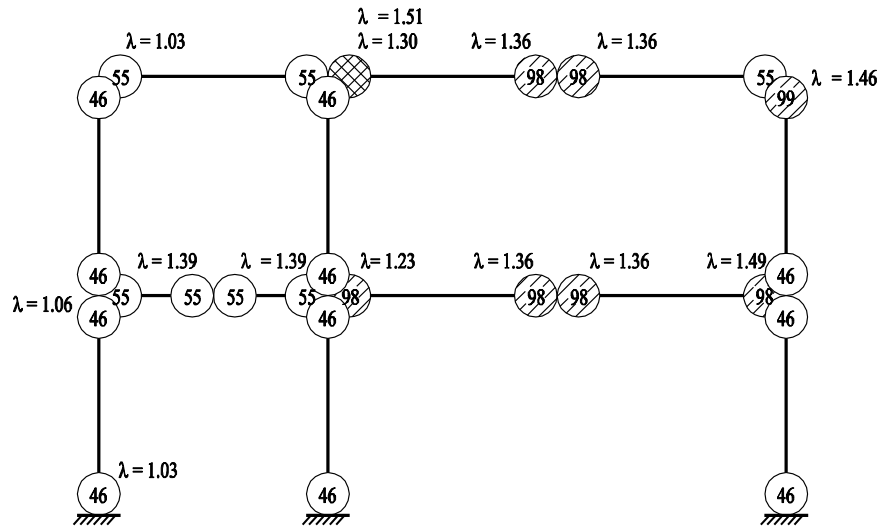


Figure 4.42: Load factor  $\lambda = 1.51$

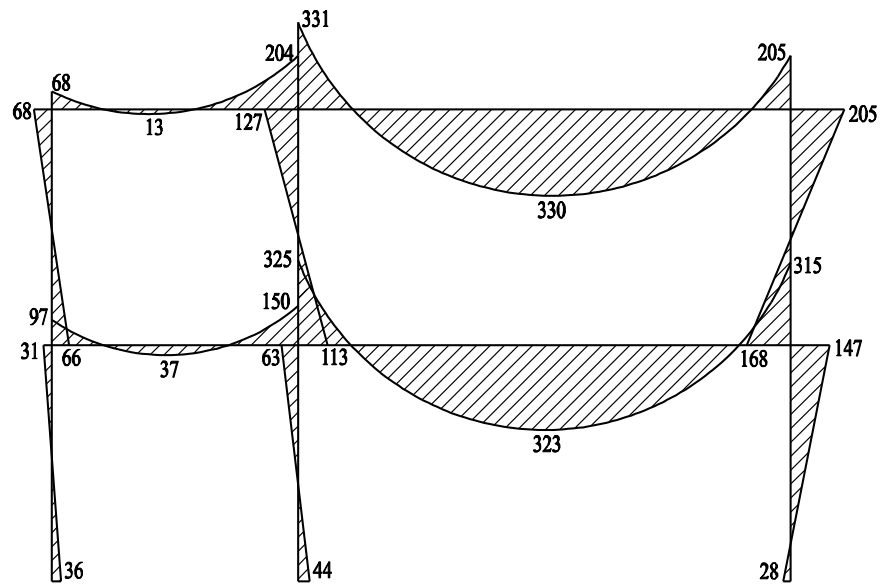


Figure 4.43: Bending moment diagram (kN-m)  $\lambda = 1.51$



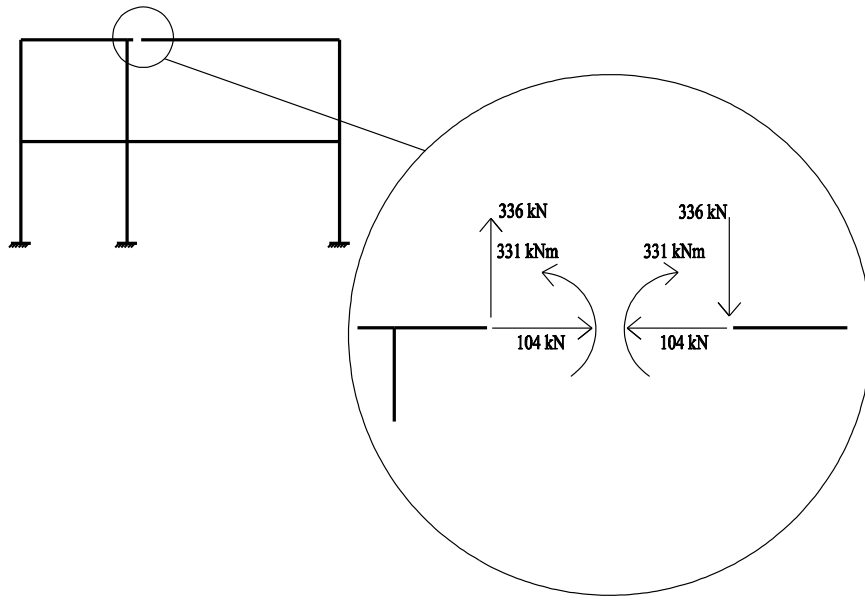


Figure 4.44: First member-end failure  $\lambda = 1.51$

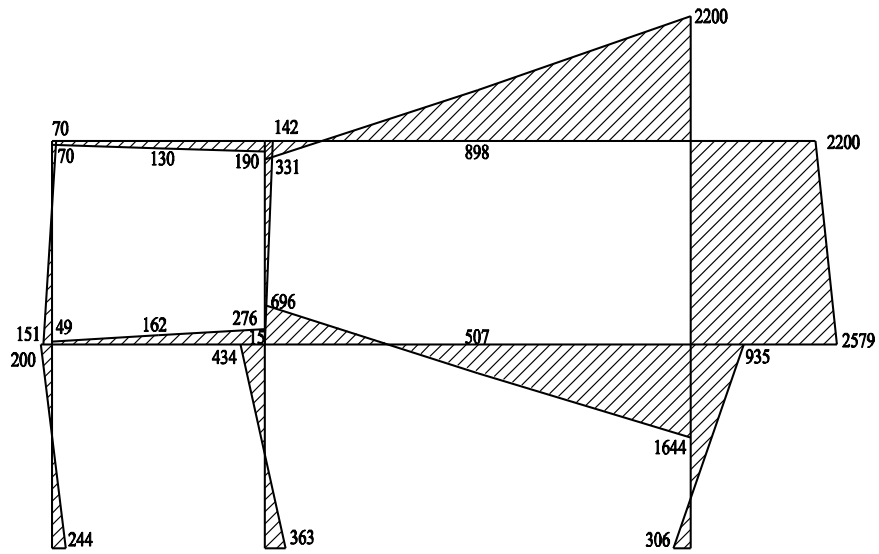


Figure 4.45: Bending moment diagram from elastic unloading (kN-m)

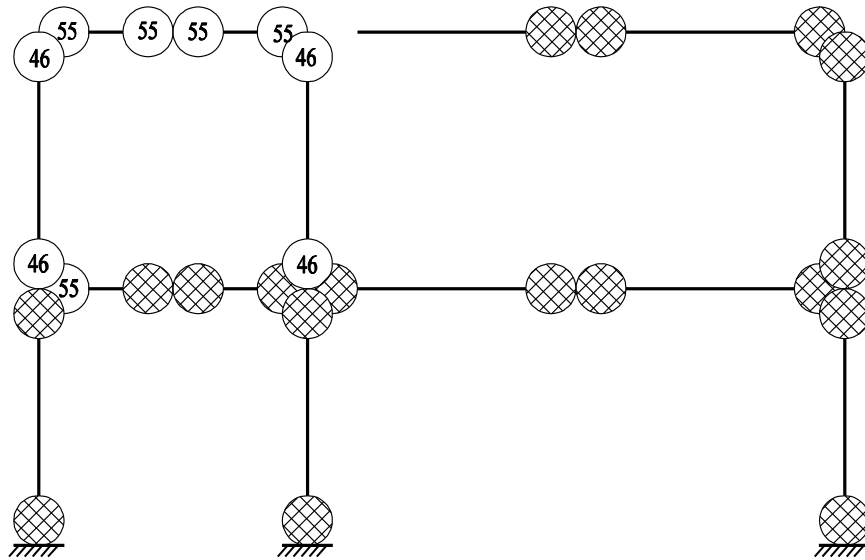


Figure 4.46: After elastic unloading

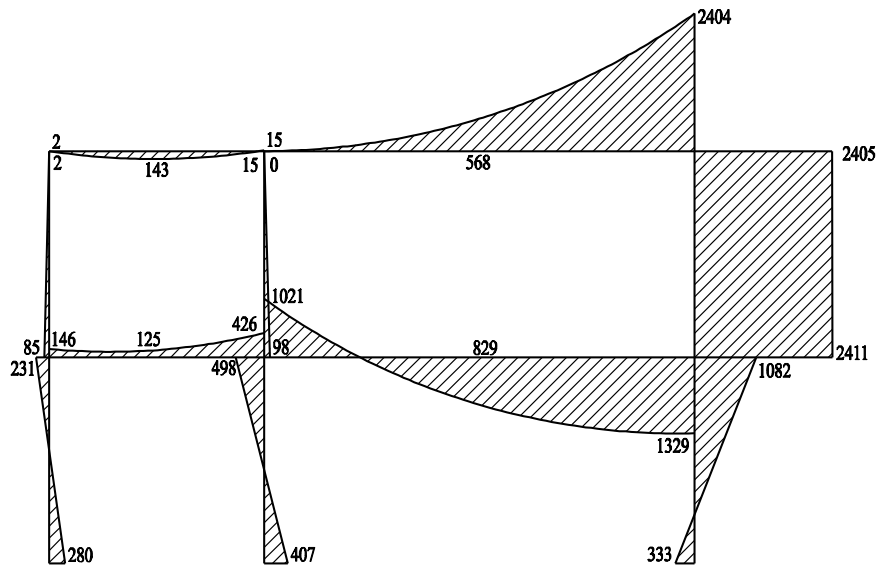


Figure 4.47: Bending moment diagram from after elastic unloading (kN-m)

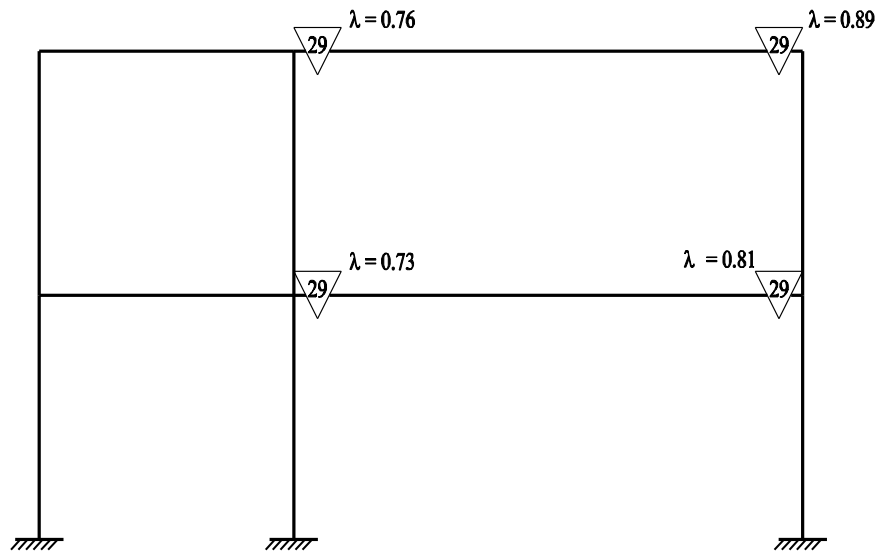


Figure 4.48: Load factor  $\lambda = 1.0$

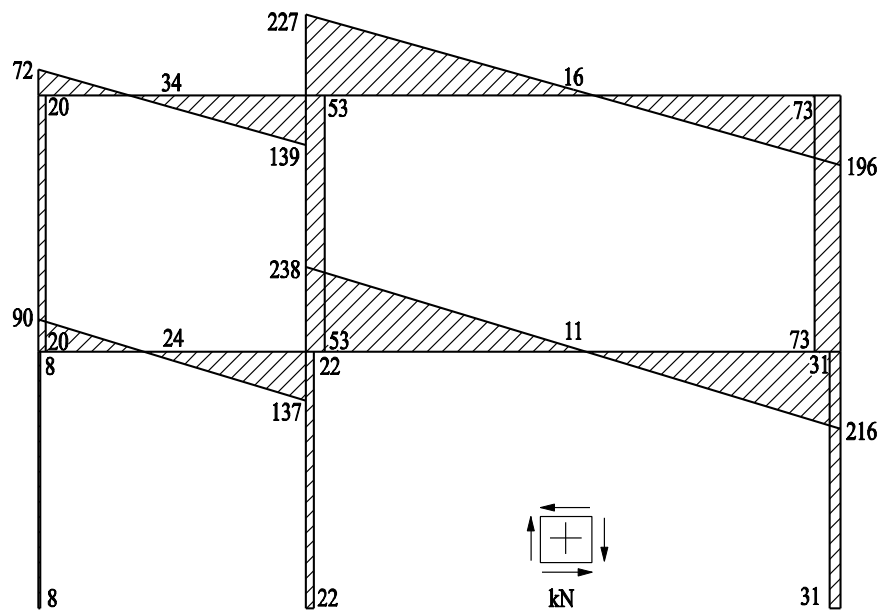


Figure 4.49: Shear diagram (kN)  $\lambda = 1.0$

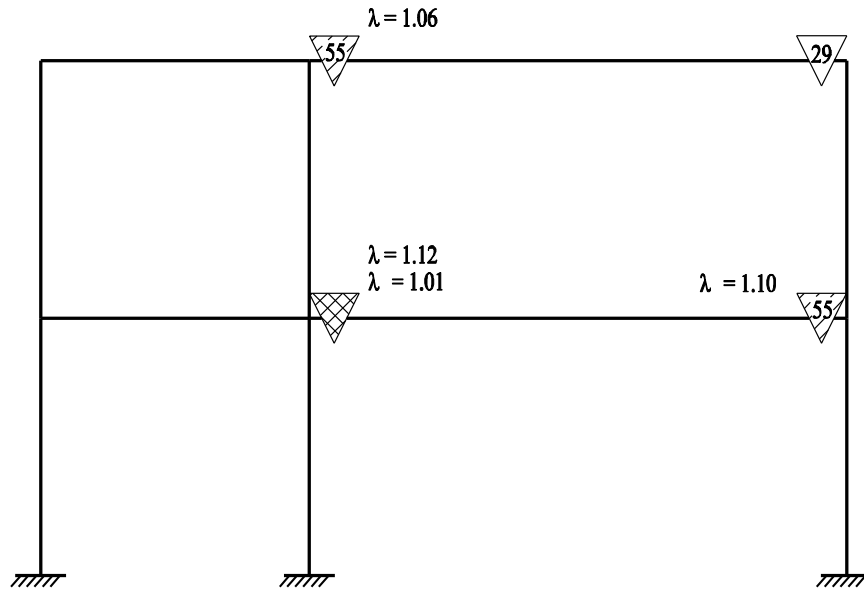


Figure 4.50: Load factor  $\lambda = 1.12$

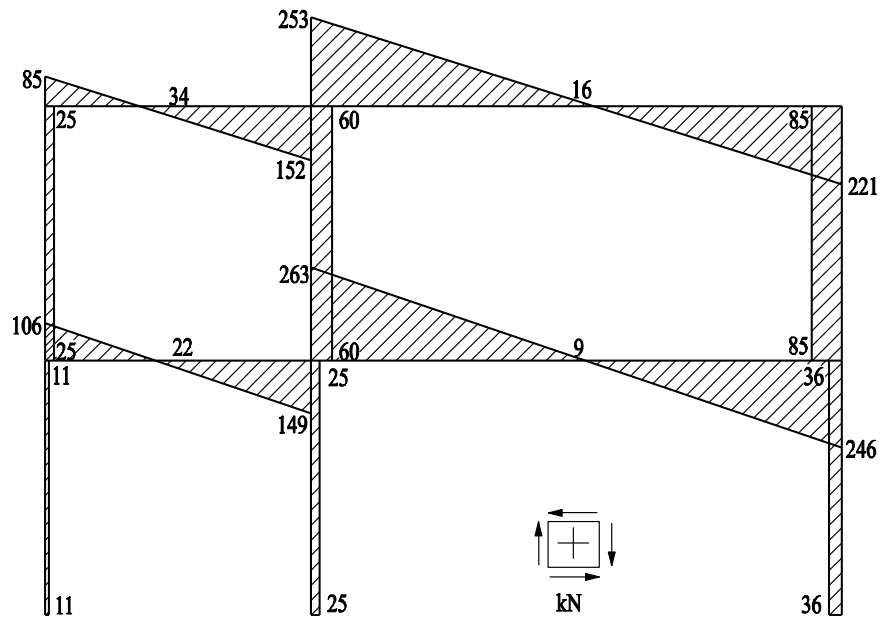
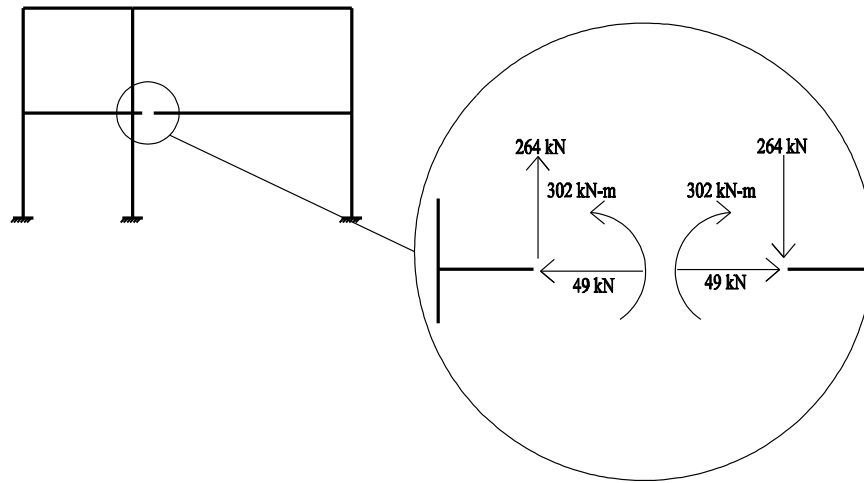
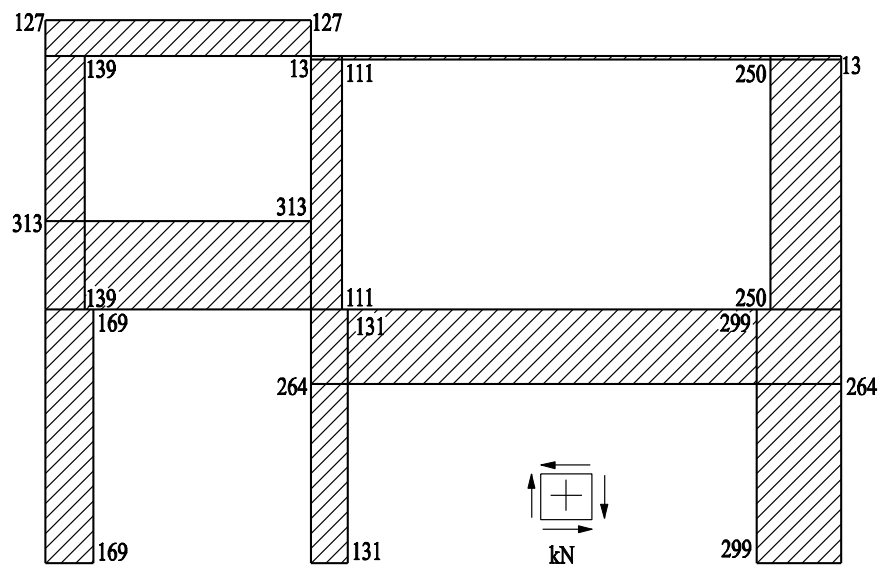


Figure 4.51: Shear diagram (kN)  $\lambda = 1.12$



**Figure 4.52: First member-end failure**



**Figure 4.53: Shear diagram from elastic unloading (kN)**

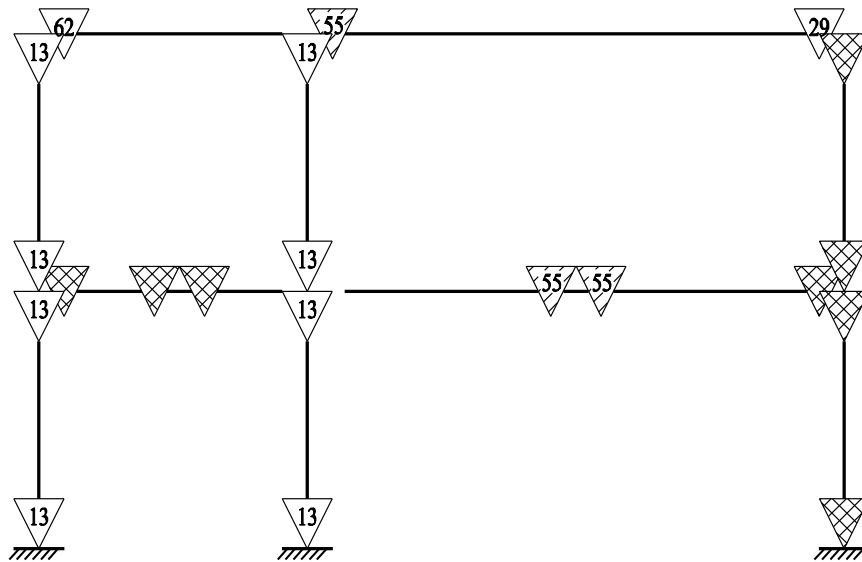


Figure 4.54: After elastic unloading

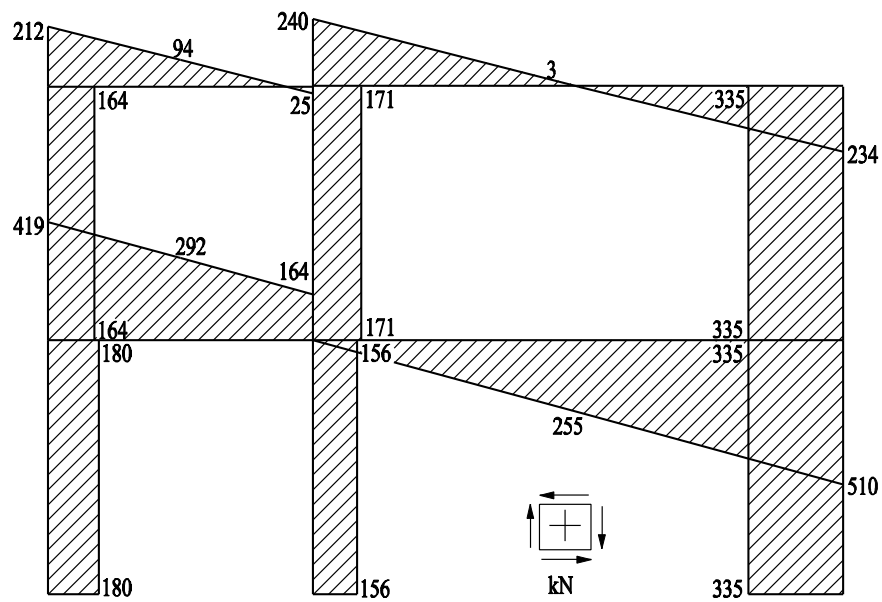


Figure 4.55: Shear diagram after elastic unloading (kN)

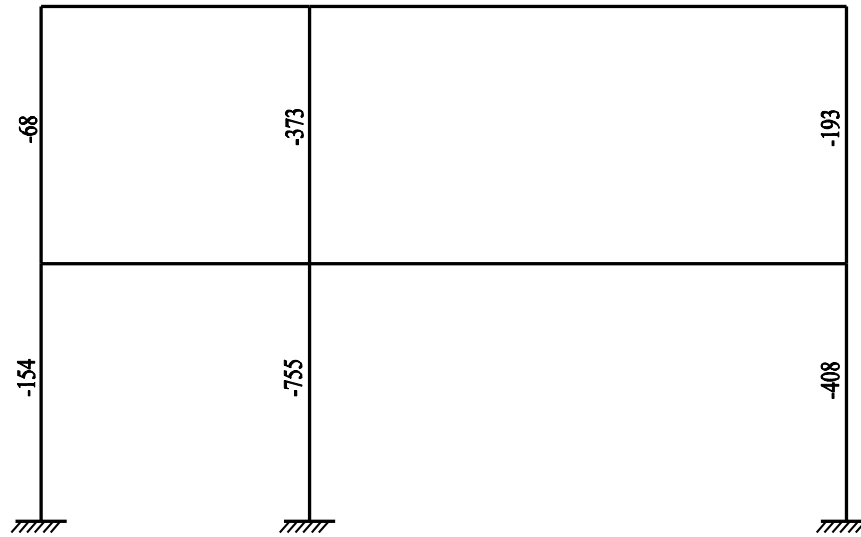


Figure 4.56: Load factor  $\lambda = 1.0$  (kN)

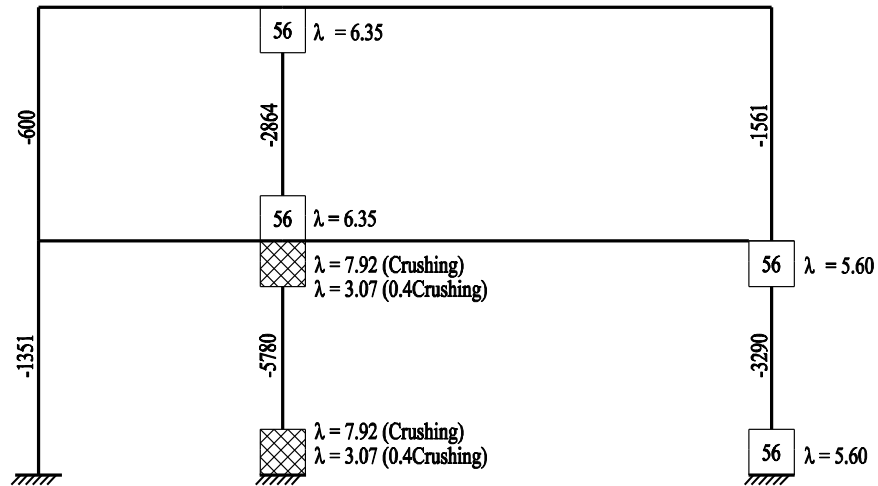


Figure 4.57: Load factor  $\lambda = 7.92$  (kN)

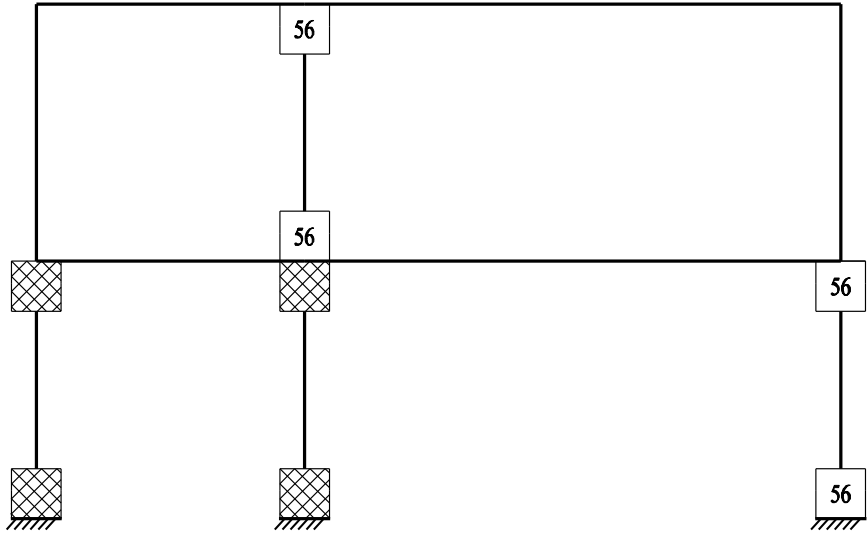


Figure 4.58: After first elastic unloading

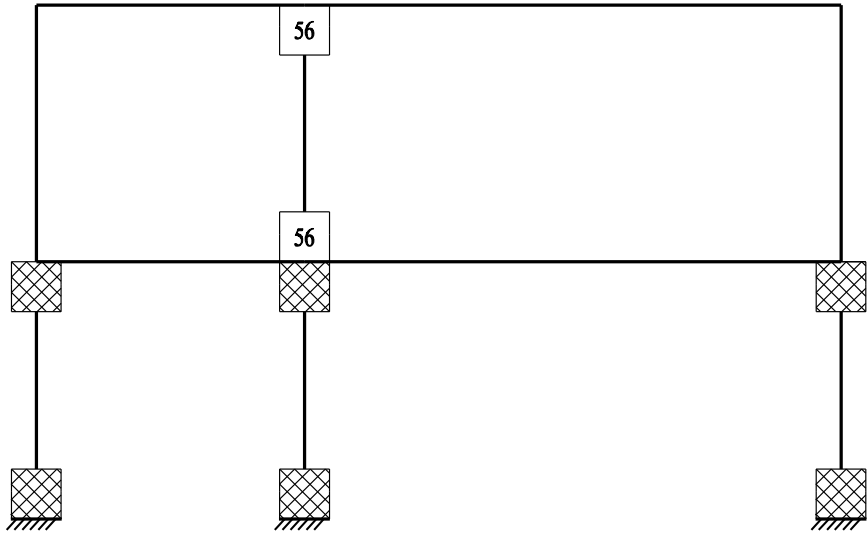
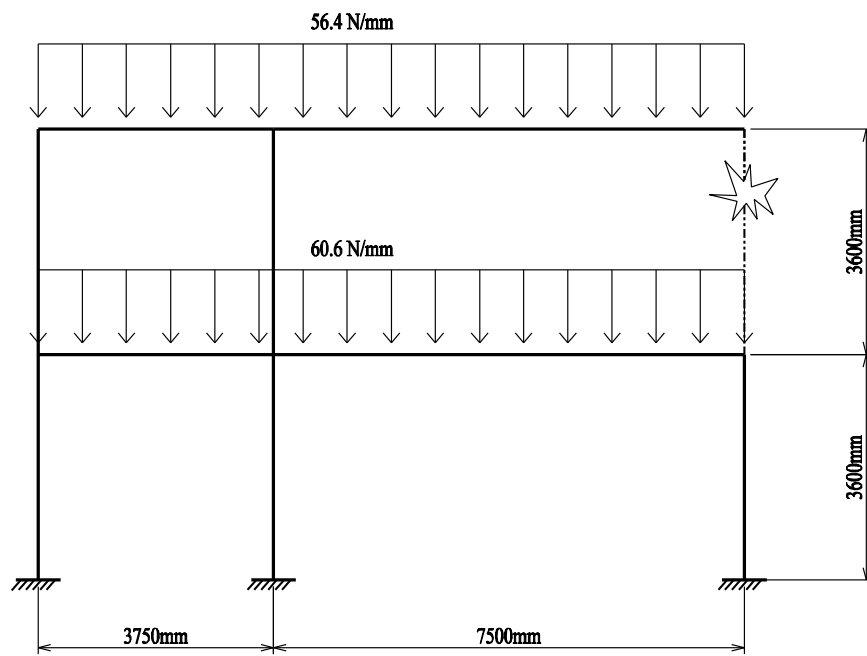


Figure 4.59: After second elastic unloading





**Figure 4.60: Geometry and loading with initial damage**

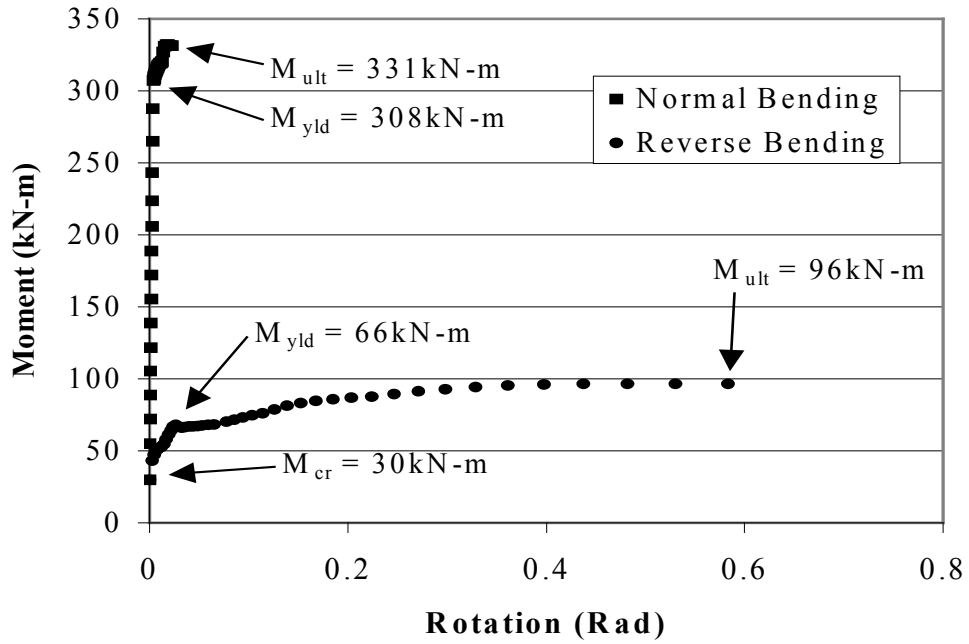


Figure 4.61: Normal and reverse bending post-elastic moment-rotation response

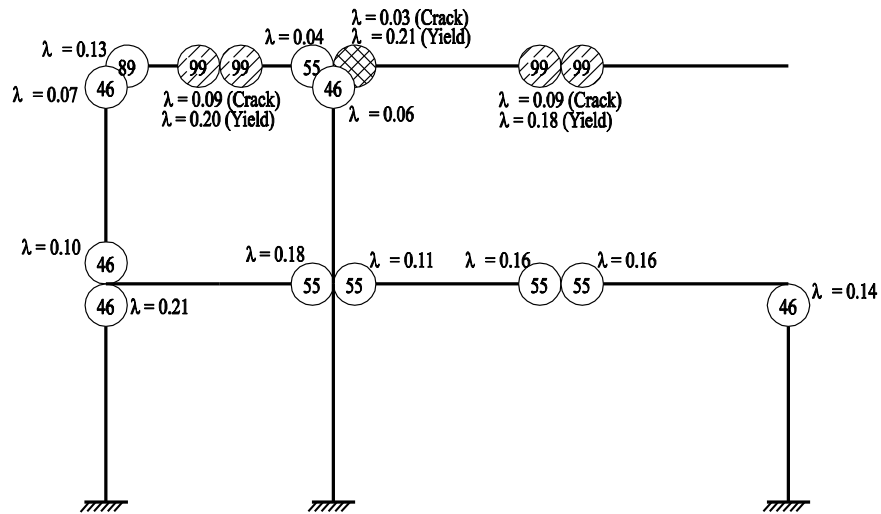


Figure 4.62: Load factor  $\lambda = 0.22$

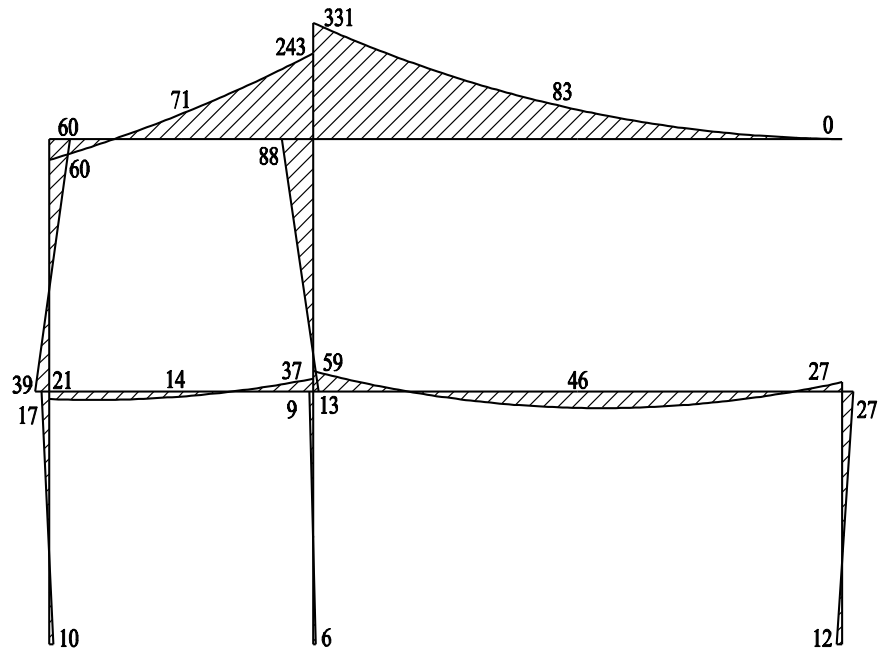


Figure 4.63: Bending moment diagram(kN-m)  $\lambda = 0.22$

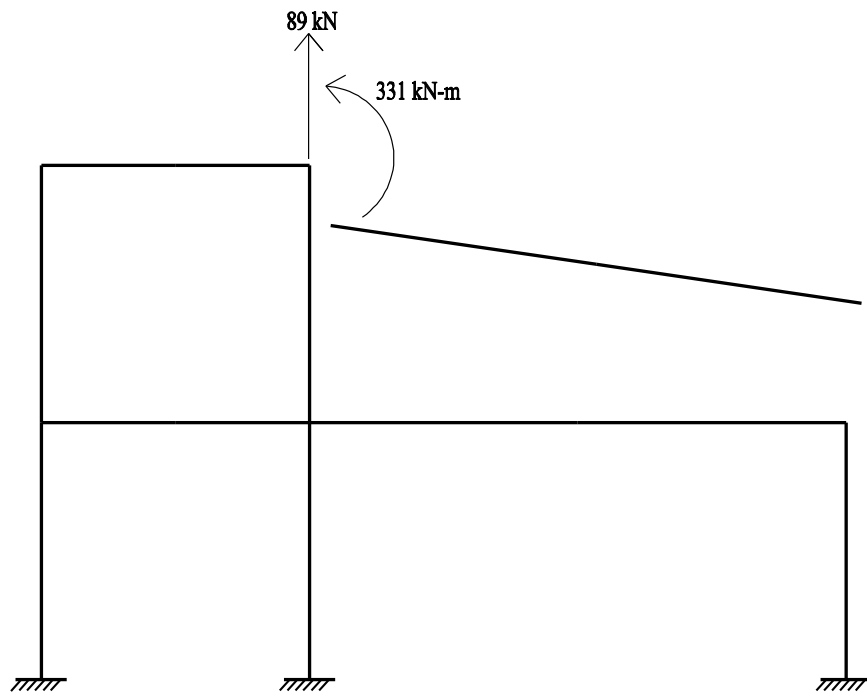


Figure 4.64: First unloading nodal loads

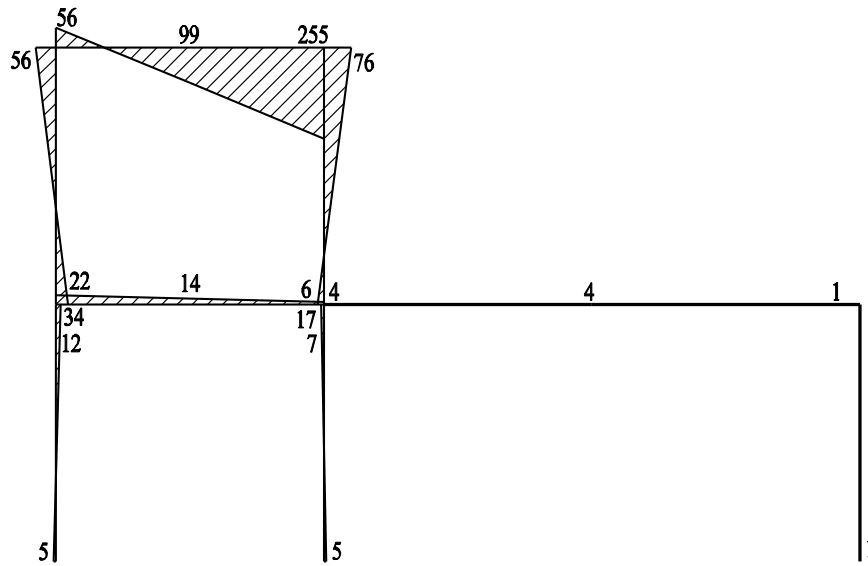


Figure 4.65: Bending moment diagram from first unloading (kN-m)

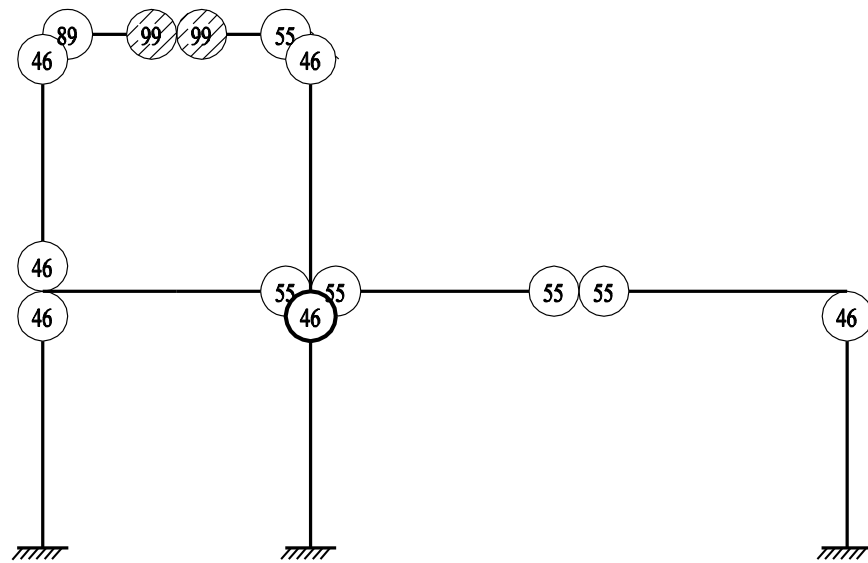


Figure 4.66: After first unloading

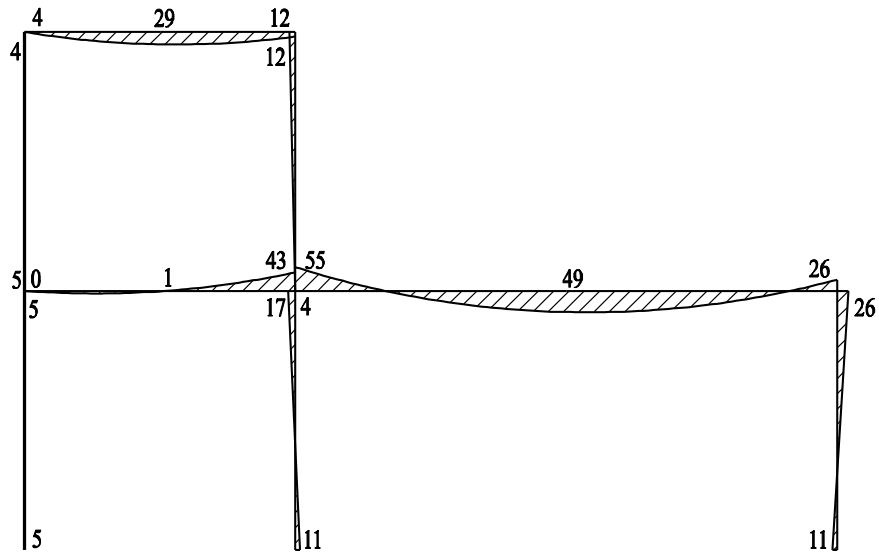


Figure 4.67: Bending moment diagram for after first unloading (kN-m)

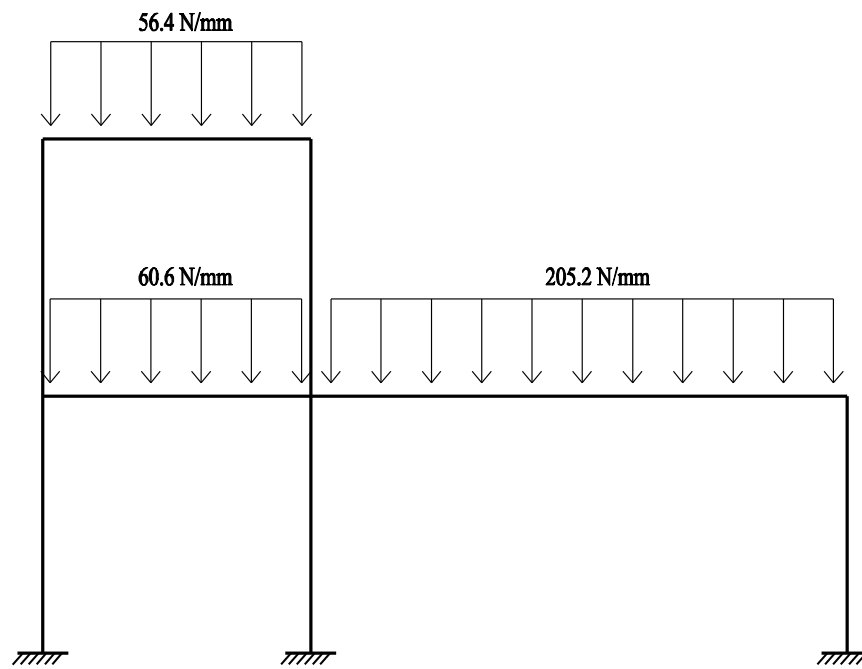


Figure 4.68: Reloading loads

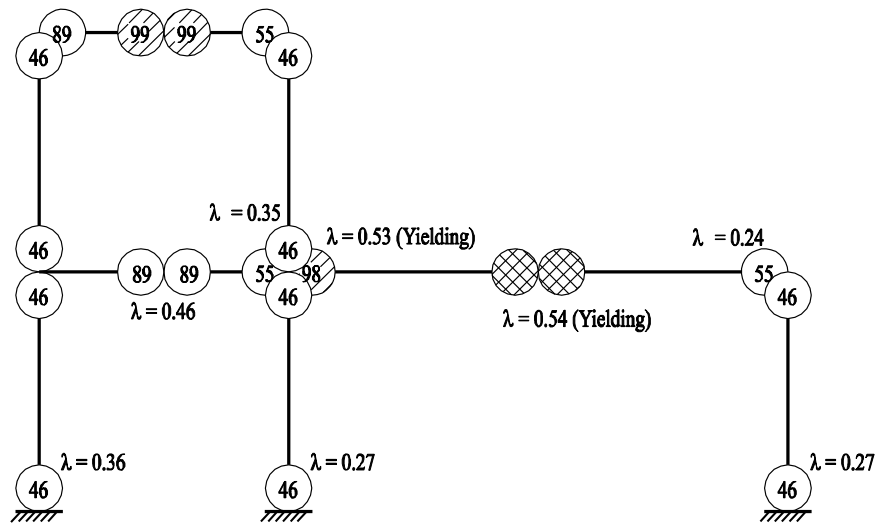


Figure 4.69: Load factor  $\lambda = 0.55$

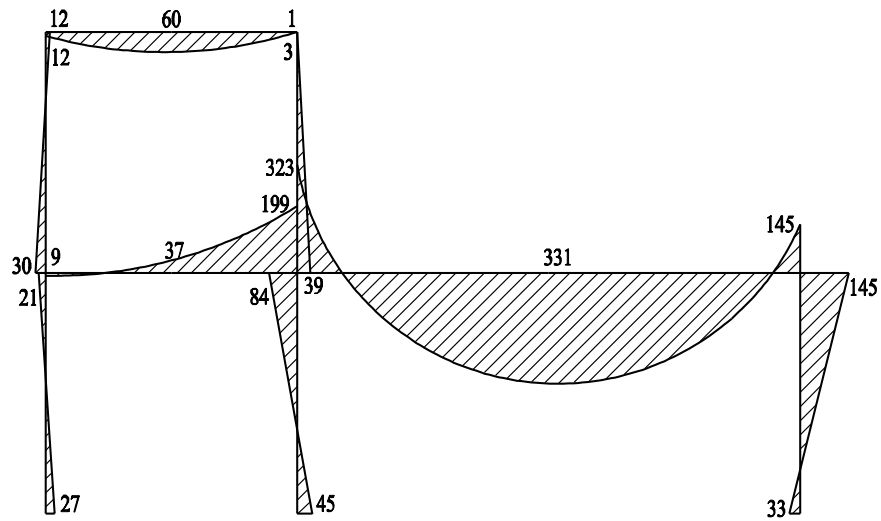


Figure 4.70: Bending moment diagram (kN-m)  $\lambda = 0.55$

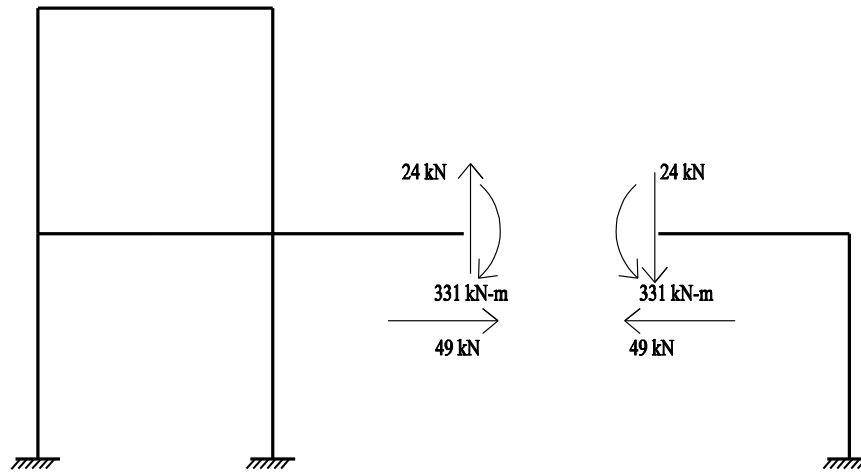


Figure 4.71: Second unloading nodal loads

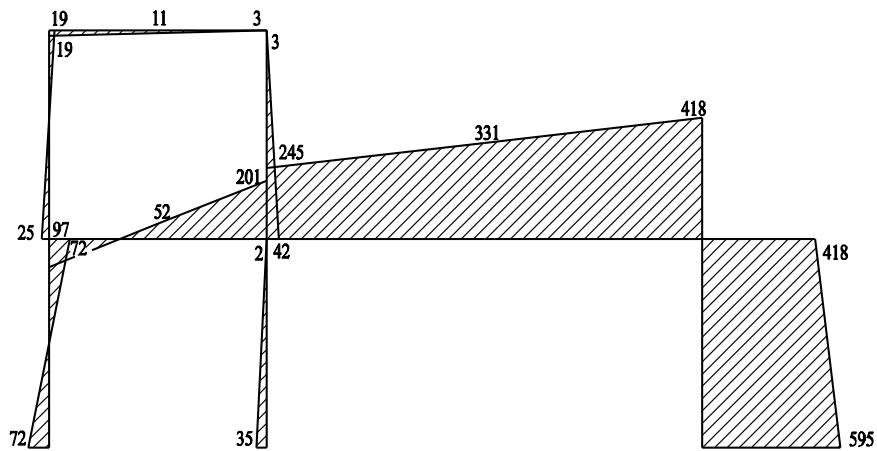


Figure 4.72: Bending moment diagram for second unloading (kN-m)

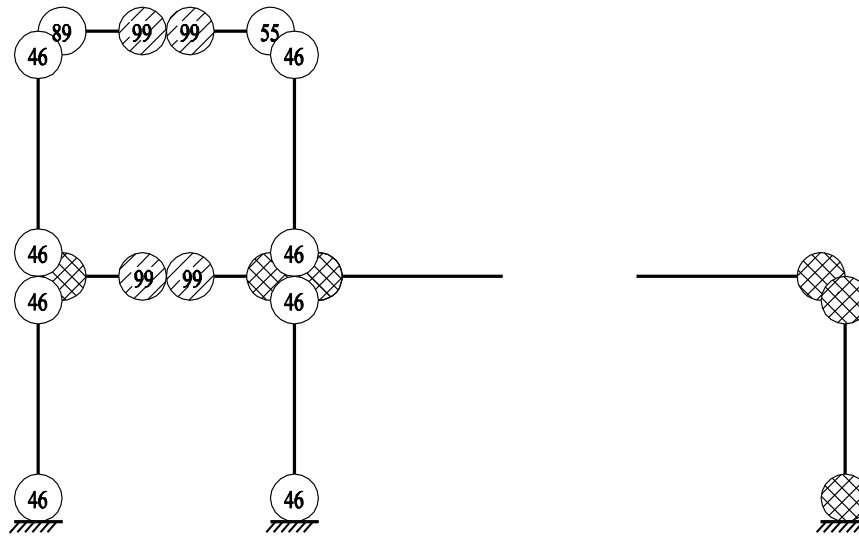


Figure 4.73: After second elastic-unloading

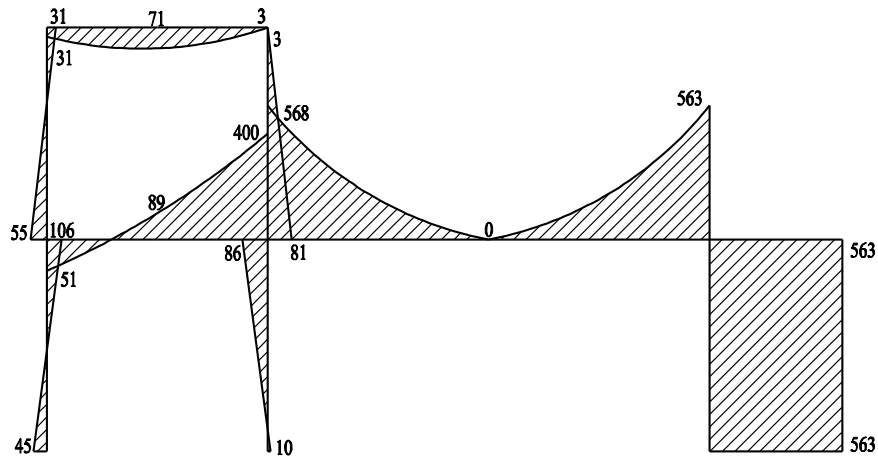
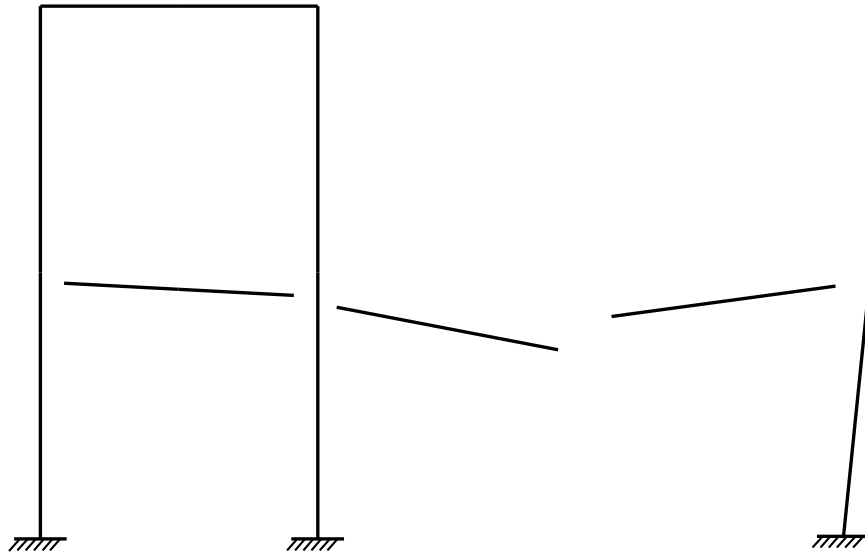


Figure 4.74: Bending moment diagram for after second unloading (kN-m)





**Figure 4.75: Remaining structure**

## **Chapter 5**

### **Conclusions**

This thesis presents the theory and methodology for analyzing reinforced concrete frames subjected to both normal and abnormal loads. A beam-column element model was developed to account for nonlinear behaviour and was employed in an incremental computer analysis program. The computer program was used to analyze examples of typical reinforced concrete frames. The following provides a summary of the work completed for this study, specific conclusions regarding nonlinear analysis of reinforced concrete frames and future work to be considered.

#### **5.1 Summary**

Chapter 1 briefly reviewed some of the analysis and design standards currently in practice, which aim to mitigate the effects of abnormal loads on structures, which can potentially lead to progressive collapse. Examples of structures that have been subjected to abnormal loads were given. The scope of work for this study was presented along with the assumptions and idealizations used throughout this study.

Chapter 2 presented the analysis concepts and theory used to develop the computer analysis program. The beam-column element used to discretize a reinforced concrete frame was developed. The nonlinear behaviour of the element was modeled using a series of end-springs which represent the post-elastic stiffness of a member-section. The post-elastic stiffness of a member-section was obtained from a post-elastic force-deformation response, which was first obtained by performing sectional analysis on a reinforced concrete section using a public domain computer program. The force-deformation responses were modeled as either bilinear or trilinear. Stiffness degradation factors were derived, based on the post-elastic force-deformation responses, which were used in modifying the elastic stiffness coefficients in the element stiffness matrix to account for the nonlinear behaviour.

Chapter 3 presented the computer analysis program which was comprised of four distinct stages. Stage zero performed an elastic analysis on the structure until the first member-section entered the post-elastic range. Stage one performed an inelastic incremental analysis on the structure which progressively tracked the deterioration of post-elastic stiffness. Stage two performed an elastic-unloading analysis on the structure which only occurred if a member-section failed. Finally, stage three performed an inelastic reloading analysis, which involved applying amplified debris loads on

the structure as a direct result of members disengaging from the main structure and falling onto the remaining structure below.

Chapter 4 presented analysis examples for reinforced concrete frames. The frame designs and analysis outputs were first explained. Each frame was analyzed for degraded post-elastic bending, shearing and axial stiffness separately. The first analysis example was for a simple portal frame used to illustrate the program outputs. The second analysis example was for a 2 bay-2 storey more redundant frame. The third analysis example was for the same 2 bay-2 storey frame but with some initial damage caused by an abnormal load. This example was used to illustrate the program's capabilities for performing a progressive collapse analysis.

## **5.2 Conclusions**

There are several specific conclusions regarding the nonlinear analysis of the reinforced concrete frames presented in this study:

- The analysis results of the 2 bay-2 storey frame for degraded bending stiffness and degraded shear stiffness as presented in Sections 4.4.1 and 4.4.2 show that the frame exhibits considerable ductility. Several member-sections continue to resist load and deform after their reinforcement has yielded.
- Cracking of a member-section (flexural, diagonal or transverse) causes a large reduction in post-elastic stiffness. This is evident by the values of the degradation factors given in the analysis examples.
- Even one member-section failure can greatly affect the remaining structure. Section 4.4.2 demonstrates this whereby after the elastic-unloading analysis is performed due to a member-section failing, several member-sections who previously had not yet experienced any post-elastic stiffness degradation now experienced either partial or complete degradation.
- For the 2 bay-2 storey frame, the amount of additional load beyond the target load level that the structure can resist is governed by the structure's shear resistance.
- Post-elastic axial stiffness degradation in compression has little effect on the structure's strength and stability. Section's 4.3.3 and 4.4.3 show that post-elastic axial stiffness degradation in compression only occurs at high load factor levels. The load factor levels

are high enough, that, if post-elastic bending or shearing stiffness degradation were also accounted for, failure of the frame would occur due to degraded bending or shearing stiffness before any degradation in axial stiffness.

- For the frames analyzed in this study, buckling does not preclude material failure.

### **5.3 Future Work**

There are several areas of future work that should be investigated in regards to this study:

- The effects of combined stress states should be incorporated into the computer analysis program. Currently, the program tracks the deterioration of post-elastic bending, shearing or axial stiffness separately and ignores moment-shear or moment-axial force interaction. Undoubtedly, accounting for force interaction would yield more realistic results.
- The degree of end-fixity should be accounted for when determining the column critical buckling load. Currently a  $k$  value of unity is used. The degree of end-fixity might be derived from the value of the column's bending stiffness degradation factors as they represent the amount of post-elastic stiffness degradation at an end-section.

## Appendix A

### Examples of Calculating $\mu$

#### 600x250mm Beam

$$\rho = 1.09\%$$

$$f'_c = 35 \text{ MPa}$$

$$E = 26540 \text{ MPa}$$

$$L = 7500 \text{ mm}$$

$$I_g = 4500 \times 10^6 \text{ mm}^4$$

$$I_e = 2027 \times 10^6 \text{ mm}^4$$

% of Length	r
01	0.869
10	0.399
20	0.249
30	0.181
40	0.142
50	0.117
60	0.100
70	0.087
80	0.077
90	0.069
100	0.062

$$\mu = 0.451 \rightarrow 9\% \text{ of length}$$

#### 500x400mm Beam

$$\rho = 1.57\%$$

$$\rho' = 0.22\%$$

$$f'_c = 35 \text{ MPa}$$

$$E = 26540 \text{ MPa}$$

$$L = 7500 \text{ mm}$$

$$I_g = 4167 \times 10^6 \text{ mm}^4$$

$$I_c = 2295 \times 10^6 \text{ mm}^4$$

% of Length	r
01	0.892
10	0.453
20	0.292
30	0.216
40	0.171
50	0.142
60	0.121
70	0.106
80	0.094
90	0.084
100	0.076

$$\mu = 0.551 \rightarrow 7\% \text{ of length}$$

### 300x300mm Column

$$\rho = 2.02\%$$

$$\rho' = 2.02\%$$

$$f'_c = 35 \text{ MPa}$$

$$E = 26540 \text{ MPa}$$

$$L = 3600 \text{ mm}$$

$$I_g = 675 \times 10^6 \text{ mm}^4$$

$$I_c = 366 \times 10^6 \text{ mm}^4$$

% of Length	r
01	0.941
10	0.617
20	0.446
30	0.349
40	0.287
50	0.243
60	0.211
70	0.187
80	0.167
90	0.152
100	0.139

$\mu = 0.542 \rightarrow 14\%$  of length

450x450mm Column

$\rho = 1.57\%$

$\rho' = 1.57\%$

$f'_c = 35 \text{ MPa}$

$E = 26540 \text{ MPa}$

$L = 3600 \text{ mm}$

$I_g = 3417 \times 10^6 \text{ mm}^4$

$I_e = 1922 \times 10^6 \text{ mm}^4$

% of Length	r
01	0.947
10	0.640
20	0.471
30	0.372
40	0.308
50	0.262
60	0.229
70	0.203
80	0.182
90	0.165
100	0.151

$\mu = 0.562 \rightarrow 14\%$  of length



## Appendix B

### Axial Stiffness Reduction Coefficient

The derivation of the axial stiffness reduction coefficient of Eq. (2.22) follows that found in Liu (2007) with a correction given here. In order to find the end reaction when end 1 displaces a unit distance as shown in Figure B.1, the force method of analysis is used, whereby from the primary structure, the displacement of end 1 due to imposed unit force  $F$  is given by,

$$f_{11} = \frac{1}{N_1} + \frac{L}{EA} + \frac{1}{N_2} \quad (\text{B.1})$$

where we solve for  $N_1$  and  $N_2$  from Eq. (2.18) of Chapter 2 where,

$$n_1 = \frac{1}{1 + \frac{AE}{N_1L}} \quad \text{and} \quad n_2 = \frac{1}{1 + \frac{AE}{N_2L}}$$

Solving for  $N_1$  gives,

$$1 + \frac{AE}{N_1L} = \frac{1}{n_1} \quad (\text{B.2})$$

$$\frac{AE}{N_1L} = \frac{1}{n_1} - 1 \quad (\text{B.3})$$

$$\frac{AE}{N_1L} = \frac{1 - n_1}{n_1} \quad (\text{B.4})$$

$$\frac{N_1L}{AE} = \frac{n_1}{1 - n_1} \quad (\text{B.5})$$

$$\therefore N_1 = \frac{AE}{L} \left( \frac{n_1}{1-n_1} \right) \text{ and } N_2 = \frac{AE}{L} \left( \frac{n_2}{1-n_2} \right) \quad (\text{B.6})$$

Then, from Eq. (B.1),

$$f_{11} = \frac{L}{AE} \left( \frac{1-n_1}{n_1} \right) + \frac{L}{AE} + \frac{L}{AE} \left( \frac{1-n_2}{n_2} \right) \quad (\text{B.7})$$

$$f_{11} = \frac{L}{AE} \left[ \left( \frac{1-n_1}{n_1} \right) + 1 + \left( \frac{1-n_2}{n_2} \right) \right] \quad (\text{B.8})$$

$$f_{11} = \frac{L}{AE} \left[ \frac{n_2 - n_1 n_2 + n_1 n_2 + n_1 - n_1 n_2}{n_1 n_2} \right] \quad (\text{B.9})$$

$$\therefore f_{11} = \frac{L}{AE} \left[ \frac{n_1 + n_2 - n_1 n_2}{n_1 n_2} \right] \quad (\text{B.10})$$

Then, as given in Eq. (2.21a), stiffness coefficient  $k_{11} = \frac{1}{f_{11}} = \frac{AE}{L} \chi_0$

where the axial stiffness reduction coefficient is,

$$\chi_0 = \frac{n_1 n_2}{n_1 + n_2 - n_1 n_2} \quad (\text{B.11})$$

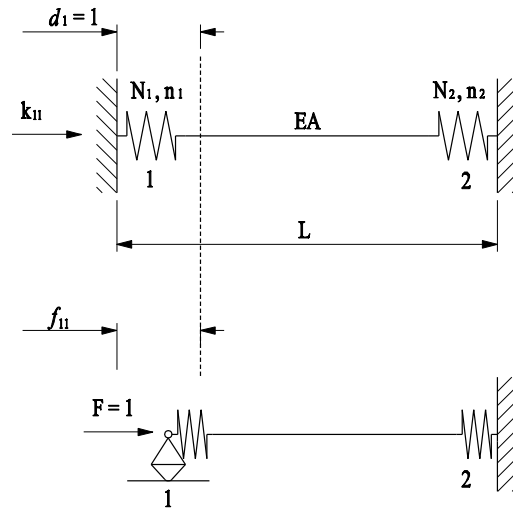


Figure B.1: Member model and primary structure (Liu, 2007)

## Appendix C

### Frame Design

The following presents the analysis and design of the reinforced concrete frames of Chapter 4. Although the analysis and design may be rather crude by a practicing engineer's standards, the intention of the designs is to help illustrate the analysis capabilities of the program.

#### Portal Frame

The following criteria were used in analyzing the portal frame of Figure 4.2 in accordance with the National Building Code of Canada 1995:

Unfactored Snow = 1.84 kPa

Unfactored Wind = 1.0 kPa

Concrete Dead = 23.6 kN/m<sup>3</sup>

250 mm thick one-way concrete slab with 7500 mm tributary width

Beams: 500 x 450 mm,  $A_g = 225000 \text{ mm}^2$ ,  $I_g = 4688 \times 10^6 \text{ mm}^4$

Columns: 450 x 450 mm,  $A_g = 202500 \text{ mm}^2$ ,  $I_g = 3417 \times 10^6 \text{ mm}^4$

All concrete 35 MPa.

The design forces were obtained from an elastic analysis using section properties as per Clause 10.14.1 of CSA Standard A23.3-94.

#### Governing Design Forces

Beams:  $M_f = 277 \text{ kN-m}$ ,  $V_f = 308 \text{ kN}$

Columns:  $M_f = 311 \text{ kN-m}$ ,  $V_f = 150 \text{ kN}$ ,  $P_f = 308 \text{ kN}$

#### Beam Reinforcement

Select  $\rho = 1.07\%$ ,  $\rho' = 0.2\%$ ,  $\therefore K_r = 2.7$ ,  $K'_r = 0.6$

Then,  $M'_r = 0.6(450\text{mm})(435\text{mm})^2 \times 10^{-6} = 51 \text{ kN-m}$

$M_r = 2.7(450\text{mm})(435\text{mm})^2 \times 10^{-6} = 230 \text{ kN-m}$

Then,  $M_r = 51 \text{ kN}\cdot\text{m} + 230 \text{ kN}\cdot\text{m} = 281 \text{ kN}\cdot\text{m}$

$$\frac{M_f}{M_r} = \frac{277 \text{ kN}\cdot\text{m}}{281 \text{ kN}\cdot\text{m}} = 0.98$$

Select 10M stirrups at 150mm o.c.

Then,  $V_s = (0.85)(200\text{mm}^2)(400\text{MPa})(435\text{mm})/150\text{mm} = 197 \text{ kN}$

$$V_c = 0.2(0.6)(\sqrt{35\text{MPa}})(450\text{mm})(435\text{mm}) = 139 \text{ kN}$$

Then,  $V_r = V_c + V_s = 139 \text{ kN} + 197 \text{ kN} = 336 \text{ kN}$

$$\frac{V_f}{V_r} = \frac{308 \text{ kN}}{336 \text{ kN}} = 0.92$$

### Column Reinforcement

Select  $\rho = 2.02\%$ ,  $\therefore K_r = 5.45$

Then,  $M_r = 5.45(450\text{mm})(385\text{mm})^2 \times 10^{-6} = 363 \text{ kN}\cdot\text{m}$

$$\frac{M_f}{M_r} = \frac{311 \text{ kN}\cdot\text{m}}{363 \text{ kN}\cdot\text{m}} = 0.86$$

Select 10M stirrups at 250mm o.c.

Then,  $V_s = (0.85)(200\text{mm}^2)(400\text{MPa})(385\text{mm})/250\text{mm} = 105 \text{ kN}$

$$V_c = 0.2(0.6)(\sqrt{35\text{MPa}})(450\text{mm})(385\text{mm}) = 123 \text{ kN}$$

Then,  $V_r = V_c + V_s = 123 \text{ kN} + 105 \text{ kN} = 228 \text{ kN}$

$$\frac{V_f}{V_r} = \frac{150 \text{ kN}}{228 \text{ kN}} = 0.66$$

## 2 Bay-2 Storey Frame

The following criteria were used in analyzing the 2 bay-2 storey frame of Figure 4.36 in accordance with the National Building Code of Canada 1995:

Unfactored Snow = 1.84 kPa

Unfactored Wind = 1.0 kPa

Unfactored Live = 2.4 kPa

Concrete Dead = 23.6 kN/m<sup>3</sup>

250 mm thick one-way concrete slab with 5000 mm tributary width

Beams: 500 x 350 mm,  $A_g = 175000 \text{ mm}^2$ ,  $I_g = 3646 \times 10^6 \text{ mm}^4$

Columns: 350 x 350 mm,  $A_g = 122500 \text{ mm}^2$ ,  $I_g = 1250 \times 10^6 \text{ mm}^4$

All concrete 35 MPa.

The design forces were obtained from an elastic analysis using section properties as per Clause 10.14.1 of CSA Standard A23.3-94.

### Governing Design Forces

Beams:  $M_f = 237 \text{ kN-m}$ ,  $V_f = 220 \text{ kN}$

Columns:  $M_f = 159 \text{ kN-m}$ ,  $V_f = 90 \text{ kN}$ ,  $P_f = 220 \text{ kN}$

### Beam Reinforcement

Select  $\rho = 1.04\%$ ,  $\rho' = 0.26\%$ ,  $\therefore K_r = 3.18$ ,  $K'_r = 0.76$

Then,  $M'_r = 0.76(350\text{mm})(438\text{mm})^2 \times 10^{-6} = 51 \text{ kN-m}$

$M_r = 3.18(350\text{mm})(438\text{mm})^2 \times 10^{-6} = 213 \text{ kN-m}$

Then,  $M_r = 51 \text{ kN-m} + 213 \text{ kN-m} = 264 \text{ kN-m}$

$$\frac{M_f}{M_r} = \frac{237 \text{ kN} \cdot \text{m}}{264 \text{ kN} \cdot \text{m}} = 0.90$$

Select 10M stirrups at 150mm o.c.

$$\text{Then, } V_s = (0.85)(200\text{mm}^2)(400\text{MPa})(438\text{mm})/250\text{mm} = 119 \text{ kN}$$

$$V_c = 0.2(0.6)(\sqrt{35\text{MPa}})(350\text{mm})(438\text{mm}) = 109 \text{ kN}$$

$$\text{Then, } V_r = V_c + V_s = 109 \text{ kN} + 119 \text{ kN} = 228 \text{ kN}$$

$$\frac{V_f}{V_r} = \frac{220\text{kN}}{228\text{kN}} = 0.96$$

### Column Reinforcement

Select  $\rho = 2.10\%$ ,  $\therefore K_r = 5.51$

$$\text{Then, } M_r = 5.51(350\text{mm})(285\text{mm})^2 \times 10^{-6} = 157 \text{ kN}\cdot\text{m}$$

$$\frac{M_f}{M_r} = \frac{159\text{kN}\cdot\text{m}}{157\text{kN}\cdot\text{m}} = 1.01$$

Select 10M stirrups at 200mm o.c.

$$\text{Then, } V_s = (0.85)(200\text{mm}^2)(400\text{MPa})(285\text{mm})/200\text{mm} = 97 \text{ kN}$$

$$V_c = 0.2(0.6)(\sqrt{35\text{MPa}})(350\text{mm})(285\text{mm}) = 70 \text{ kN}$$

$$\text{Then, } V_r = V_c + V_s = 70 \text{ kN} + 97 \text{ kN} = 167 \text{ kN}$$

$$\frac{V_f}{V_r} = \frac{90\text{kN}}{167\text{kN}} = 0.54$$

**Appendix D**  
**2 Bay - 2 Storey Frame Members Post-Elastic Force-Deformation**  
**Response**

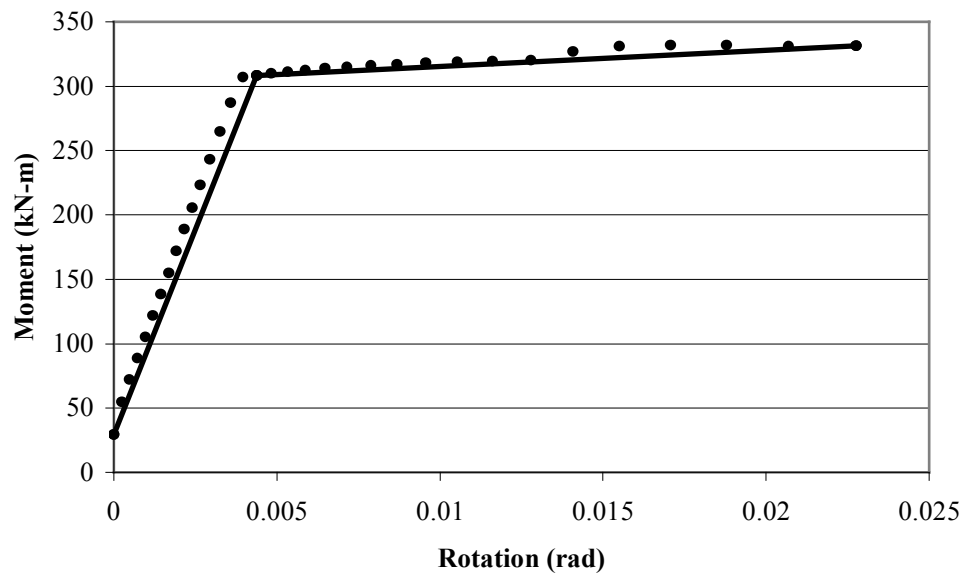


**Figure D.1: Beam post-elastic moment - rotation response**



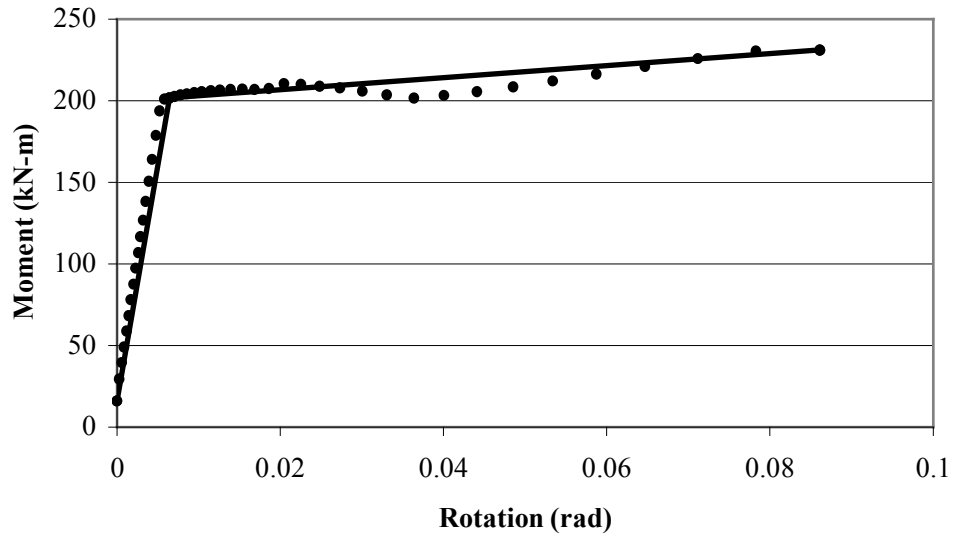


**Figure D.2: Column post-elastic moment - rotation response**

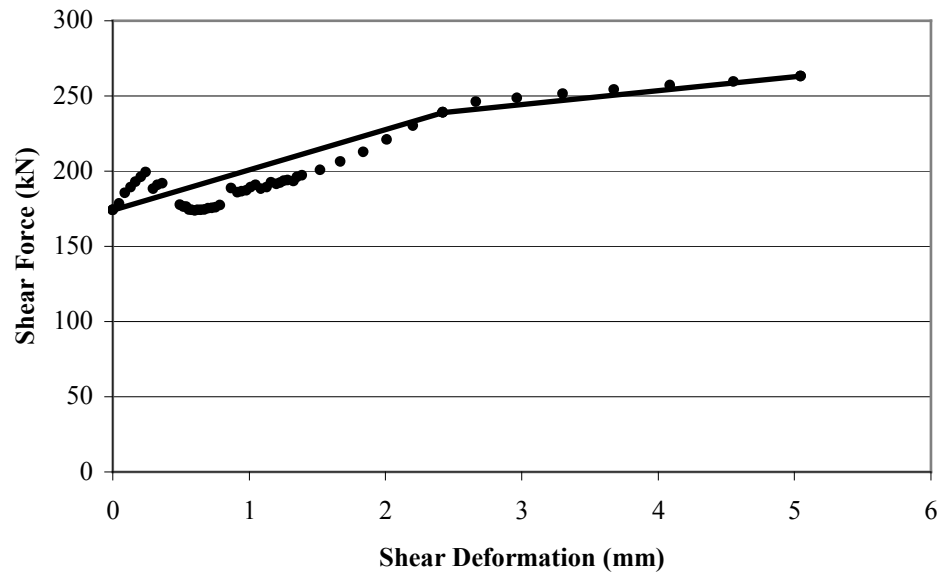


**Figure D.3: Smaller bay beam post-elastic shear force - shear deformation response**

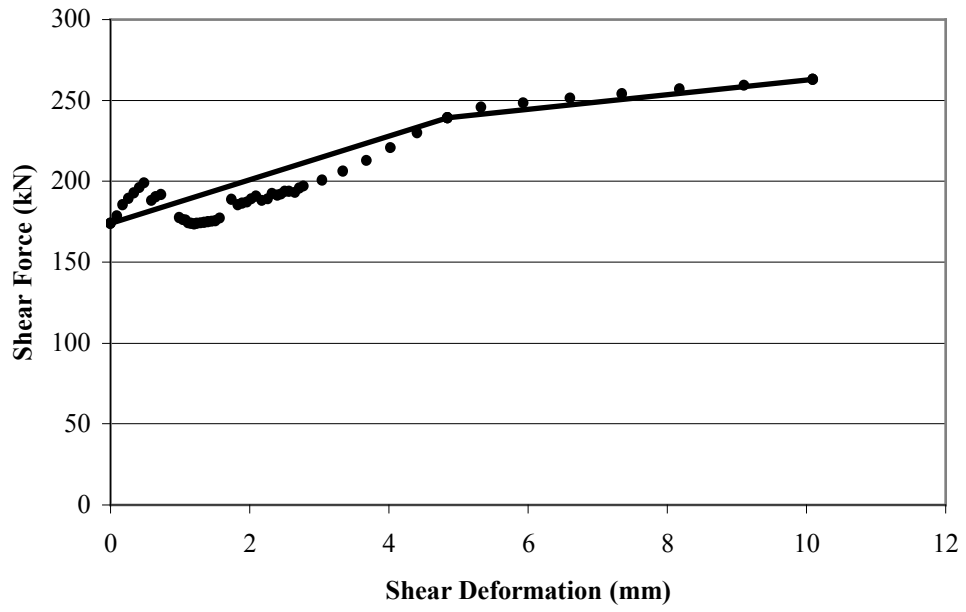


**Figure D.4: Larger bay beam post-elastic shear force - shear deformation response**

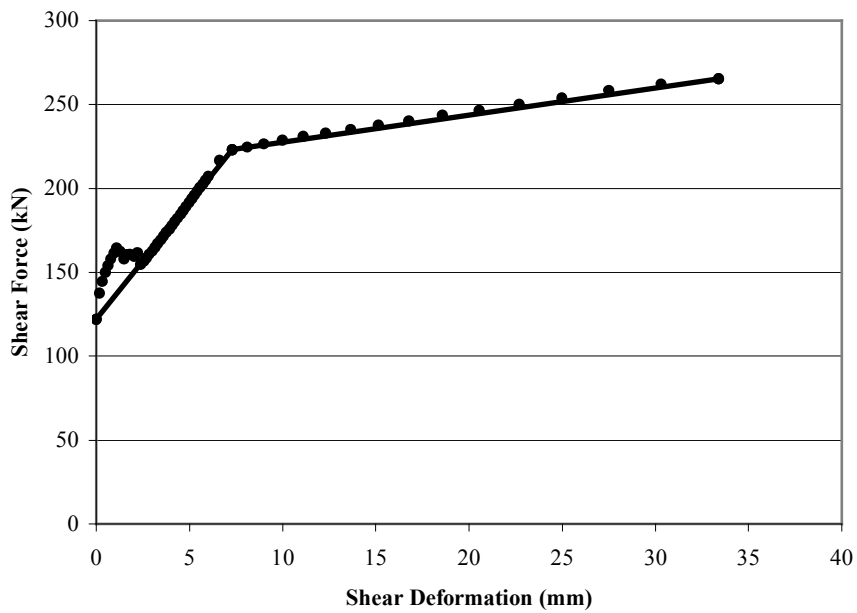


**Figure D.5: Column post-elastic shear force - shear deformation response**

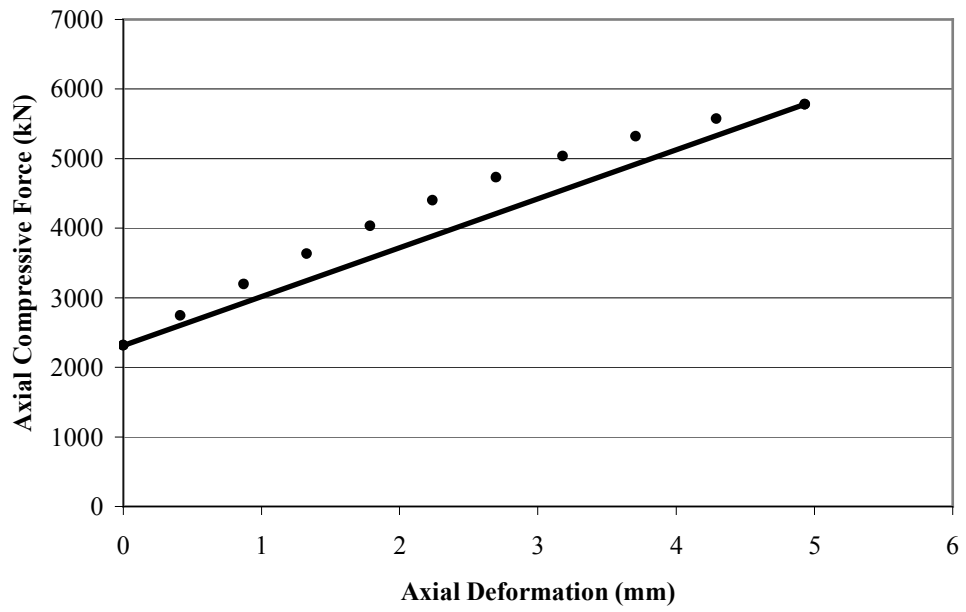


**Figure D.6: Column post-elastic axial compression - axial deformation response**

## References

- ACI. (2004). "Control of Deflection in Concrete Structures." *435R-04*, American Concrete Institute (ACI), USA.
- Bentz, E. (2000). "Sectional Analysis of Reinforced Concrete Members." PhD thesis, University of Toronto, Ontario, Canada.
- CAC. (1995). *Concrete Design Handbook*. Cement Association of Canada (CAC), Ottawa, Canada.
- Collins, M.P. & Mitchell, D. (1991). *Prestressed Concrete Structures*. Prentice-Hall, Inc., New Jersey.
- CSA. (1994). "Design of Concrete Structures." *A23.3-94*, Canadian Standards Association, Toronto, Ontario.
- Daily Telegraph. (1968) [http://apps.newham.gov.uk/History\\_canningtown/pic47.htm](http://apps.newham.gov.uk/History_canningtown/pic47.htm)
- DoD. (2005). "Design of Buildings to Resist Progressive Collapse." *Unified Facilities Criteria 4-023-03*, Department of Defense, USA.
- GSA. (2003). "Progressive Collapse Analysis and Design Guidelines for New Federal Office Buildings and Major Modernization Projects." Office of Chief Architect, General Services Administration, Washington, D.C.
- Hibbeler, R. C. (1994). *Mechanics of Materials*. Macmillan College Publishing Company, New York.
- Hinman, H. (1997). "Lessons from the Oklahoma City Bombing: Defensive Design Techniques." American Society of Civil Engineers (ASCE), New York.
- Liu, Y. (2007). "Progressive-Failure Analysis of Steel Building Structures Under Abnormal Loads." PhD thesis, University of Waterloo, Ontario, Canada.
- MacGregor, J. G., and Bartlett, F. M. (2000). *Reinforced Concrete - Mechanics and Design*. Prentice-Hall Canada, Inc., Scarborough, Ontario.
- NRCC. (1995). "National Building Code of Canada." National Research Council of Canada, Ottawa, Ontario.
- Pillai, S.U., Kirk, D.W., & Erki, M.A. (1999). *Reinforced Concrete Design*. McGraw-Hill Ryerson Ltd, Canada.
- Response-2000. (2000). Version 1.0.5. "Reinforced Concrete Sectional Analysis using the Modified Compression Field Theory." Evan C. Bentz & Michael P. Collins.  
<http://www.ecf.utoronto.ca/~bentz/r2k.htm>

Sennett, R. E. (1994). *Matrix Analysis of Structures*. Prentice-Hall, Inc., New Jersey.

Stamets, J. (1987) [http://www.historylink.org/essays/output.cfm?file\\_id=2947](http://www.historylink.org/essays/output.cfm?file_id=2947)

Timoshenko, S.P., & Gere, J.M. (1972). *Mechanics of Materials*. D. Van Nostrand Company, New York.

Xu, L. (1994). "Optimal Design of Steel Frameworks with Semi-Rigid Connections." PhD thesis, University of Waterloo, Ontario, Canada.

Xu, L., Liu, Y., and Grierson, D. E. (2005). "Nonlinear Analysis of Steel Frameworks Through Direct Modification of Member Stiffness Properties." *Advances in Engineering Software*, 36(5), 312-324.